SULFIDE MONITORING IN THE BALTIC SEA USING THE OPUS UV *IN-SITU* SENSOR

Monographic Dissertation

for the Award of the Academic Degree

Doctor rerum naturalium (Dr. rer. nat.)

of the Faculty of Mathematics and Natural Sciences

of the University of Rostock

Submitted by

Malin Maria, Waern

born on 07.02.1996 in Slaka, Sweden

Rostock, February 2025

(Reviewed May 2025)

https://doi.org/10.18453/rosdok_id00004905

TABLE OF CONTENT

ABSTRACT

The spread of hypoxic and anoxic zones is linked to the stability of both the sulfur and oxygen cycles. Prolonged deoxygenation in the ocean interior increases the spread of sulfides, which can lead to loss of biodiversity. However, the co-occurrence of sulfides and oxygen in natural environments is not fully understood, as high-resolution *in-situ* measurements of sulfides are rare. Here, a comprehensive investigation was conducted to 1) determine which regression method is the most optimal for measuring total H_2S ($H_2S + HS^-$) in the Baltic Sea using the OPUS UV sensor (TriOS GmbH, Germany), and 2) determine the distribution of total H_2S along a transect with ca. 1 m depth resolution from the Arkona Basin to the Eastern Gotland Basin. The results show that the OPUS sensor measurements agree well with the control method (wet chemistry from Niskin bottles) and have a lower limit of detection (LOD) compared to the control method in four out of five cruises. In addition, the high-resolution OPUS data showed co-occurrence of total H_2S and oxygen on multiple casts for all cruises. Plumes of sulfidic water were also detected around and above the oxygen LOD, but were not persistent. These results show that the co-occurrence of total H_2S and oxygen is a recurring phenomenon in the Baltic Sea and that the distribution of sulfides is more dynamic than suggested by historical records.

ZUSAMMENFASSUNG

Die Ausbreitung hypoxischer und anoxischer Zonen hängt mit der Stabilität sowohl des Schwefel- als auch des Sauerstoffkreislaufs zusammen. Längerer Sauerstoffmangel im Inneren der Ozeane verstärkt die Ausbreitung von Sulfiden, was zu einem Biodiversitätsverlust führen kann. Das gleichzeitige Auftreten von Sulfiden und Sauerstoff in der Natur ist jedoch nicht vollständig geklärt, da hochauflösende In-situ-Messungen von Sulfiden selten sind. Hier wurde eine umfassende Untersuchung durchgeführt, um 1) festzustellen, welche Regressionsmethode für die Messung von Gesamt- H_2S (H_2S + HS^-) in der Ostsee unter Verwendung des OPUS-UV-Sensors (TriOS GmbH, Deutschland) am besten geeignet ist, und 2) die Verteilung von Gesamt- H_2S entlang eines Transekts mit ca. 1 m Tiefenauflösung vom Arkona-Becken zum östlichen Gotland-Becken zu bestimmen. Die Ergebnisse zeigen, dass die OPUS-Sensormessungen gut mit der Kontrollmethode (Nasschemie aus Niskin-Flaschen) übereinstimmen und in vier von fünf Fahrten eine niedrigere Nachweisgrenze (LOD) im Vergleich zur Kontrollmethode aufweisen. Darüber hinaus zeigten die hochauflösenden OPUS-Daten bei allen Fahrten das gleichzeitige Auftreten von H_2S und Sauerstoff bei mehreren Probenahmen. Sulfidische Wasserfahnen wurden auch in der Nähe und oberhalb der Sauerstoff-LOD festgestellt, waren aber nicht persistent. Diese Ergebnisse zeigen, dass das gleichzeitige Auftreten von H_2S und Sauerstoff ein wiederkehrendes Phänomen in der Ostsee ist und dass die Verteilung von Sulfiden dynamischer ist, als es die historischen Aufzeichnungen vermuten lassen.

List of Abbreviations

AB	Arkona Basin
AOX	alternative oxidase
BB	Bornholm Basin
CDOM	Colored dissolved organic matter
df	Data frame
EGB	Eastern Gotland Basin
EMB	R/V Elisabeth Mann Borgese
H_2S	Hydrogen sulfide
HS^-	Bisulfide ion
IQR	Interquartile range
ISD	Linear regression highlighting the use of a derived background spectra
ISL	Linear regression highlighting the use of a linear background spectra
ISP	Linear regression highlighting the use of a poly-4 background spectra
ISQ	Linear regression highlighting the use of a quadratic background spectra
LM	Linear model
LOD	Limit of detection
LOQ	Limit of quantification
LOZ	Low oxygen zone
NBS	National Bureau of Standards
NO_3	Nitrate
NTU	Nephelometric Turbidity Unit
O_2	Oxygen
OMZ	Oxygen Minimum Zone
OPUS	The OPUS-DS UV sensor (TriOS GmbH, Germany)
Poly-4	A function over wavelengths expressed as λ^{-4}
S	Sulfur
S^{2-}	Sulfide ion
$S_2O_3^{2-}$	Thiosulfate ion
SD	Standard deviation
SO_3^{2-}	Sulfite ion
SO_4^{2-}	Sulfate ion
SQR	Sulfide-quinone oxidoreductase

LIST OF FIGURES

LIST OF TABLES

ACKNOWLEDGEMENT

When I received the opportunity to start a PhD at the Leibnitz Institute for Baltic Sea Research Warnemünde (IOW), I was overjoyed! This meant that I would be able to fulfill one of my biggest dreams so far and take another big step on my journey towards becoming a full-fledged researcher. Although I had to move from Sweden to Germany, I did not hesitate. The fact that I had already lived abroad, as well as moved from my hometown in pursue of my university studies, probably made the decision easier. My family have always been supportive in all of my endeavors, and their unwavering support and reassurance throughout my journey has been enormous. As if that was not enough, my PhD-journey led me to find a second family, here in Germany. My partner always listens patiently to my ramblings, and support me, along with many more, when things get tough. The number of people I have met and had the pleasure of getting to know during this time is too many to mention by name, however, I truly hope that all my friends and colleagues, new and old, realize my heart-felt appreciation. Everyone I have met and interacted with has influenced my work in one way or another.

I started my PhD-journey in September 2020 in the midst of Corona regulations and lockdowns. The restrictions were at times difficult to cope with, however, thanks to the diving department at IOW, led by Dipl. Ing. Erik Stohr, I got a good first contact with the institute as well as the Rostock University despite the otherwise limited human interaction. Despite these challenges, the fantastic colleagues on R/V Elisabeth Mann Borgese had a positive outlook, and without their help, I would not have been able to get so much good data in such a short amount of time. Thank you all for your support. I would especially like to thank Dr. Ing. Robert Wagner, Jan Donath, Ingo Schuffenhauer and the Marine Technology department at IOW for their invaluable help with all the fieldwork. I would also like to thank the Nutrient-group, led by Prof. Dr. Joanna Waniek, at IOW for their unwavering support and assistance with my calibration work and for providing me with all the control data used for this thesis. I could not have done it without your expertise and regular monitoring. Also, a special thank you to Mareike Floth-Peterson for always assisting me in the lab and Prof. Dr. Joanna Waniek for your immense support during my final months writing my thesis. Thank you also to MBARI and NKE, who provided calibration spectra for comparison and further investigations.

A large portion of my work in the earlier days was about verifying the overall performance of the OPUS sensor. The support I received from my thesis committee was very important, and I learnt a lot from our discussions. Thank you Prof. Dr. Arne Körtzinger, Dr. Birgit Klein, and Dr. Peter Holtermann for taking the time to help me. A special thank you to

Dr. Ralf Prien who was not only part of my committee, but who also always greeted me with a smile whenever I would drop by for yet another question or concern, in what seemed to be a never ending stream of thoughts that needed an outlet.

Lastly, I would like to thank Prof. Dr. Gregor Rehder and Dr. Henry Bittig for your insights and for giving me this opportunity. I have gained many new experiences, and grown as a person.

There are many more I would like to thank; whose support gave me strength when I needed it most, and whose comments kept me grounded when I let my imagination run wild. There are no words to express my gratitude, I can only say thank you!

This work was supported by the DArgo2025 and C-SCOPE project of the German Federal Ministry of Education and Research (BMBF).

CHAPTER 1. INTRODUCTION

The environment is an ever-changing system. Areas once high above sea level can nowadays be found deep below the surface. These continuous changes are necessary in order to both build up resilience and to drive evolution. The natural cycle of the environment is very complex, where weathering, physical and chemical barriers, and landscape play a big role. At steady state, the processes and driving forces that affect the cycles coupled to these parameters are constant; however, depending on location and parameter, steady state could be defined by a period of seconds to millennia. Short-term variations affect resilience and long-term variations influence evolution. However, when these changes happen at an increased speed, e.g. due to anthropogenic contributions, they might do more harm than good.

Between 1960 and 2010, the global oxygen inventory decreased with about 2% (Stramma & Schmidtko, 2019). Although a seemingly small amount, the oxic diffusion from the atmosphere to the oceans is one of the main driving forces to keep the chemocline (water mass with strong chemical gradient) from reaching the sea surface (Kump et al., 2005). Therefore, prolonged deoxygenation can have a substantial impact on – among other things – the sulfur cycle and the spread of hypoxic (oxygen < 1.47-2.75 ml/l) and anoxic (oxygen depletion) zones (Stramma & Schmidtko, 2019; Bhuiyan et al., 2024). A reduced oxygen inventory could thus compress oxygenated habitats as the Oxygen Minimum Zones (OMZ) expand (Stramma & Schmidtko, 2019) and chemicals other than oxygen will be needed for remineralisation. In fact, prolonged episodes of hypoxia and anoxia have already been found to affect bottom living organisms, causing a loss in biological diversity (Rabalais, 2019; EEA, 2023). On geological time scales, oceanic anoxic events have been found to be a consequence of abrupt temperature rise caused by an increase in carbon dioxide (CO_2) flux to the seawater (Jenkyns, 2010). Given the trends of today, with increasing temperature (Samset et al., 2024) and CO_2 emission (Liu et al., 2024) along with deoxygenation, it becomes increasingly important to have a clear picture of the spread of anoxia – and thereby sulfides – and their relationship to oxygen minimum zones.

1.1 Sulfides in the environment

Sulfur (S) is a very common chemical element in the world's oceans as well as in the crust (Charlson et al., 1992), and can be found in various forms depending on physical and chemical factors, such as biological composition and water properties involving pH (Millero et al., 1987). The reaction rates between the sulfur forms have been found to increase with pH

(Avrahami & Golding, 1968). The most stable form, as well as the most abundant in seawater, is sulfate (SO_4^{2-}), and additions to the water can come from weathering or leaching from sediments and rocks (Charlson et al., 1992; Sievert et al., 2007). Hydrogen sulfide (H_2S), another form found in marine environments, is believed to be formed primarily by heterotrophic sulfate-reducing bacteria, and to lesser degree through putrefaction of amino acids containing sulfur (Cline & Richards, 1969). In addition, H_2S can also be found in soil or rock minerals. Its moderate solubility in water along with dissociation behavior contribute to the formation of bisulfide (HS^-) (Dahl, 2020).

Bisulfide, HS^-, is dominating between pH 9 – 12 (97-99%, **Figure 1.1**), and can oxidize into several forms of sulfur-bearing ions depending on the amount of dissolved oxygen (O_2) (Cline & Richards, 1969):

$$2HS^- + O_2 = 2S^0 + 2OH^- \quad 1.1$$

$$2HS^- + 2O_2 = S_2O_3^{2-} + H_2O \quad 1.2$$

$$2HS^- + 3O_2 = 2SO_3^{2-} + 2H^+ \quad 1.3$$

$$HS^- + 2O_2 = SO_4^{2-} + H^+ \quad 1.4$$

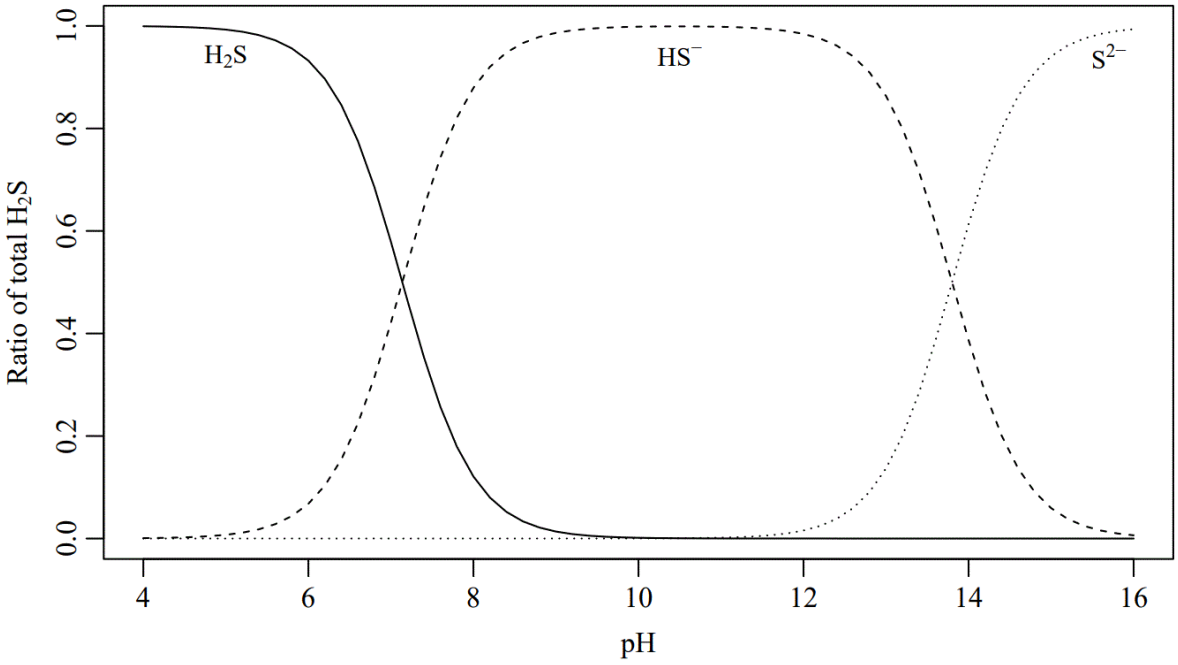

Figure 1.1. Bjerrum plot showing ratios between hydrogen sulfide (H_2S), bisulfide (HS^-), and sulfide (S^{2-}) as a function of pH at 15 °C.

Sulfate can also be formed when sulfite (SO_3^{2-}), the product from bisulfide (HS^-) oxidation, is oxidized. In addition, thiosulfate ($S_2O_3^{2-}$), together with HS^- and oxygen (O_2), can also form SO_4^{2-} (Avrahami & Golding, 1968). It has been found that $S_2O_3^{2-}$ has an important contribution factor to the dark assimilation of carbon dioxide (CO_2), and subsequently the microbial growth in marine environments with low organic material concentrations (Tuttle & Jannasch, 1977). Although sulfate, SO_4^{2-}, is the most stable form, it may only oxidize H_2S, and is not involved in oxidizing HS^-. However, when SO_3^{2-} is present along HS^- and SO_4^{2-}, $S_2O_3^{2-}$ rapidly forms. Furthermore, SO_3^{2-} alone in an oxic solution is oxidized into SO_4^{2-}, which also has a higher rate than HS^- oxidation (Avrahami & Golding, 1968). A schematic flow of the conversions can be seen in **Figure 1.2.**

Given the peculiar effect of the SO_4^{2-} and SO_3^{2-} ions on the potential oxidation process of HS^- to sulfide (S^{2-}) or $S_2O_3^{2-}$, it is also important to understand the oxidation process of H_2S. If HS^- is oxidized, the equilibrium between H_2S and HS^- shifts to the left, and more H_2S will dissociate. This has been well documented in e.g. Reverberi et al. (2016), Kamyshny et al. (2013), and Cline and Richards (1969). According to Avrahami and Golding (1968), for solutions with low sulfide concentrations, SO_3^{2-} is the first ion to form, which is rapidly removed as SO_4^{2-}. The remaining SO_3^{2-} will further oxidize the solution and form $S_2O_3^{2-}$, which will slowly oxidize into SO_4^{2-} as well. The oxidation of H_2S is thus highly affected by the O_2

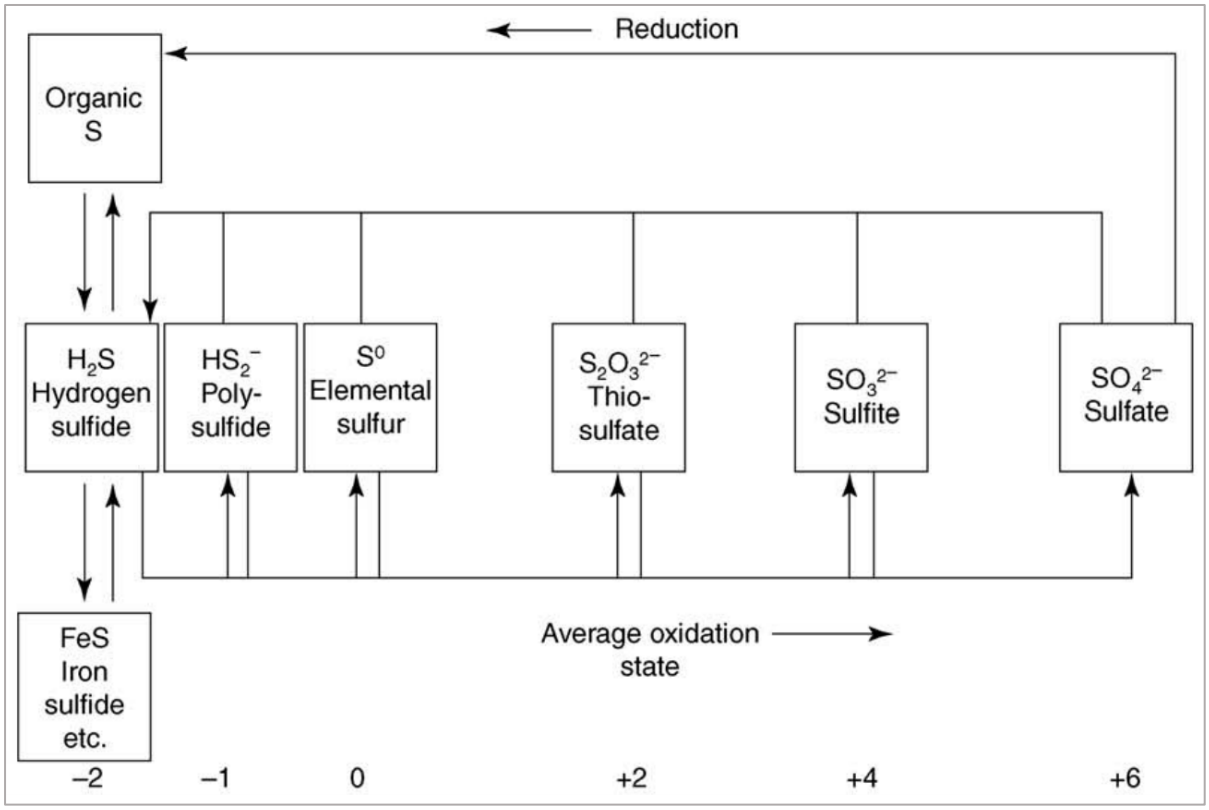

Figure 1.2. Schematic flow of the sulfur forms as presented by Lloyd (2006).

concentrations as well. The oxidation rate (within the ranges of temperature: 5-65 °C, pH: 4-8 and ionic strength: 0-6 M) can be calculated through (Millero et al., 1987):

$$\frac{d[H_2S]}{dt} = k[O_2][H_2S] \quad 1.5$$

where $[H_2S]$ is the concentration of H_2S. The rate constant, k, can be determined by:

$$log\ k = 10.50 + 0.16pH - (3.0 \cdot 10^3)/T + 0.44I^{1/2} \quad 1.6$$

The foundation of the sulfur cycle in the marine environment is hypothesized to originate from the large pool of marine sulfate (SO_4^{2-}) coupled with a supply of high organic matter available to heterotrophic sulfate-reducing bacteria (Callbeck et al., 2021). The lower energy yield through sulfate reduction compared to other oxidizers such as nitrate and manganese oxides is generally non-favorable, however, the substantially larger pool of marine sulfate (approximately 28 mM compared to nano- or micomolar levels) can compensate for this (Canfield, 2004; Callbeck et al., 2021). Despite the lower energy yield, many bacteria and archaea utilize dissimilatory sulfur metabolism, forming a key process of the planets sulfur cycle (Sievert et al. (2007), see also section **1.2**).

Depending on the oxygen concentration in the water column, the sulfur cycle can act as either a sedimentary cycle during non-sulfidic events or diffuse into the lower water column during sulfidic events (**Figure 1.3**). High productivity zones around coastal OMZs tend to have an active sulfur cycle as the sulfide-rich sediments form a strong benthic-pelagic interface with the overlying water column. Productivity zones have an increased potential to intensify eutrophic and anoxic conditions which can lead to the expansion of OMZs and consequently release of sulfides from the sediments, potentially changing the biogeochemical cycle in the area (Callbeck et al., 2021). In addition, although sulfate and sulfur reduction are both an anaerobic process, sulfur oxidation can occur as both an aerobic and anaerobic process (Sievert et al., 2007).

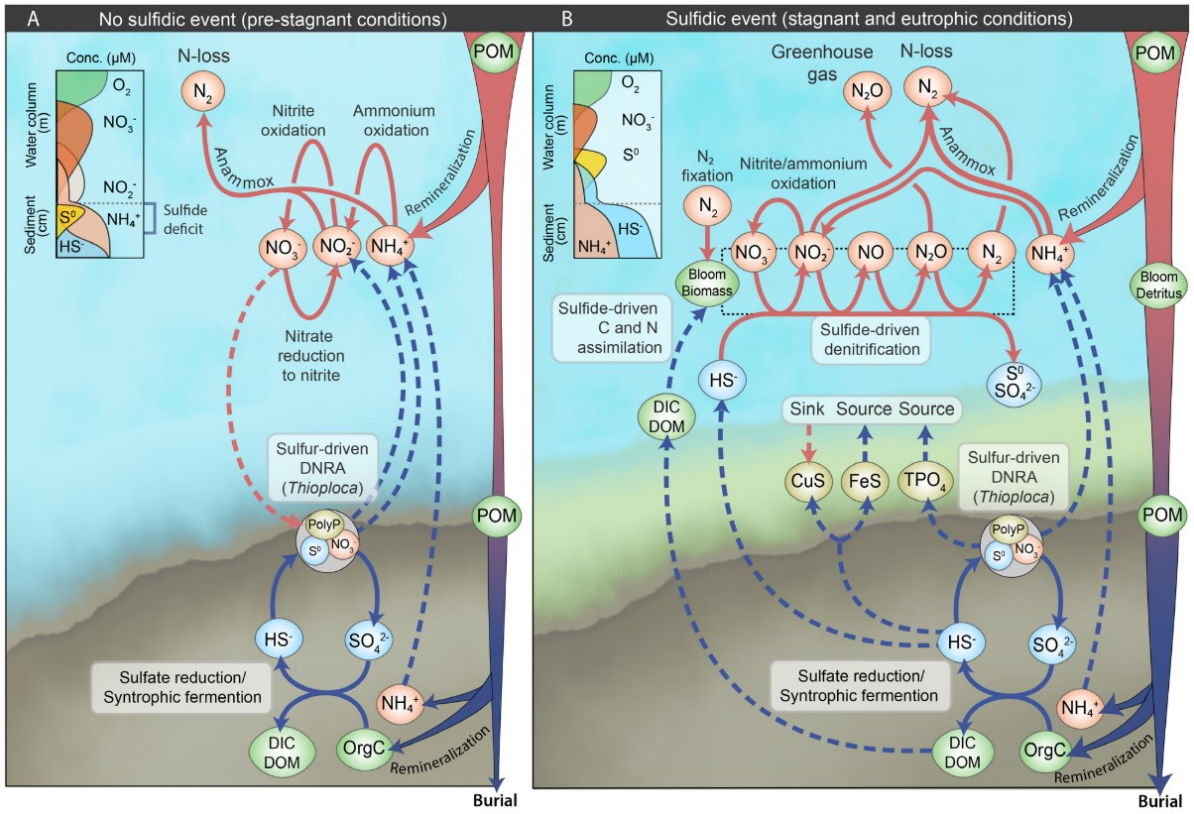

Figure 1.3. Connection between the sulfur, nitrate, carbon, and phosphorous cycle on the upper shelf of the oxygen minimum zone (OMZ; < 200 m) as summarized by Callbeck et al. (2021). The figure indicates two scenarios: A) no H_2S in the bottom waters, and B) an accumulation of elemental sulfur (yellow-green background color) generated through oxidation of sulfide. Solid lined arrows represent processes within the water column (red) and sediment (blue), while dotted lined arrows represent water-sediment fluxes.

1.2 Ecological importance of sulfides

Although much of the H_2S is dissociated into HS^-, little is known about the effect of HS^- on organisms and the environment. On the other hand, high concentrations of H_2S is believed to lead to oxidative stress, which can result in death if no detoxifying pathways are active. Kelley et al. (2016) found in their study, that evolutionary independent lineages of the same species of fish had a significant difference in gene expressions depending on if they had colonized a sulfidic or non-sulfidic area. Individuals that were exposed to higher concentrations of sulfides had, e.g., an upregulated gene associated with H_2S detoxification and oxidized sulfur transportation. The sulfide-quinone oxidoreductase (SQR) pathway in metazoans is one such pathway, and is linked to ATP production in the respiratory chain (Tobler et al., 2016). The SQR pathway can efficiently detoxify up to 10 µM H_2S, however a loss of function of enzymes in this pathway may result in lethal accumulation of endogenously produced sulfide. In addition, exposure to sulfide-rich environments consistently downregulated genes responsible for skin barriers, and fish in these environments also had a greater gill surface area to body

mass ratio, suggesting that H_2S flux regulation is not the main technique for coping with stress due to sulfide exposure (Kelley et al., 2016).

However, not all is bad when it comes to the toxicity of H_2S. Lloyd (2006) suggested in his review that H_2S, at μM levels, could in fact be vital for redox balancing in aerobic organisms. At higher H_2S concentrations, *Acanthamoeba castellanii*, a soil amoeba, has shown that although H_2S acts as a respiratory inhibitor, other pathways were opened to allow further electron transport. In addition, H_2S has also been found to regulate genes involved in aging, which in turn can lead to longevity by increasing the resistance to oxidative stress and overall stress resistance (Tabibzadeh, 2016). If these effects are solely due to the H_2S form and not influenced by the HS^- form, however, is unknown, as the studies only looked at the resulting changes in organisms after exposure to a sulfidic solution or environment. The studies did not go into detail about the ratio between H_2S and HS^- in their respective scenarios.

Sulfur-oxidizing bacteria (SOB) may also play a vital role in the various nutrient cycles (Hu et al., 2018). While marine heterotrophic bacteria release H_2S through organic sulfur decomposition (desulfurization) during the metabolism of organic matter, SOB can recycle the reduced sulfur back to its oxidized form through dissimilatory sulfur oxidation. Furthermore, magnetotactic bacteria contain cells that specialize in oxidizing sulfide to sulfate, which can later be reduced back to sulfide, and reducing nitrate to ammonium or nitrogen (Li et al., 2020). This process, along with their magnetotaxis behavior (ability to move using metabolic energy guided by geomagnetic fields) across the oxic-anoxic interface, make these bacteria efficient shuttles for carbon, nitrogen, sulfur, and iron.

Noteworthy is that large-scale hypoxia (low oxygen levels), and even anoxia, in the Baltic Sea is a reoccurring phenomenon (Conley et al., 2009). The Baltic Sea was in fact ranked second in 2020 as the most impacted area in terms of cultural eutrophication; defined as "increases in the supply of organic matter to an ecosystem that is fueled by anthropogenic inputs of inorganic nutrients where increases in organic matter are most often due to excess phytoplankton production" (Malone & Newton, 2020). The Chesapeake Bay (estuary) ranked first, with other highly affected areas being the northern Adriatic Sea (semi-enclosed marginal sea), the northern Gulf of Mexico (bay), and the Santa Barbara Channel (region) - all of which are influenced by multiple river discharges.

1.3 Motivation and Structure of Thesis

Monitoring of the marine environment is a good first step towards a healthy ecosystem; however, without a good understanding of all processes and their respective influences and dynamics this effort is of no vail. The complexity of the sulfur system is gradually becoming clearer, and the various forms of sulfur are beginning to demonstrate capabilities beyond mere toxicity. Therefore, it is crucial to obtain a better understanding of the extent of the sulfides in the marine environment, in order to untangle the mystery still surrounding these chemicals. However, classical wet-chemistry analysis procedures are slow and require both additional time and effort to provide this data, not to mention the relative low resolution. There is also an increased risk of human error in the handling of such measurements, both in the actual measurement phase and in the often manual recording of outputs. A solution for this predicament comes from the fast growing technology sector, and new autonomous instruments are continuously introduced to society. Still, not all solutions are yet reliable, and care needs to be taken when implementing any new technology into a larger system.

The aim of this thesis is to extend the knowledge of the location of total sulfides (total H_2S; H_2S_t) in the Baltic Sea using one such new technological development, namely the OPUS DS nitrate ultraviolet (UV) sensor (TriOS GmbH, Germany), hereafter referred to as OPUS sensor. However, since a variety of analytical methods have been found in the literature, a comprehensive investigation is first needed to determine the best method to use with this sensor in the Baltic Sea. Thus, the first part of the results chapter (**3.1**) focuses on method development for UV measurements in the Baltic Sea - specifically for the OPUS sensor. The second part of the results chapter (**3.2**) is dedicated to the investigation of the distribution of total H_2S along a transect from the Arkona Basin to the Eastern Gotland Basin using the high resolution OPUS measurements.

CHAPTER 2. MATERIALS AND METHOD

2.1 The Baltic Sea as a research area

The Baltic Sea has historically attracted significant attention due to its unique characteristics and geographic position. Both its structure and composition has changed tremendously since its formation around 13.5-13.0 ka BP (10^3 years before present); from being subjected to heavy sea ice and deposits of glacial varved clays giving a freshwater environment to for a short period allow marine water to enter the area in 10.0-9.9 ka BP allowing diatoms and mollusks to thrive, only to go back to a freshwater environment around 9.6-9.5 ka BP until ca. 8.0 ka BP when traces of marine influences were once again detectable (Björck, 1995). Today, this marginal sea has a unique water signature (Snoeijs-Leijonmalm & Andrén, 2017), with its several sills developed during the time of formation dividing the area into 11 basins (from Arkona Basin to the Bothnian Bay) and giving rise to drastic changes in water properties in both vertical and horizontal directions (HELCOM, 2023).

The input of freshwater (~660 km^3 / year) from river run-offs, precipitation, and other anthropogenic sources, along with inflows of highly saline waters (~475 km^3 / year) from the Kattegatt are two of the main driving forces of water circulation in the Baltic Sea today (as discussed by e.g. Björck (1995) and Lehmann et al. (2022)). The Arkona Basin is positioned in the south-western part of the Baltic Sea, where inflow of saline water from the Drogden and Darss Sills mix with the brackish water in this basin, forming a mixed upper layer and a saline bottom water (Lass & Mohrholz, 2003; Lass et al., 2005). The saline bottom water can form a central pool which discharges in to the Bornholm Basin through the Bornholm Gatt, resulting in a net flow in an eastward direction through the Bornholm Basin (Lehmann & Hinrichsen, 2003; Lass et al., 2005). Strong westerly winds, as well as major Baltic inflow events, drives saline water through both the Arkona Basin and the Bornholm Basin towards the Eastern Gotland Basin (Krauss & Brügge, 1991; Kuijpers et al., 2012). Since the Baltic Sea has many basins and low inter-circulation, it is stratified with a salinity between 5-8 down to ~100 meters and 8-12 below. The O_2 concentrations also vary over depth with an overall strong gradient around 75-100 meters, where it goes from ~7.75 to 0 ml/l. The Bornholm Basin and Gotland Basin are both areas with greater depths (≥ 90 m) where periods of stagnation occur. Organic matter mineralization can accumulate continuously due to stagnation, and will halt when there is a renewal event. Thus, the prerequisites of steady state are changed, and will only be fulfilled when concentrations and fluxes are averaged over decades (Schneider et al., 2017).

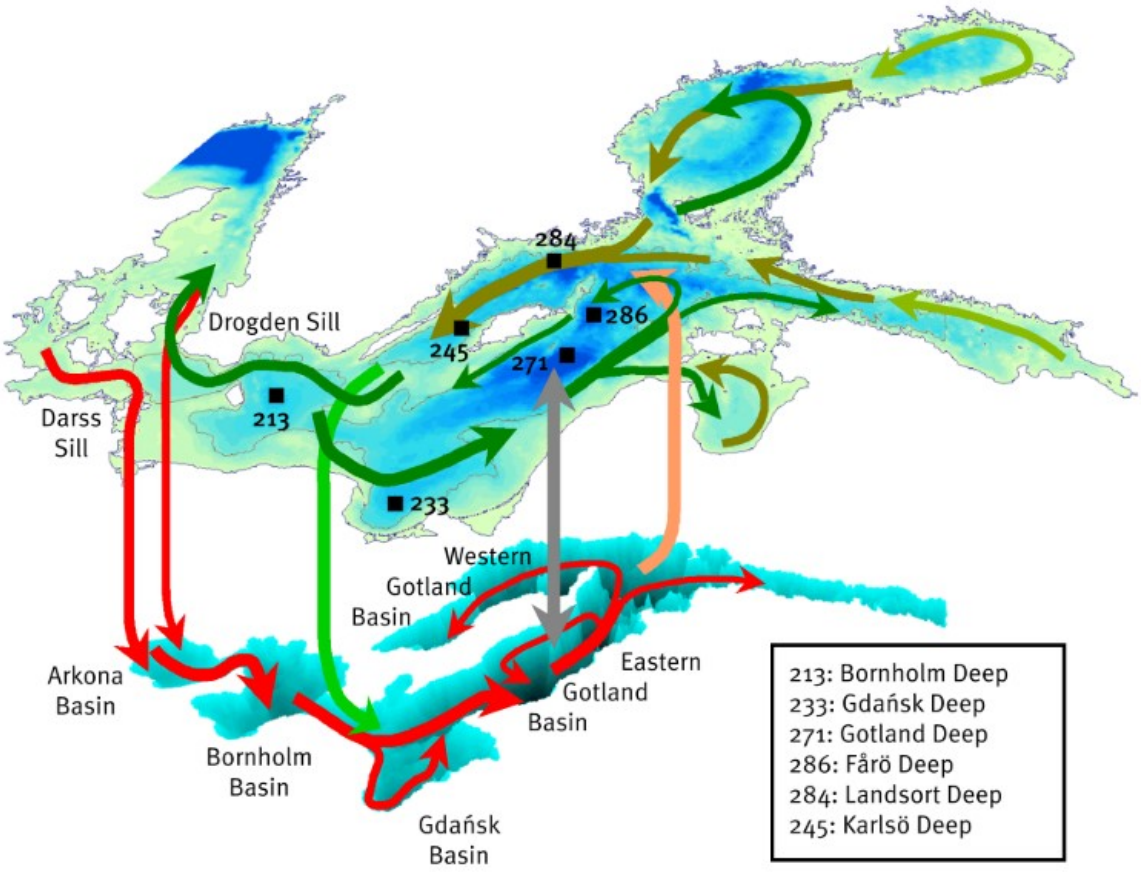

Figure 2.1. Map of the Baltic Sea including water circulation over the basins (modified by Feistel et al. (2016)).

Studies on the residence time in the Baltic Sea have shown that the age of the water masses varies greatly between basins and over decades due to the bathymetry and water circulation (**Figure 2.1**), as well as seasons, but can be estimated to have a median age of 1 year in the Arkona and Bornholm Basins, and 3 years in the Eastern Gotland Basin during the 20th century (e.g. Gustafsson, 2000; Meier, 2005).

Total H_2S concentrations in the Baltic Sea, here free H_2S & HS^-, can vary both over depth and area, up to 50 µM in the Bornholm Basin and 200 µM in the deeper parts of the Eastern Gotland Basin (this thesis). Indications of an increase since the 1920s has been addressed by Hopkins (2000), and as a response to increased anthropogenic impacts, the EU initiated a strategy called the Green Deal, which includes the older Marine Strategy Framework Directive (MSFD), to address the unfavorable state of the oceans (Commission, 2020). Since 2008, all member states were required to achieve, or maintain, 'good environmental status' within their marine waters by 2020, including the Baltic Sea, and special monitoring programs were deployed 2014 in order to observe and assess the progress (Commission, 2020).

HELCOM began coordination of chemical monitoring in the Baltic Sea already in 1979, however, this mainly contributed to "occasional production of theme-wise reports and periodical assessments of the state of the Baltic Sea" (HELCOM, 2013). Since the 1970's, many more conventions and directives have been adopted to improve the monitoring efforts (de Jonge et al., 2006; HELCOM, 2013), although with varying impact in the different Baltic Sea states (Hopkins, 2000). Despite this effort, little to no improvement in the status of the Baltic Sea has been recorded, and many indicators (e.g. eutrophication, number of seals, harbor porpoise, and water birds) do not reach a 'good' status (HELCOM, 2023). If this is solely due to poor environmental health, or if it is a mixture of monitoring results and the interpretation of such, is still debatable (de Jonge et al., 2006; Blackford et al., 2015).

In many areas, the baseline is unknown and monitoring efforts are often not put into perspective of the full system. In addition, Nygård et al. (2020) found in their study, that the distribution of monitoring programs may not give a representative picture of the status, as the sampling stations are unbalanced between habitats. **Figure 2.2** is a compilation of the resulting maps from Feistel et al. (2016), used to monitor the extent of the anoxic and hypoxic zones, along with rough estimations of the total H_2S concentration in the Baltic Sea. The maps use an extrapolation algorithm in order to estimate the extent of total H_2S, but are sensitive to loss of data points as they only consider the new input data. As mentioned by the authors, this may lead to different maps having different boundaries, which in the worst case can lose important information about the processes in the Baltic Sea involving the sulfur species. Nonetheless, these maps are in agreement with the probability maps for anoxic and hypoxic zones modeled by Kõuts et al. (2021).

Another aspect, which greatly influence total H_2S measurements, is pH, as higher acidity may cause instrument corrosion and can highly affect their performance. Sulfides are typically found in the deeper parts of the water column, where oxygen has been depleted, and according to data in Sharkweb, gathered by the Swedish Metrological and Hydrological Institute (https://sharkweb.smhi.se/hamta-data/), pH in the Baltic Sea varies between 7.2-8.8 in the upper 100 meters, and can go down to 7.1 below 100 meters. The resolution of pH data below 100 meters is limited, and often not higher than one measurement per 50 meters. Since the H_2S:HS^- ratio is partly influenced by the pH, this may be another problem for long-term and reliable high-resolution measurements in the Baltic Sea that take this variation into account.

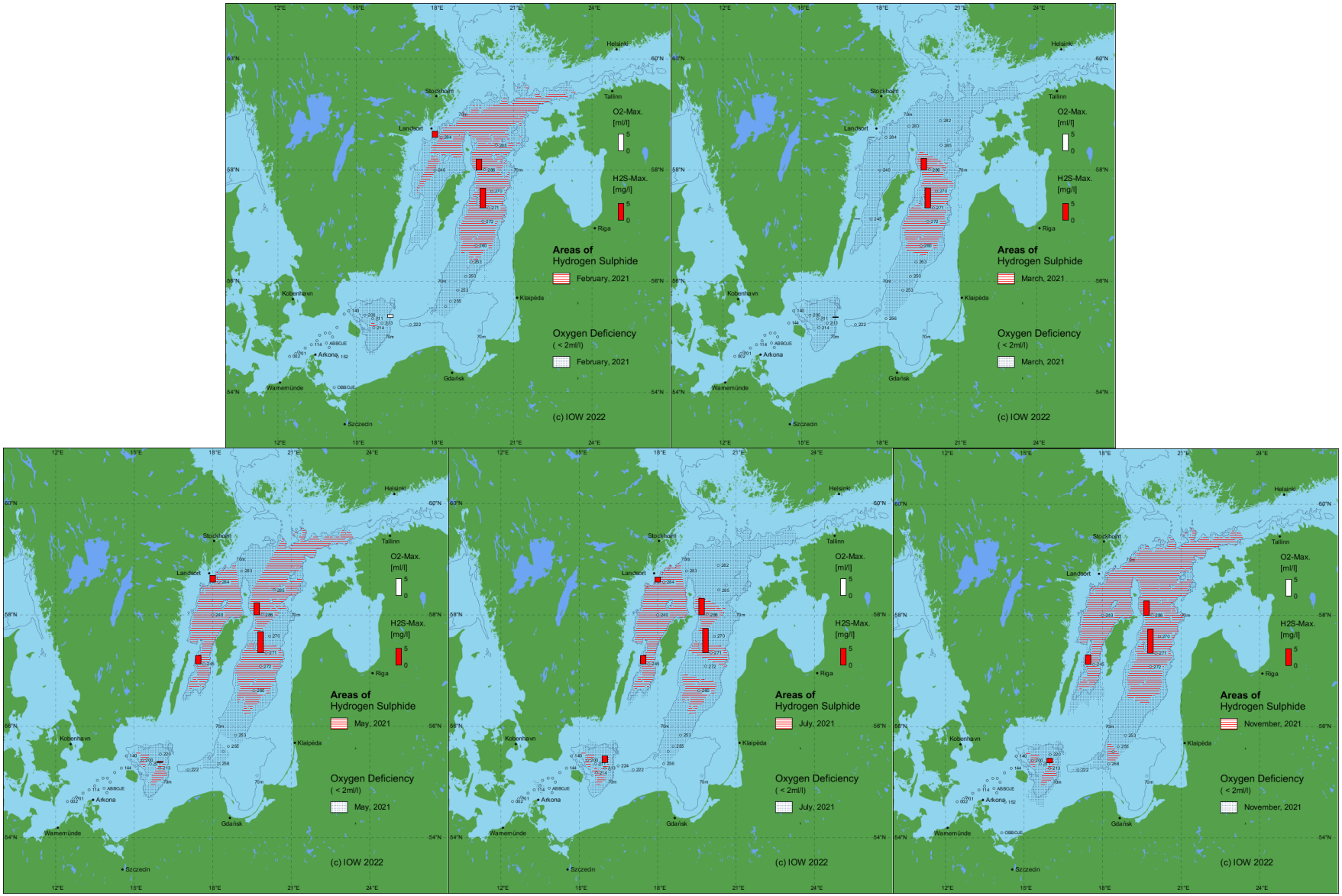

Figure 2.2. Estimated spread of total H_2S based on the control data, only considering geographical boundaries. For details see Feistel et al. (2016).

2.2 The OPUS sensor

Remote or self-operating UV/vis spectrophotometers are becoming more popular as they allow fast and extended *in-situ* measurements in nutrient monitoring applications. Many species of inorganic compounds have been found to be quantifiable through absorption spectra in the ultraviolet region (Addison et al., 1952; Armstrong & Boalch, 1961; Noto & Mecozzi, 1997). UV spectroscopy has since been used as a low cost, fast, and reliable approach to determine nitrate (Takeda & Fujiwara, 1993; Finch et al., 1998; Johnson & Coletti, 2002), sea salt characteristics (Noto & Mecozzi, 1997; Johnson & Coletti, 2002; Sakamoto et al., 2009), the presence of organic matter (Foster & Morris, 1971; Langergraber et al., 2003; Sakamoto et al., 2017; Meyer et al., 2018), as well as other inorganic compounds (such as thiosulfate ($S_2O_3^{2-}$) and iodide (I^-)) (Guenther et al., 2001) with satisfying results.

The OPUS sensor has been deemed well equipped for *in-situ* measurements in regards of the above mentioned compounds as it has gone through rigorous testing in the factory as well as in the field. This particular type of sensor has been on the market for some time (dating back to the ISUS sensor developed in early 2000's; (Johnson & Coletti, 2002)), with the mathematical approach to make use of the recorded data still under development. Most of these developments came from either laboratory tests or in combination with field data collected in the Pacific or Indian Ocean (Johnson & Coletti, 2002; Sakamoto et al., 2009; Poornima et al., 2016; Sakamoto et al., 2017; Plant et al., 2023), the Atlantic Ocean (Nehir et al., 2021), and Antarctica (Johnson et al., 2017), with few observations in the North Sea and Baltic Sea (Zielinski et al., 2011; Meyer et al., 2018; Nehir et al., 2021). However, the OPUS sensor has also been used in groundwater monitoring trials with reliable results (Burbery et al., 2021).

The OPUS sensor is designed with three main sections: (1) the outgoing light and reference diode section, (2) the 10 mm open path where the medium is measured, and (3) the receiving diode array on the other end (**Figure 2.3**).

The light from the xenon flash lamp in the first section is partially absorbed and/or scattered by molecules when it passes through the open path. The transmitted light can be used to verify what is present in a sample, as each molecule, or complex, has a unique extinction coefficient spectrum, i.e. a characteristic spectral absorbance that indicate the magnitude of absorbed or scattered light at any given spectral range. Thus, it is important to know which components may absorb in the range used. The extinction coefficient spectra of the components used in this thesis are shown in **Figure 2.4**.

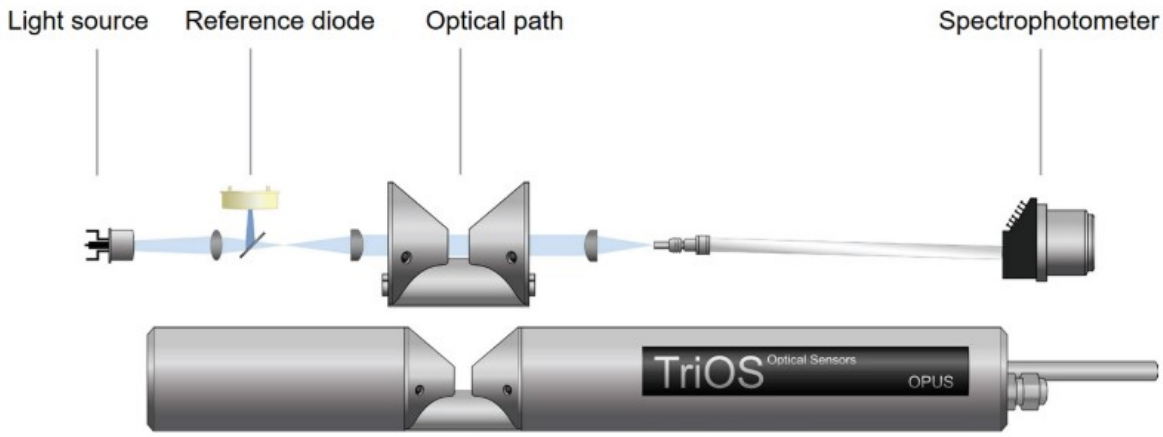

Figure 2.3. Sensor design as given by TriOS GmbH OPUS manual (2017), combined into one figure by Nehir et al. (2021).

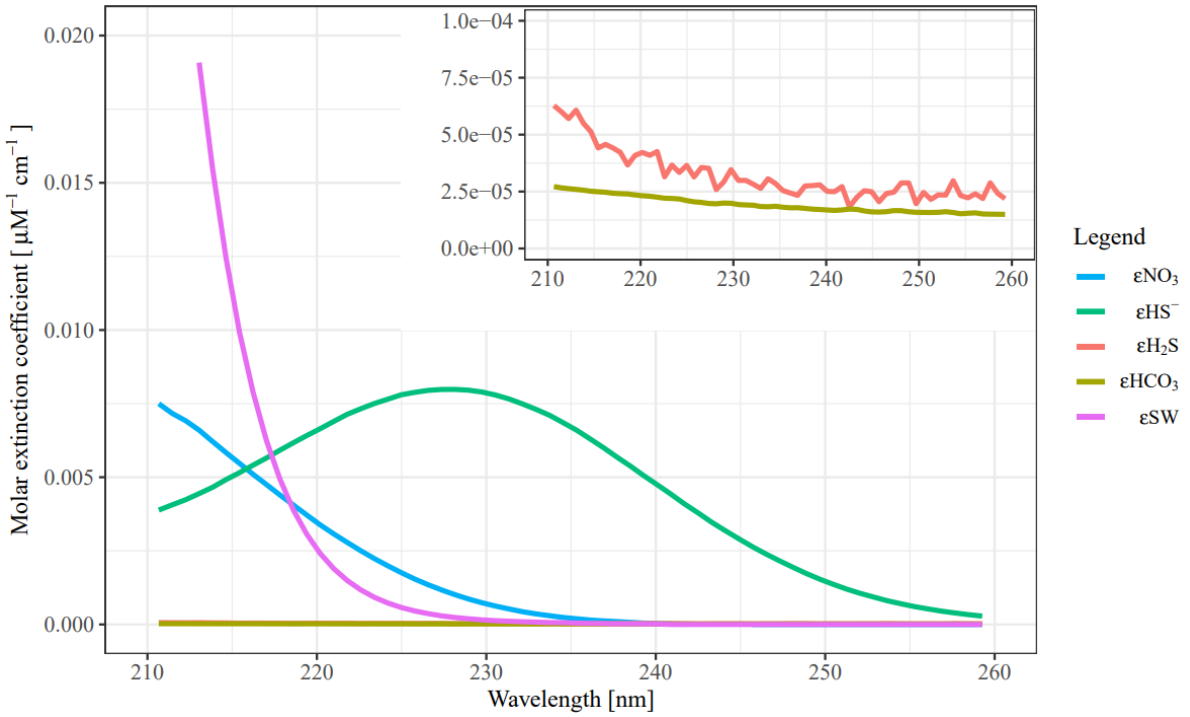

Figure 2.4. Extinction coefficient spectra (εsubstance) collected from laboratory calibrations. Details on calculations can be found in chapter **2.3.2**. Insert in top right corner shows ε_{H2St} and ε_{HCO3} at higher resolution. All spectra are per µM for a path length of 10 mm.

The intensity spectrum of the light that passed through the sample in the second section of the OPUS sensor is recorded by the detector in the third section. For the OPUS sensor, the detector, a high-end miniature spectrometer, contains a holographic grating as dispersive element and a 256-element linear photodiode array covering the wavelength range from 190 nm to 360 nm with a spacing of about 0.8 nm between elements. The resulting spectrum is called light spectrum, and is the sum of all transmitted light. However, detectors can be subjected to external influences such as dark current in the photodiode or scattered light, thus,

in order to remove such potential influences all light spectra intensities are corrected using intensities from a dark spectrum. In short, the dark spectrum indicates what the detector is sensing when no light is emitted from the light source of the instrument, and the intensities here should be small. The adjusted light spectra intensities can be converted to an absorbance value by using an ultrapure water-sample intensity spectrum as reference (**Figure 2.5**). The sample in the second section, which determines the resulting absorbance spectrum, can be either *in-situ* or calibration measurements of known solutions. By combining all known, and to some degree unknown (here termed background), spectra in a regression, it is possible to calculate their respective concentration by finding the combination of the components which

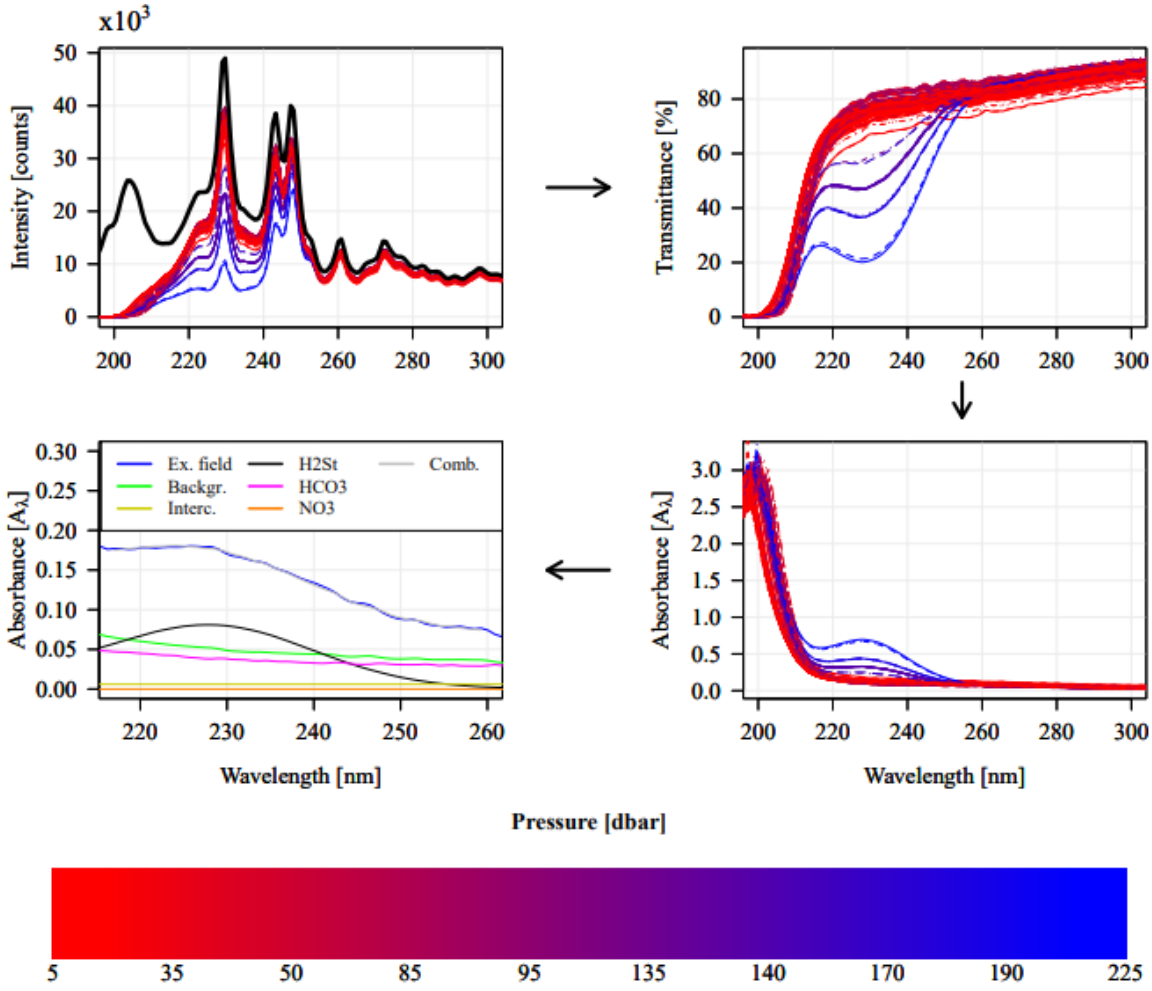

Figure 2.5. Schematic figure of data processing on a selection of the measurements from March 2021. Field measurements are plotted color coded from red (low pressure) to blue (high pressure – see color bar) by in situ pressure. Top left: Intensity spectra from field measurements compared to reference spectrum of pure MQ-water (black). Top right: Transmittance of light in percent for each field measurement. Higher percentages indicate that more light passed through the water. Bottom right: Calculated absorbance over the wavelength range. Bottom left: Example of regression result from a single field measurement (Ex. field) around 124 dbar. The combined spectra (Comb; grey) show how well the sum of all plotted absorbance (Background (Backg.) + Intercept (Interc.) + total H_2S (H2St) + HCO3 + NO3) fit to the field data (blue). The influence of salinity on the field sample has not been included in the representation. Note the limited wavelength range between 217-260 nm.

fits the *in-situ* measurements best (see section **2.3.2** for detailed equations). This generic processing allows reproducibility, and minimizes the influence of personal preferences when evaluating the data, as few constraints are put on the analytical process.

Although the OPUS sensor has a wide wavelength range, not all wavelengths will give clear outputs. It was reported by Johnson and Coletti (2002) that the xenon flash lamp used in the OPUS sensor gave varying intensities between 210-300 nm, and that the lamp had a relatively low intensity below 220 nm. It was also confirmed in the OPUS manual that if the absorbance at 210 nm or 360 nm exceeded 3 or 0.8, respectively, the measured values could become more uncertain as the signal-to-noise ratio becomes too low. In addition, both salinity concentrations and turbidity could potentially affect the readings if exceeding 1 and 200 NTU, respectively. A narrower path length is suggested for water with higher turbidities and/or salinities, as this may reduce the influence on the total absorbance, however, due to the proportionality between absorbance and path length, a shorter path length results in a lower absorbance, thus, components of low concentrations will be unfavored (Wenzel, 2024).

One of the more challenging aspects of using this type of sensor is that the measurements are made *in-situ* , meaning that the samples are not filtered or under the influence of reagents that may bind unwanted compounds to reduce background noise. The background noise is caused by substances that are either unknown or that may only contribute to the scatter of light but do not absorb in this range. Both linear (λ) and quadratic ($\lambda + \lambda^2$) regressions have been proposed for such corrections (Johnson & Coletti, 2002; Johnson et al., 2006; Sakamoto et al., 2009; Nehir et al., 2021), and Frank et al. (2014) concluded in their work on the southern North Sea that a quadratic regression parameter may be most accurate to account for colored dissolved organic matter (CDOM). Meyer et al. (2018), who did a study in the Baltic Sea, included a 4th order polynomial (λ^{-4}) instead, to account for CDOM and scatter due to particles as well as other substances. Since many ocean properties differ between various basins, part one of this thesis will investigate which of these representations of background signals function the best in the Baltic Sea. In addition, a fourth method for background correction is introduced here, namely a derived spectrum where all known components have been subtracted, only to leave the structure of the unknown. **Figure 2.6** is a visual representation of all four background spectra, where it is also visible to see the difference between the derived spectra from all cruises from the fourth method. By principle, if one can account for all parameters in a mixture, it should not matter where the mixture originated from. This should be applicable also for the OPUS sensor, however, only field tests can verify this, and only direct comparisons of the various methods proposed will indicate which method is supreme in the Baltic Sea.

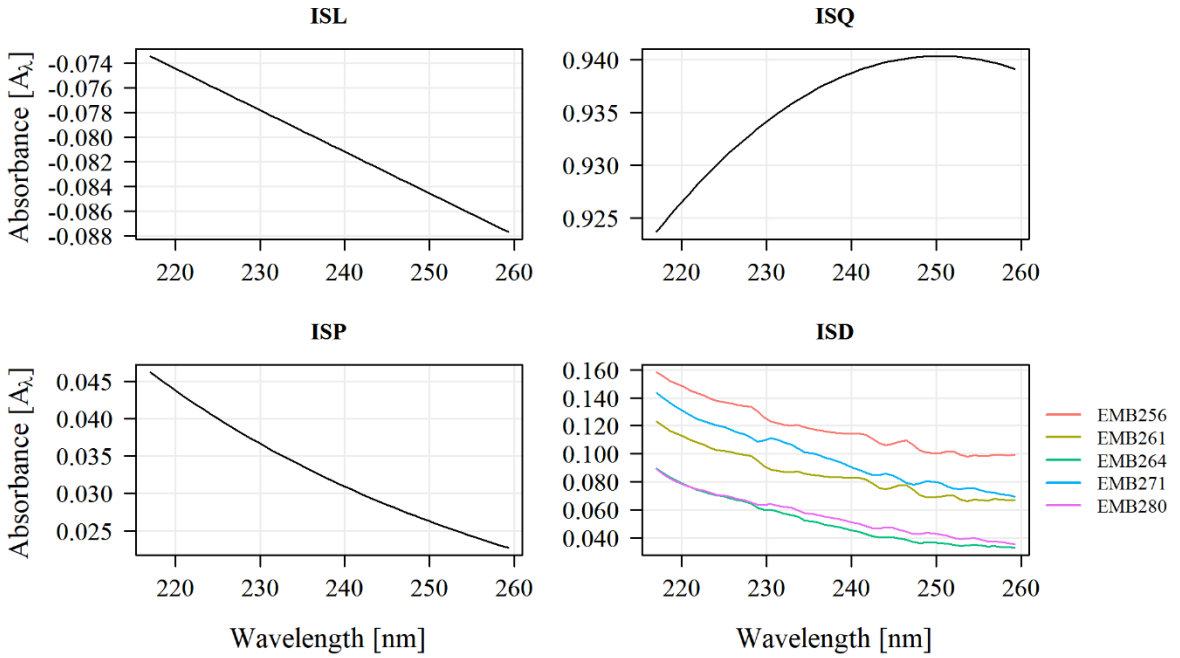

Figure 2.6. Absorbance spectra (from regression equation 2.13: $abs_{rest,\lambda}$) highlighting the difference between investigated background spectra. ISL is a linear, ISQ is a quadratic, ISP is a poly-4, and ISD is a derived *in-situ* background spectrum. A sample from station TF0214 at 91 m was used to adjust all spectra. The sample was taken in January, thus the ISD spectrum from EMB256 was used in the regression. The inclusion of all derived spectra in the ISD figure here is meant to show how all derived background spectra differ.

The OPUS sensor was attached vertically to the CTD rosette onboard the R/V Elisabeth Mann Borgese (**Figure 2.7**) and ran continuously with an average of four seconds per logged measurement. Longer measurement times were needed where intensities were low, thus requiring additional flashes from the light source to reach a satisfying light spectrum intensity. In most cases, however, no more than two flashes were needed. In May, e.g., 92.7% of the measurements were taken with only one flash, the rest with two flashes. In July, 60.7% of the measurements required one flash, while 39% needed two. The remaining 0.3% was satisfied with three flashes. No pattern could be found where more flashes was needed.

As the quickest built-in automatic triggering function for continuous measurements is ≥ 10 seconds, a remote desktop was connected to the OPUS sensor via the CTD-rig, and was used to trigger measurements at a faster pace. The remote desktop would poll the sensor 2.5 times/second to attempt a new measurement. Every 10th measurement was set to calibration where a dark measurement was also collected. No corrections were applied on these before storing on the OPUS internal memory. After extracting stored data, the total absorbance was calculated using a MQ background spectrum collected in the lab as reference (details in section **2.3.2**). The OPUS sensor was operating on 12 V.

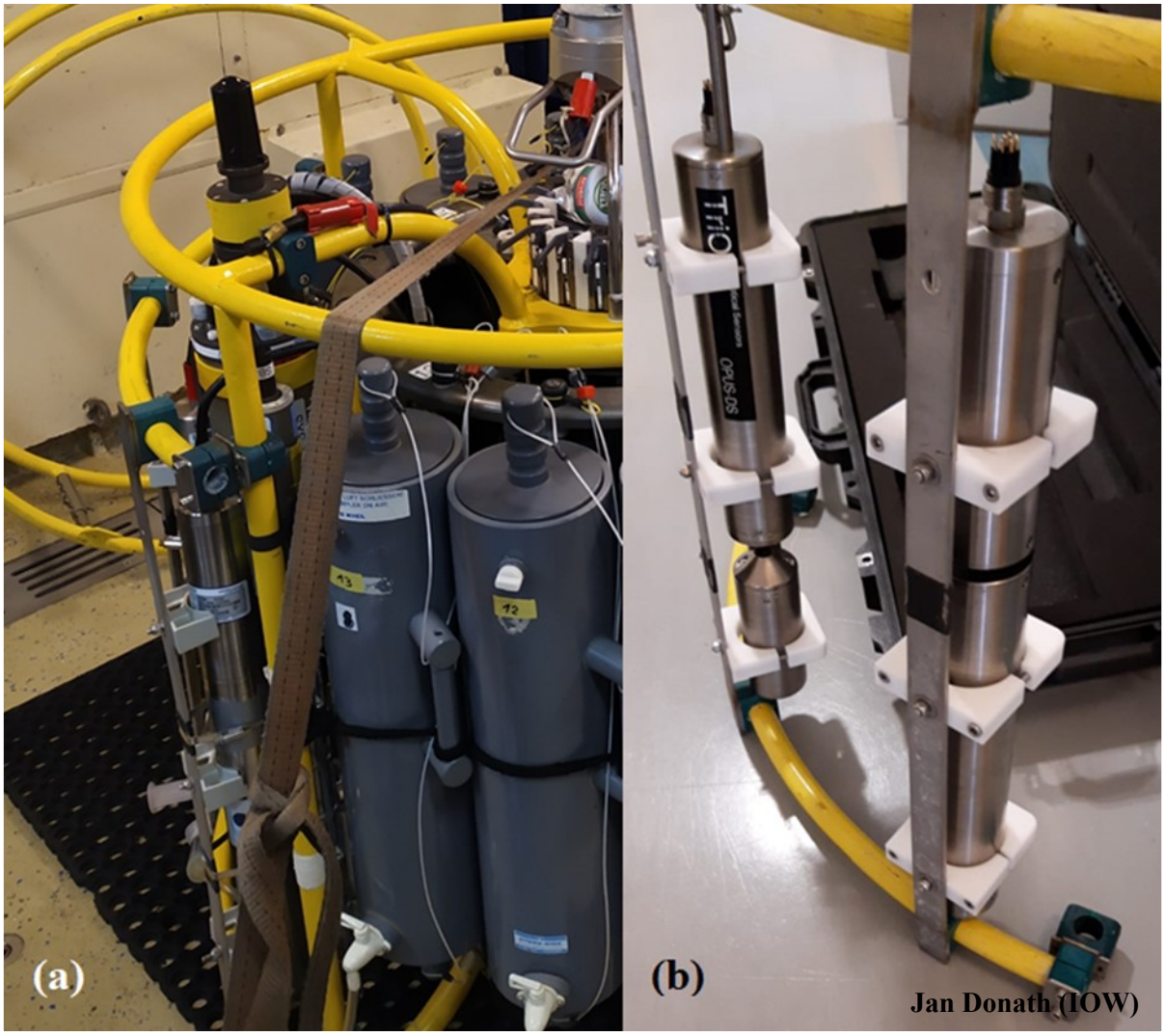

Figure 2.7. The OPUS sensor mounted on the CTD-rosette-rig onboard R/V Elisabeth Mann Borgese (EMB).

2.3 Data acquisition and processing

2.3.1 Cruises and laboratory data

In-situ field data

Five cruises with R/V Elisabeth Mann Borgese (EMB) were conducted two to three months apart in 2021. The cruises were part of a monitoring program at Leibniz Institute for Baltic Sea Research – Warnemünde, which had the advantage of following the same cruise track and the availability of certified accompanying control data, such as oxygen and total H2S measurements. (**Figure 2.8**, **Table 2.1**). The data was collected in forms of profiles from the surface down to the sea floor. The maximum depth was ca. 119 m, which is well within the limit of the OPUS sensor at ca. 600 m. The control data, here wet chemistry analyzed Niskin-bottle samples, was not always collected on the same stations for all cruises. Furthermore, bad weather conditions also reduced the number of monitoring stations for some cruises, thus, the

number of control measurements varied between the cruises (total of 24-33 measurements per cruise; see **Table 2.1**).

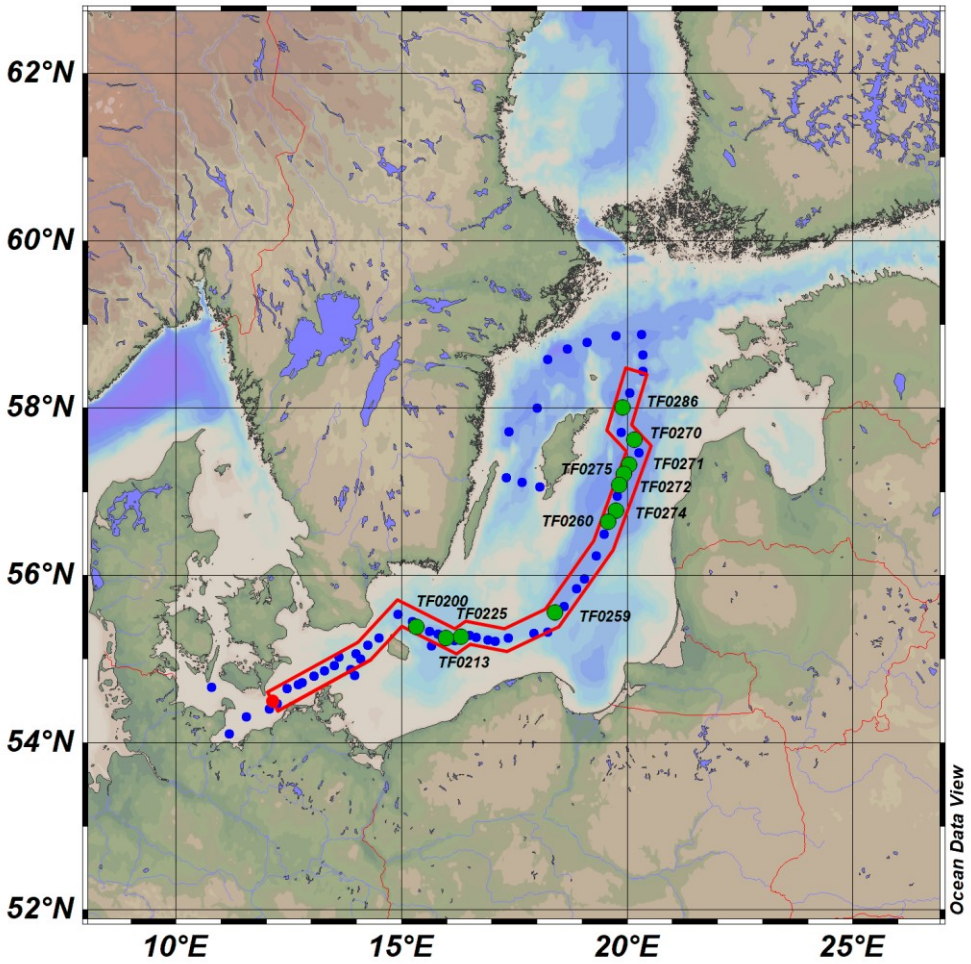

Figure 2.8. Station map with the total number of control stations in green. Not all cruises had control measurements at all stations. Red area determined the transect limits.

Table 2.1. Cruise times and the total number of unique observations from each cruise. The number of observations include values below limit of detection (LOD). The number of OPUS measurements were averaged per control in chapter **3.1** to get a homogenous data set (see details in section **2.3.3**).

Cruise	Time (day and month in 2021)	N observations used in chapter 3.1		N observations used in chapter 3.2
		Control	OPUS	OPUS
EMB256	25.01-05.02	24	67	6 293
EMB261	18.03-30.03	27	71	6 333
EMB264	04.05-14.05	29	70	4 048
EMB271	20.07-29.07	26	97	4 007
EMB280	04.11-15.11	33	96	3 545

All control measurements were carried out on-board the ship immediately after sample collection from the Niskin bottles attached to the CTD rosette. Nutrient measurements (NO_3 and total H_2S) were taken following the standard procedure described in DIN EN ISO/IEC 17025 (IOW procedures) using a FlowSys Nutrients Autoanalyzer from Alliance Instruments (NO_3, SD = ± 0.36 µM) and a Shimadzu UV mini 1240 photometer (total H_2S, SD = ± 1.52 µM). Since the volume taken from the Niskin bottle before sample extraction is unknown, a buffer depth of ± 1 m from the recorded bottle depth was applied to all control samples. This allowed a match to OPUS measurement that might have been taken on water collected in the very top or bottom of the bottle. In addition, the 1 m limit allowed a match between control and OPUS data which might, theoretically, be outside of the bottle volume depth range, but taken on the exact same cast. It was deemed that these measurements had higher likelihood to be more similar to the controls than OPUS measurements taken within the theoretical bottle volume depth range but on a different cast. This range limit also reduces the risk of control measurements being lost due to the unfortunate occurrence of a dark measurement (used for noise reduction) which could result in the OPUS resolution to decrease.

Laboratory calibrations for the OPUS sensor

Calibrations were conducted in order to acquire an extinction coefficient spectrum for nitrate, hydrogen sulfide, bisulfide, and salinity. The extinction coefficient for bicarbonate was taken from Meyer et al. (2018). Calibrations procured through sensors other than the OPUS sensor used for field measurements were linearly interpolated to the wavelengths of this sensor.

Milli-Q (MQ; Merck Milli-Q® Reference) reference spectra were taken in conjugation with the calibrations. The MQ spectrum taken closest to the cruise was used for background correction, except for the November data when MQ from February the following year was used. **Figure 2.9** shows the collected MQ spectra and the variance seen between occasions. An absorbance normalization between MQ measurements was done by using the measurement from June 2021 as reference. The measurements taken over three consecutive days in March 2021 are consistent with each other, but differ from the other measurements.

Low nutrient Atlantic seawater (SW, < 1µM of nutrients), salinity 35, (OSIL, UK) was used to obtain the seawater extinction coefficient (ε_{SW}). A 23.738 µM nitrate (NO_3) solution for ε_{NO3} was prepared by solving 2.4 mg KNO_3 in 1 L MQ-water. Both solutions were measured with the OPUS DS nitrate sensor using a glass measuring cup. The cup was cleaned three times with MQ-water and once with solution before each measurement. The solution was measured for five minutes to test for any drift in data.

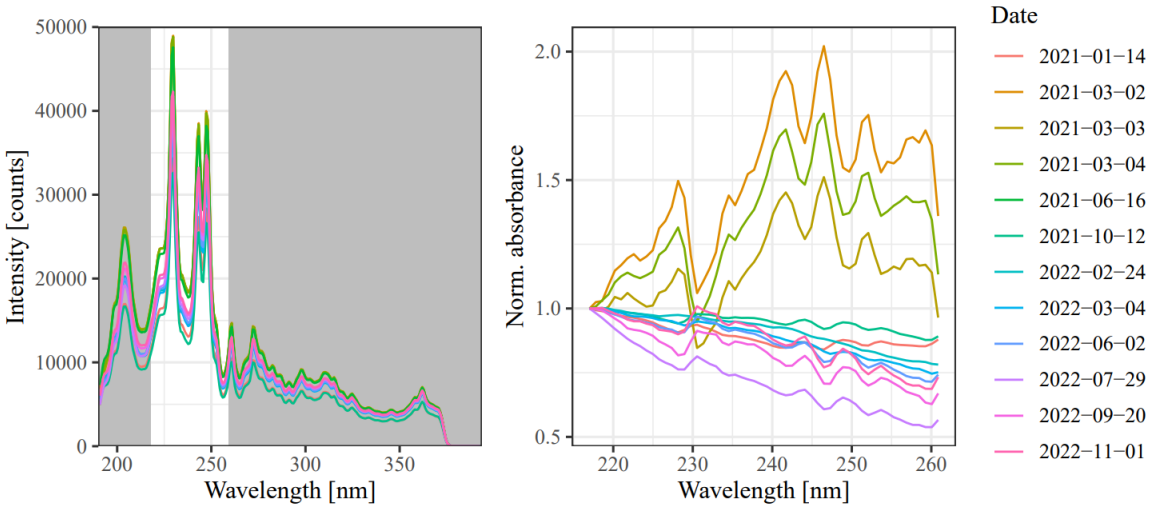

Figure 2.9. Intensity variations from MQ measurements. Left: full range MQ spectra from measurements in 2021 and 2022. Grey area is outside the used spectral range. Right: Normalized absorbance to wavelength 217 nm using a measurement from 2021-06-16 as reference for intensity conversion (see chapter **2.3.2** for details). This highlights the difference between the spectra over their wavelength range and time.

Hydrogen sulfide (H_2S) and bisulfide (HS^-) were prepared in anoxic solutions and measured with a Shimadzu UV mini 1240 photometer, following Grashoff et al. (1983). The half-life of H_2S has been determined to be approximately 20 minutes in seawater (Avrahami & Golding, 1968), or as low as a few minutes when the ratio between dissolved O_2 (DO) and H_2S is above one (Siang et al., 2017). Due to the rapid oxidation rates of the sulfide ions, it is important to take the amount of DO in the solutions used into particular consideration. It is also important to keep the solutions from becoming exposed to air for a prolonged time, as oxygen from the air easily diffuses into the solution. Deionized water used in most experiments can have DO of up to 8.8 ml/l. Thus, it is important to degas the dilution solution (often MQ-water) before mixing the sulfide solution. However, it is not as important to degas pH buffers or adjusters if a higher sulfide concentration is used, as the overall added volume is low. It is noteworthy to remember the half-life of H_2S when conducting the experiments.

Using Iron-III and p-Aminodimethylaniline for catalytic and oxidizing effects on the H_2S species, the intermediate indammonium salt condense with H_2S to form a thiazine dye, which was subsequently determined colorimetrically. Oxygen (O_2) free MQ-water for solution dilution was prepared by bubbling nitrogen (N_2) gas while heated to 100 °C for 40 minutes. N_2-gas was continuously bubbling while the MQ-water cooled down to the working temperature 22.3 and 22.7 °C (HS^- and H_2S, respectively). All glass bottles used to prepare the solutions were initially filled with argon (Ar) gas to reduce the oxidation rate. The solutions were then prepared by dissolving 0.15 g Na_2S*9H_2O in 200 ml O_2-free MQ water. A 1:10

working solution was prepared for each of the two substances and did not stand for more than 30 minutes before further use. A new working solution was prepared if this time limit was exceeded. The final solution was prepared by diluting 60 ml working solution to 200 ml with O_2-free MQ water. The pH value of this solution was 9.5 (HS^-), and to measure H_2S 10 ml 0.02 M HCl was added to adjust the pH to 4.7. To remove the influence of the HCl on the H_2S spectrum, a MQ solution with the same HCl addition (10 ml 0.02 M) was used. Thus, instead of using a pure MQ spectrum for correction, the H_2S spectrum was corrected on a mixture with HCl. The Grashoff et al. (1983) method (DIN EN ISO/IEC 17025; IOW procedures) was used to determine the final total H_2S concentration, here accounting for all sulfide species (H_2S, HS^-, S^{2-}, and complexes thereof). The concentration HS^- and H_2S was derived from total H_2S (H_2S_t) using the rate constant equation from Millero (1986) and the Henderson-Hasselbalch equation to account for the ratio (*f*) H_2S:HS^- (equation **2.9**-**2.11**). Since the Grashoff method gives concentrations in mg/L, the respective substances concentrations were converted to µM via:

$$[x]\ (\mu M) = (1 - f_x) \cdot \frac{[H_2S_t]\ (mg/L)}{M_x\ (g/mol)} \cdot 10^3 \qquad 2.1$$

where *x* is either H_2S or HS^-. The final calibration concentration was 84.67 µM for HS^- and 74.45 µM for H_2S.

Each solution was measured for at least five minutes, or a duration giving a minimum of 15 spectra. These were used to evaluate if there was any inconsistency in measured intensity over time. If inconsistencies were found, a new calibration was done or, if reasonable causes could be assumed (e.g. through visual inspection), the most appropriate measurements were used.

2.3.2 General processing approach from literature

This section presents the data processing steps that were derived from literature. The equations presented here were utilized to process both laboratory and field data. A general schematic proceeding on field data can be found in **Figure 2.5**, section **2.2**.

Acquired sensor data were converted from intensity over wavelength (Int_λ) to absorbance over wavelength (A_λ) using the negative decadic logarithm of the intensity divided by a clean reference spectrum over wavelength using MQ-water ($Int_{0,\lambda}$). The intensities were adjusted on their respective dark current measurement ($Int_{\lambda,D}$ and $Int_{0,\lambda,D}$):

$$A_\lambda = -\log_{10}\left(\frac{Int_\lambda - Int_{\lambda,D}}{Int_{0,\lambda} - Int_{0,\lambda,D}}\right)$$

2.2

A set of spectra of known contributors to the absorbance within the used wavelength range were measured in the lab in order to obtain the absorbance of each chemical per unit. These molar extinction coefficients were calculated through the Beer-Lambert law:

$$\varepsilon_{\lambda,Tcal} = \frac{A_\lambda}{l \cdot c}$$

2.3

where A_λ is the absorbance at wavelength λ (nm), l is the path length in cm and c is the sample concentration in μM.

It was found that bromide, one of the components with high absorbance in the lower wavelengths region and a major contributor to the salinity profile, is influenced by physical factors, such as temperature and pressure. Total absorbance, $A_{\lambda,field\ data}$ (equation **2.2**), was thus corrected for salinity influences by first calculating the molar *in-situ* seawater extinction coefficient ($\varepsilon_{SW,\lambda,Tis}$) following the steps from Sakamoto et al. (2009):

$$\varepsilon_{SW,\lambda,T_{is}} = \frac{\varepsilon_{SW,\lambda,T_{cal}} \cdot ASW_{(\lambda,T_{is})}}{ASW_{(\lambda,T_{cal})}}$$

2.4

where $\varepsilon_{SW,\lambda,T_{cal}}$ is derived from Beer-Lambert's law (equation **2.3**) at calibration temperature, and *ASW* is temperature (*T*, in °C) corrected sea water absorbance; derived using the following equation with *in-situ* temperature (T_{is}) and calibration temperature (T_{cal}):

$$ASW_{(\lambda,T)} = (A + B \cdot T) \cdot e^{(C+D\cdot T)\cdot W_\lambda}$$

2.5

W is a function of λ and a scaling parameter of [wavelength – 210 nm]. A, B, C, and D are constants derived from resultant regression parameters, and are 1.1500276, 0.02840, –0.3101349, and 0.001222, respectively.

To account for the pressure dependency found by de Fommervault et al. (2015), the improved pressure correction suggested by Sakamoto et al. (2017) was applied through:

$$\varepsilon_{SW,\lambda,p} = \varepsilon_{SW,\lambda,Tis} \cdot \left(1 - \frac{0.026 \cdot pressure\ [dbar]}{1000}\right)$$

2.6

where pressure is the *in-situ* pressure for each field measurement. The salinity absorbance ($SW_{abs,p}$) for each field measurement could thus be calculated using $\varepsilon_{SW,\lambda,p}$ with the corresponding CTD salinity ($S_{CTD,p}$; equation **2.7**). This was subsequently subtracted from the total absorbance measured (equation **2.8**). In addition, a bicarbonate (HCO_3) spectrum was also subtracted following the recommendations of Meyer et al. (2018) using a depth-dependent fraction of the concentration 1615 µM (equation **2.8**, $f_{HCO3,p}$ = 1 at p < 60 dbar, 1.1 at p = 60-80 dbar, and 1.2 at p > 80 dbar). The remaining absorbance ($abs_{rem,\lambda}$) was used in equation **2.13**.

$$SW_{abs,p} = \varepsilon_{SW,\lambda,p} \cdot S_{CTD,p} \tag{2.7}$$

$$abs_{rem,\lambda} = abs_{total,\lambda} - SW_{abs,p} - (\varepsilon_{HCO3,\lambda} \cdot [HCO_3] \cdot f_{HCO3,p}) \tag{2.8}$$

Calculating the total sulfide concentration in the field data (total H_2S) was done by combining the species-specific extinction coefficient spectra (here HS^- and H_2S) to a total sulfide extinction coefficient spectrum (equations **2.11** and **2.12**). Millero et al. (1988) published a set of equations regarding the ratio between HS^- and H_2S depending on salinity, temperature, and pH. Since there is a very small absorbance of H_2S within our wavelength region (**Figure 2.4**), it is important to adjust the total sulfide extinction coefficient spectrum accordingly. The dissociation constant of H_2S was calculated through:

$$pK_1 = -98.080 + \frac{5765.4}{T} + 15.0455 \cdot \ln(T) \tag{2.9}$$

$$pK_1^* = pK_1 + AS^{1/2} + BS \tag{2.10}$$

where *T* is temperature in Kelvin, *S* is salinity, and *A* and *B* are constants of values -0.1570 and 0.0135, respectively when using pH on total scale (Millero et al., 1988). The ratio H_2S: HS^- was calculated by:

$$f = 10^{-(pH - pK_1^*)} \tag{2.11}$$

where pH is on total scale.

The combined total H_2S extinction coefficient spectrum was thus calculated via the derived equation:

$$\varepsilon_{H2St,\lambda} = \frac{\varepsilon_{HS-} + f \cdot \varepsilon_{H2S}}{1 + f} \quad 2.12$$

where ε_{HS-} is the extinction coefficient spectrum for bisulfide and ε_{H2S} is the extinction coefficient spectrum for hydrogen sulfide calculated with equation **2.3**.

Nitrate and total sulfide concentrations were derived using a simple linear (lm) regression with the format:

$$abs_{rem,\lambda} = \varepsilon_{NO3,\lambda} \cdot c_{NO3} + \varepsilon_{H2St,\lambda} \cdot c_{H2St} + abs_{rest,\lambda} + I \quad 2.13$$

where I is the intercept, $\varepsilon_{x,\lambda}$ is the extinction coefficient spectrum for substance x over waveleng th λ, c_x is the fitted concentration of substance x, and abs_{rest} is the background correction term (see chapter **3.1.1** for details). The term abs_{rest} changes depending on the correction used, and can be expressed as $a \cdot \lambda$ for linear correction, $a \cdot \lambda + b \cdot \lambda^2$ for quadratic correction, $a \cdot \lambda^{-4}$ for poly-4 correction, and $a \cdot abs_{\text{derived}}$ for derived correction, with a and b as the coefficients being fitted.

2.3.3 Processing laboratory measurements and *in-situ* field data

All solutions measured in the laboratory and used for calibration were post-processed using equations **2.2** and **2.3**. The hydrogen sulfide and bisulfide spectra were shifted by 2 nm on the wavelength axis as the characteristic peak from bisulfide was offset to all field and other control data. This offset is believed to be due to a setup error of the UV spectrometer or during transfer of data in text format, allowing this correction to be made. The calibrations' success was partially verified by investigating the precision of repeated measurements. Since the mean contribution was used as the extinction coefficient, a low precision could result in a poorly representing spectrum. The SD was determined based on the variance of these measurements. The SD was within reasonable bounds for nitrate (KNO_3; 0.63 µM), low nutrient sea water for salinity determination (0.28), and HS^- (0.16 µM). Higher SD was found for H_2S (5.1 µM), which may have an effect on the combined spectrum output used as extinction coefficient for the OPUS sensor. A comparison between field and lab derived SD was made in chapter **3.1.2** to see if the SD from the two individual sulfide spectra could influence their combined spectrum.

The OPUS timestamp differed from the CTD timestamp at initialization for the first two cruises. The real-time clock of the OPUS sensor was set by a different computer than that

for the CTD data recording when the instrument was calibrated. Thus, a separate program was used to update the OPUS clock on-board the EMB; however, small differences could still be detected. To match the profiles from the two data files accurately, a temporary salinity was calculated from the OPUS data to be used as a matching criterion when combining the data. The temporary salinity was calculated using equations **2.2** to **2.7** described in chapter **2.3.2**. An average *in-situ* temperature for each cruise was used to calculate $ASW_{(\lambda,Tis)}$ (equation **2.4**). The resulting theoretical salinity profile from the OPUS sensor was fitted to the CTD salinity using a simple linear fit over a select time span, allowing checks on both positive and negative time adjustments. The matching of the two salinity profiles was initially done on all cruise data simultaneously, allowing for hourly corrections if needed. Once all stations were overlapping, another match was done for each station separately, allowing for minutes to seconds corrections in the case of drift in the OPUS clock due to the system being turned on and off repeatedly. Since the CTD data used for post-processing had measurements every second (average descent rate ca. 0.25 m/s) and the OPUS sensor was recording measurements approximately every four seconds, the resulting resolution for the matched data was around 1 m. The data used in the result sections **3.1.2** and **3.1.3** include OPUS measurements that were a maximum of ± 1 m from the recorded control data depth, obtained from the same CTD cast as controls were collected on. If multiple casts were taken in order to collect the control data, the time recorded for the control measurement was used to determine which of the CTD casts to use, giving priority to the cast closest to the time of the control. If more than one OPUS measurement was matched to the control data, these would be averaged before any further analysis.

Values for pH and alkalinity were collected from the SMHI Sharkweb database (https://sharkweb.smhi.se/hamta-data/) and matched to the present data based on shortest geographical distance and smallest density profile difference for each cruise, separately. The pH values were originally on the National Bureau of Standards (NBS) scale with a standard deviation of ± 0.06, which – when applied – had the largest impact on the ratio H_2S:HS^- at the chemocline (up to 22% difference between -0.06 and 0.06 pH adjustment), where strong gradients in temperature and salinity were observed (see also section **3.1.2**). With the accompanying alkalinity data as well as *in-situ* temperature, salinity, and pressure, the NBS-scale was recalculated to the total proton scale using CO2SYS in Octave. No further regard was taken to the NBS-scale standard deviation (SD) from this point on. Converted pH values to ratio H_2S:HS^- (*f*) using equations **2.9** to **2.11** have been plotted in **Figure 2.10**.

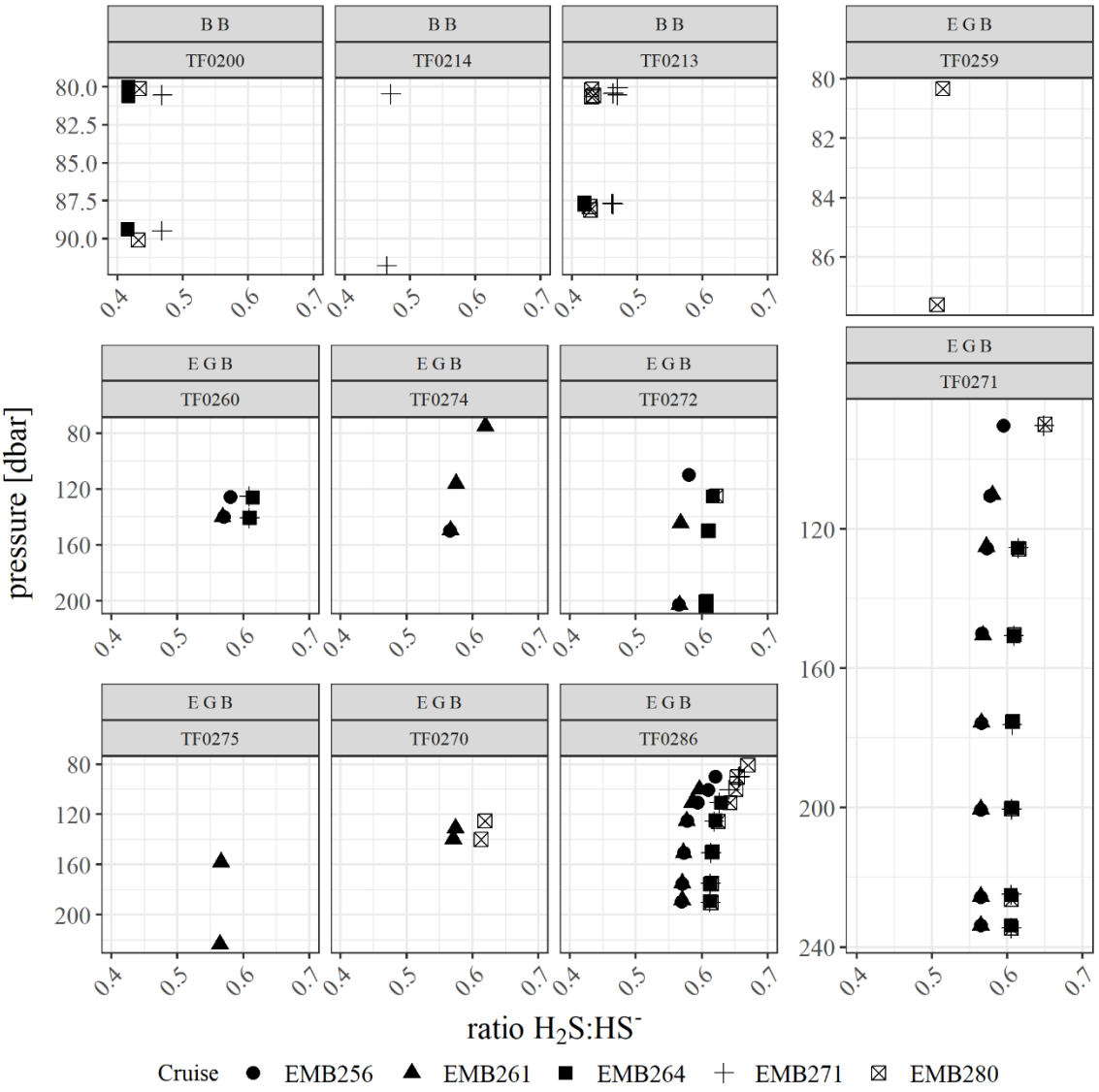

Figure 2.10. Calculated ratio H_2S to HS^- in 2021 for OPUS measurements with matching wet chemistry control data (used in section **3.1**). The ratio H_2S to HS^- increases in a northward direction, and is either stable or decreasing with depth. Variations throughout the water column and seasons can be above 10%. BB = Bornholm Basin, EGB = Eastern Gotland Basin.

All field data prepared for any regression analysis were processed using equations **2.2** to **2.13**. A check on the distribution of field data, presumed to represent the blank and/or where the signal-to-noise was presumed high (here upper 20 m of the water column), indicated that the data was not normally distributed. This could happen if the water mass measured changes or if the sensor gives a skewed output. Therefore, the estimated limit of detection (LOD) for OPUS measurements was determined through the partially non-parametric equation described by Linnet and Kondratovich (2004):

$$LOD_{est} = LOB_{est} + \frac{z_{1-\beta}}{1 - \frac{1}{4 \cdot df}} \cdot SD_s \qquad 2.14$$

where LOB_{est} is the estimated blank value, $z_{1-\beta}$ is the $1-\beta$ percentile of the standard Gaussian distribution, *df* is the degrees of freedom, and SD_s is the sample standard deviation. The SD_s and LOB_{est} were calculated using field measurements (at reasonable concentrations and in the upper 20 m of the water column, respectively) when the CTD was still in the water column. The LOB_{est} was determined as the 95th percentile of the observed concentrations when ranked by size. To determine the SD_s, all samples with repeated measurements were pooled, and an estimate was calculated as the weighted average of the sample variances. The *df* was calculated as $\text{sample size} \cdot (\text{replicate size} - 1)$. A power ($\beta$-value) of 95% gave a sensitivity ($z_{1-\beta}$) of 1.645. For control total H_2S, the standard deviation (1.52 µM) and LOD (2.36 µM) found during lab calibration was used. The OPUS LOD along with the corresponding *df* can be found in **Table 3.1**, section **3.1.2**, and **Table 3.4**, section **3.1.3**.

Two approaches were used when analyzing the field data depending on the background method used. 1) In the case where the empirical background spectra (linear, quadratic, or poly-4) were applied, all field data with accompanying control measurements were used (unless otherwise stated). 2) For analysis using a derived background spectrum, field data from the oxic zone with matching control data were initially divided 70:30 into training and test data, respectively. The training data was used to derive the 'rest' absorbance while the test data was used to verify the outcome in the result section. Thus, the test data included all measurements with corresponding control total H_2S and fewer measurements from the upper water column. The background spectrum (abs_{rest}) was derived by subtracting the salinity and HCO_3 absorbance, calculated with equations **2.3** to **2.8**, and the nitrate absorbance, calculated with our calibration spectrum and control data, for each month. Areas with total sulfide were excluded due to the low number of control measurements.

2.3.4 Statistical approaches and data visualization

The Kruskal-Wallis rank sum test was used to examine whether the methods investigated in chapter **3.1** differed. This test is capable of managing both non-parametric data and groups of data of varying sizes, while also being more robust against outliers. It functions on a ranking system instead of the actual values, i.e. it reorganizes all data from the various groups (here methods) from small to big and allocate a number sequence to the whole data set, and compare these to the χ^2 distribution (Kruskal & Wallis, 1952). This is ideal for the data presented in this thesis as the derived background method (ISD) has a reduced number of measurements due to the derived background spectrum.

The Kruskal-Wallis rank sum test can, however, not tell which group of data differ, if more than one is compared. This test will only be able to answer the question if samples come from identically distributed populations. In order to specify which group is different in a multi-group comparison, the Dunn rank sum test was used. The Dunn test combines all samples and subsequently ranks the values from smallest to largest. The different groups can thus be compared on the sum of their respective ranks (Dunn, 1964).

Taylor diagrams have been used to compare three mathematical operations in a visual manner rather than table. Since the ISD method had a reduced number of measurements compared to the linear (ISL), poly-4 (ISP), and quadratic (ISQ) background methods, all control data were normalized with a standard deviation of 1. All sensor data was therefore also normalized on their specific control data standard deviation. It is important to recognize that the standard deviation (SD) presented in conjunction with the Taylor diagram is a normalized standard deviation and is not appropriate for comparison with the non-normalized standard deviation, which is a more common definition for the abbreviation SD. In essence, the Taylor diagram is a "summary of how well patterns [in a general sense between groups] match each other in terms of their correlation, their root-mean-square difference, and the ratio of their variance [to control]" (Taylor, 2001).

All data conversions and processing were done in RStudio (2022.07.2, Build 576) using the packages: tidyverse, lubridate, tibbletime, hms, oce, data.table, utils, rlang, stats, lmtest, FSA, rstatrix, Metrics, patchwork, flextable, officer, gridExtra, plotrix, seacarb, and plotly.

2.4 Limitations and problems with *in-situ* measurements

This thesis is limited to the area of three basins: Arkona Basin, Bornholm Basin, and Eastern Gotland Basin, in the Baltic Sea. Although the OPUS sensor produced profiles in other basins as well, these were neglected due to the low number of control measurements of total H_2S needed to verify the accuracy of the OPUS sensor as well as if a correction is needed. This thesis focuses on 1) the application of methods suggested in literature to calculate total H_2S and the comparison of these to the method developed here, as well as, 2) investigating the distribution of total H_2S in the aforementioned three basins. Only one of the methods from the literature has previously been used to analyze water from the Baltic Sea (the 4^{th} order polynomial, poly-4 (Meyer et al., 2018)). Variations due to physical changes in the instrument, like changes in the path length or variations in the output spectrum of the light source or biofouling of the instrument windows will not be considered within the scope of this work. In addition, a limited number of cruises with varying temporal cover, as well as control

measurements per cruise, were conducted. Due to unpredictable weather conditions, a 1:1 comparison of the same stations and depths throughout the year could not be done. The investigation in chapter **3.1** is thus an approximation of the fluctuations in the Baltic Sea, averaged over all basins and cruises combined.

The pH was not measured onboard the ship in 2021, thus all pH related data was collected from the Swedish Meteorological and Hydrological Institute (SMHI). Each OPUS measurement was allocated a pH value from SMHI data based on closest geographical location and density profile. This can result in a pH value being collected from a different basin than the one where the measurement took place, if a station there was closer on the geographical criteria. However, the effects of this are only briefly discussed in section **2.3.3** and chapter **3.1.2**.

When plotting and analyzing the transect data in ODV, the same transect section was used for all cruises. Although stations were revisited, there is a potential of some station locations to be positioned further away for some cruises than others, although still being within reasonable distance of the transect section. The local variation in bathymetry resulted in a few stations being deeper for some of the cruises compared to others. In the transect section figures from ODV, these stations seem to go into the sediments, however, this is not the case. The cause of this 'coring' is due to the bathymetric resolution and the fact that these stations are not in the center of the transect line. Care has been taken when analyzing this data, as to not allow artificial boundaries affect the outcome.

CHAPTER 3. RESULTS & DISCUSSION

This chapter is divided into two parts. Section **3.1** investigates which method is the most appropriate to use to measure total sulfides (free H_2S + HS^-) in the Baltic Sea with the OPUS sensor. Processed data from the OPUS sensor is compared to control measurements taken from bottle samples. In addition, the section investigates if there is a need to correct the regression outcome on the OPUS sensor data, or if the methods applied give appropriate outputs directly. Section **3.2** examines the spread of total sulfides in the Baltic Sea using the method with the best outcome from the previous section. The spread of total sulfides will be considered on both spatial and temporal scales using transect data from the southern Arkona Basin through to the northern Eastern Gotland Basin over five months. The results are discussed in an environmental context in section **3.2.6**.

3.1 Method development for sulfide monitoring

Unless otherwise stated, control data, or simply control, refers to the data obtained through the wet chemistry method described in section **2.3.1**. Raw data refers to unadjusted total sulfide data (free H_2S + HS^-) from the OPUS sensor, obtained via the regression described in chapters **2.2** and **2.3**. Corrected data refers to adjusted total sulfide OPUS data, where a mean offset and linear slope correction have been applied. Except for the removal of control data below the control LOD, no further adjustments were made on the remaining control data. Details on OPUS data adjustments are highlighted in the respective relevant sections.

3.1.1 Purpose and method abbreviation

As mentioned in chapter **2.2**, there are two main correction methods used to account for the background signal caused by colored dissolved organic matter (CDOM), particles, and other possibly unknown constituents, namely linear and quadratic regression. The linear correction uses a simple function over all wavelengths ($a \cdot \lambda_{wl}$), whereas the quadratic correction uses a quadratic function over all wavelengths ($a \cdot \lambda_{wl} + b \cdot \lambda_{wl}^2$). In addition, a method using a poly-4 function ($a \cdot \lambda^{-4}$) has also been tested specifically in the Baltic Sea. All three methods are purely empirical approaches, which is ideal for, e.g., float deployments, where no control measurements are made. However, the linear and quadratic approaches are approximations from studies on mostly Case I water types (open oceans dominated by phytoplankton), whereas this study, which is in the Baltic Sea, is a Case II water type (other water bodies highly affected by CDOM and phytoplankton; Matsushita et al. (2012)). The only study in the Baltic Sea, using the poly-4 function (Meyer et al., 2018), had very few

measurements in total (15 measurements over 3 stations combining H_2S, HS^-, and S^{2-}), making a validation for the best method difficult. In addition, previous focus has mainly been on monitoring nitrate. In order to evaluate which method would be most suited for monitoring sulfides on a large scale in the Baltic Sea, a comparison to a derived *in-situ* spectrum has been included, using a substantially bigger data set than before, spanning over five cruises and five different months.

All tested methods are simple linear regressions with a total sulfide spectrum (S) comprising of the HS^- and H_2S specific extinction coefficient spectra (S^{2-} estimated at a fraction of $< 5 \cdot 10^{-6}$ at pH 7 and 4 °C and therefore neglected). The regression includes an intercept (I), and uses derived (D), linear (L), poly-4 (P), or quadratic (Q) background correction methods, respectively. These methods are abbreviated as ISD, ISL, ISP, and ISQ. The derived (D) background spectrum is based on the remaining absorbance after known constituents are subtracted (see chapters **2.2** and **2.3**).

3.1.2 Initial outcome from regression analysis

This section presents the raw data outcome of total H_2S concentrations using the four methods ISD (derived background), ISL (linear background), ISP (poly-4 background), and ISQ (quadratic background). A comparison of all four methods against control (wet chemistry) was made to determine the potential of each method. Hence, this section focusses on the first main aim of this thesis: evaluating which method is best suited for the Baltic Sea when no corrections are applied, using the hypothesis 'all methods have equal error to control'.

The data used to calculate the statistics presented in **Table 3.1** was not normally distributed (Shapiro-Wilk test: W = 0.957, 0.966, 0.951, and 0.978 for ISD, ISL, ISP, and ISQ respectively; $p < 0.001$ for all methods), therefore, non-parametric tests were used for statistical testing and a semi-parametric method was used to calculate the limit of detection (LOD; see details for equation **2.13**). The LOD tended to be higher in May (EMB264) and July (EMB271), with ISQ also having high LOD in November (EMB280). The field SD was relatively similar between all methods (**Table 3.1**), with March (EMB261) being slightly higher than the other cruises. All following analyses were carried out on data where measurements below the cruise specific LOD had been removed, and treating all cruises as one. The SD used was thus 0.93 µM (ISD), 0.87 µM (ISL), 0.89 µM (ISP), and 1.20 µM (ISQ), which was lower than the SD of control at 1.52 µM and the SD from the laboratory calibration at 5.26 µM ($H_2S + HS^-$). Applying the cruise specific LOD, allowed for a more accurate data set, with reduced risk of including/excluding data below/above the field LOD.

Table 3.1. Summary of limit of blank (LOB), limit of detection (LOD), degrees of freedom (df), as well as blank and field standard deviations (SD) of raw data (total H_2S). Outliers (defined as ± 1.5 · interquartile range (IQR) from the first and third quartile based on peak variation) were removed before calculating field SD. The LOD obtained for each cruise was applied on the data. Blank statistics presented for all cruises combined is meant for comparison only. Field SD for all cruises combined was calculated after the cruise specific LOD was applied and where more than one measurement was taken per control. Control LOD = 2.36 µM, and control SD = 1.52 µM.

Cruise	Method	Blank				Field	
		LOB [µM]	SD [µM]	df	LOD [µM]	SD [µM]	samples
EMB256	ISD	0.51	0.31	12	1.03	0.69	32
	ISL	2.57	0.33	124	3.12	0.64	33
	ISP	1.51	0.33	124	2.06	0.65	33
	ISQ	1.06	1.08	124	2.84	0.95	33
EMB261	ISD	0.58	0.56	76	1.50	1.41	51
	ISL	1.17	0.50	342	1.99	1.26	53
	ISP	0.23	0.62	342	1.24	1.30	53
	ISQ	2.45	1.43	342	4.80	1.49	54
EMB264	ISD	1.35	1.16	42	3.27	0.63	38
	ISL	5.69	0.85	375	7.09	0.59	46
	ISP	5.69	0.89	375	7.15	0.59	46
	ISQ	8.82	2.87	375	13.54	0.99	35
EMB271	ISD	-0.13	0.23	8	0.27	0.96	42
	ISL	4.44	0.51	125	5.28	0.94	42
	ISP	3.83	0.61	125	4.84	0.98	41
	ISQ	13.36	1.67	125	16.12	1.42	41
EMB280	ISD	0.71	0.48	58	1.50	0.69	79
	ISL	2.06	0.48	402	2.85	0.69	79
	ISP	1.48	0.56	402	2.39	0.70	79
	ISQ	8.78	1.80	402	11.75	0.99	71
All cruises combined	ISD	0.82	0.71	200	1.99	0.93	242
	ISL	4.52	1.43	1 372	6.87	0.87	253
	ISP	4.46	1.83	1 372	7.47	0.89	252
	ISQ	10.16	3.82	1 372	16.45	1.20	234

Figure 3.1 shows a concentration profile comparison (calculated via equation **2.13** including all methods and control from all stations and cruises. The general error between control and the results from the different methods was promising, with no method visually diverting from either control or the other methods. However, two control measurements at 80 m at station TF0213 in July (EMB271; see **Figure 3.1**) were visually different from all other measurements in this region. No clear indication of this measurement being false was found, thus it remained in the analyzed data (**Figure 3.1**).

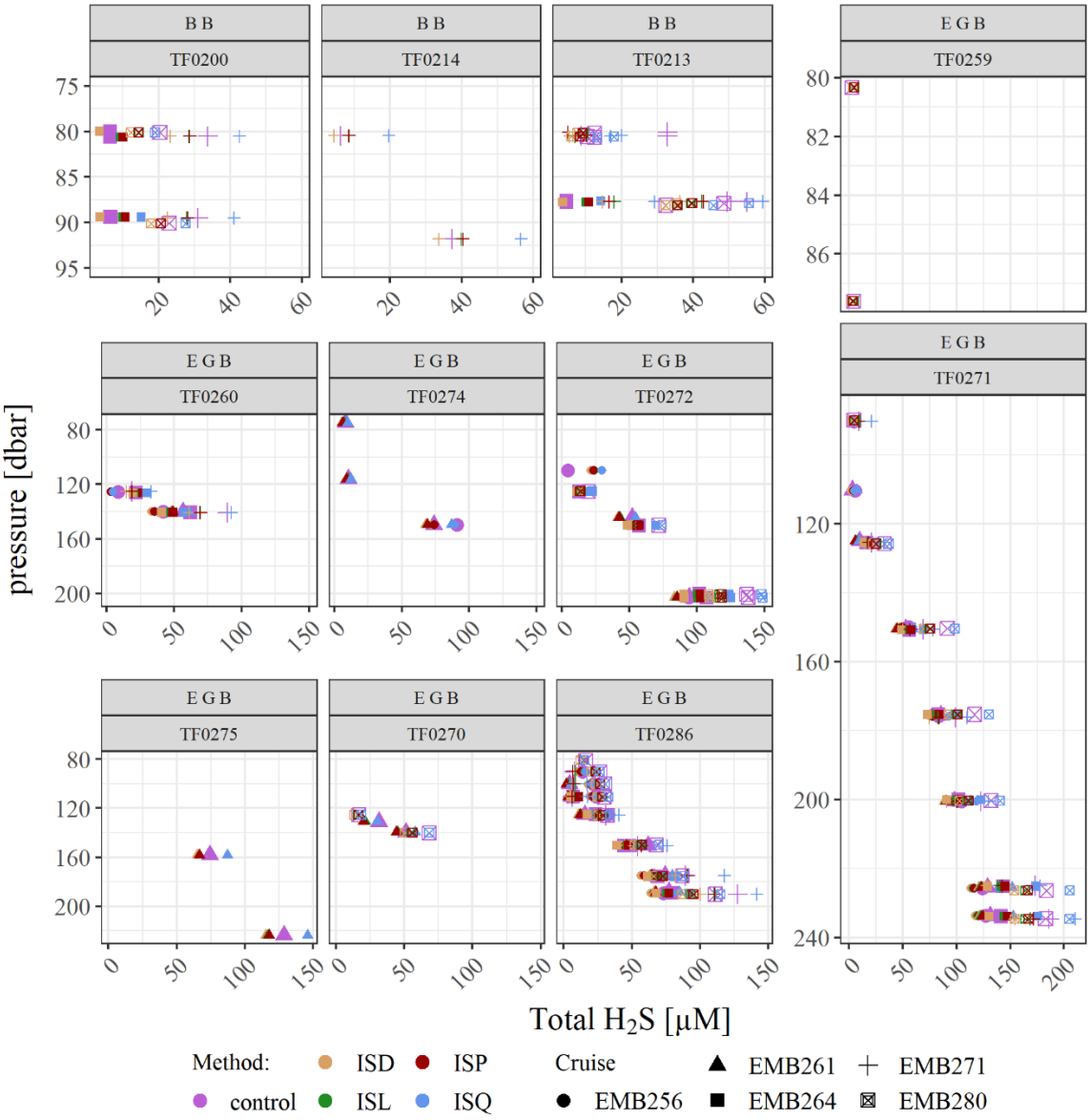

Figure 3.1. Raw outcome of total H_2S concentrations from ISD, ISL, ISP, ISQ, and control values over pressure. Stations appear in the order of the transect, from the Bornholm Basin (BB) to Eastern Gotland Basin (EGB).

Although all four methods had a good overlap with control, **Figure 3.2** clearly shows that the difference to control was not the same throughout the water column. A tendency

towards higher difference between sensor concentrations and control over depth was observed for all methods. In addition, stations in the Bornholm Basin had a larger difference compared to stations with similar depths in the Eastern Gotland Basin. However, no method was constrained to being only higher or lower than control; rather a change between positive and negative offsets could be observed on some stations, e.g. TF0270, TF0271, TF0272, and TF0286 (**Figure 3.2** and **Figure 3.3**).

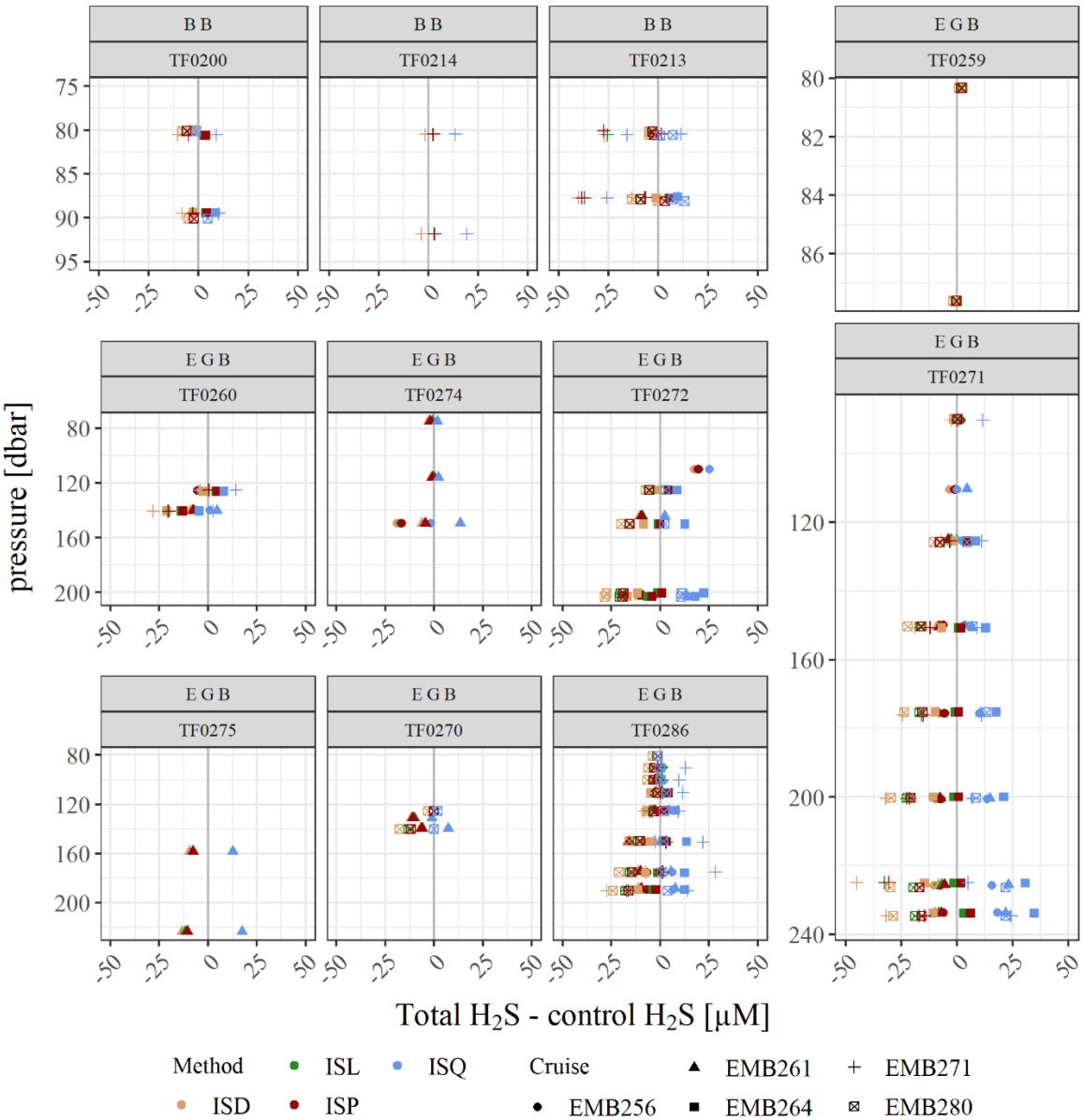

Figure 3.2. Difference between total H_2S calculated by each method from sensor data and the control concentrations over pressure. Stations appear in the order of the transect, from the Bornholm Basin (BB) to Eastern Gotland Basin (EGB). Ca. 94% of the measurements lies within ± 12.5 µM for ISD, ISL, and ISP for all cruises. ISQ had 95% of all measurements within ± 25 µM, except for the May cruise which was still only at ca. 89%.

The top panel in **Figure 3.3** shows the relative error of total H_2S to control over control concentrations. The cubic root of the relative error was found to have both positive and negative

values for all methods (although only two measurements from ISD was positive), further indicating that no method was constrained to being only higher or lower than control. In addition, the panel also highlight that the ISD and ISQ methods gave more homogenous readings compared to ISL and ISP. Nevertheless, the relative error to control drastically increased below ca. 10 µM control concentration for ISL (n=21), ISP (n=21), and ISQ (n=17; up to 576%). Some spread was also found for ISD (n=19, one value at 395% and another at -65%), however, most were ± 25% (**Figure 3.3**).

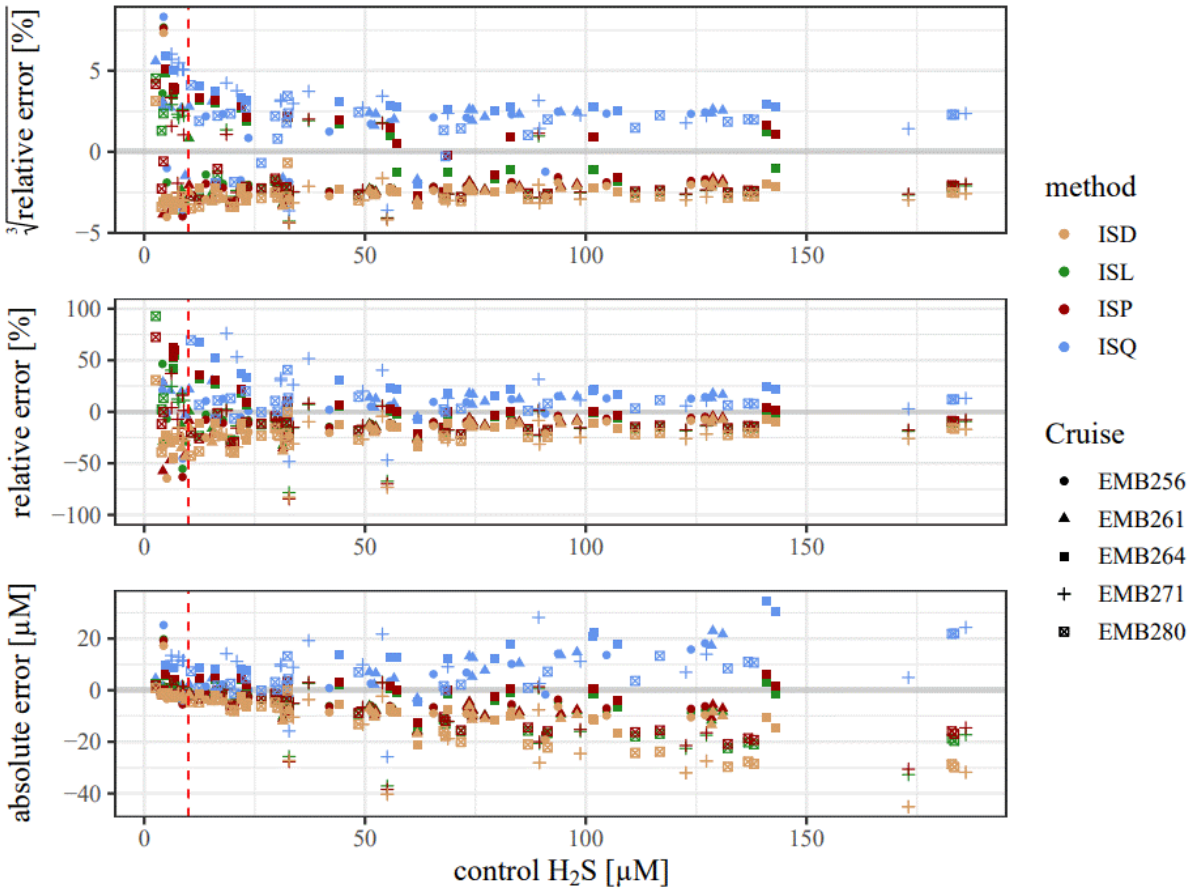

Figure 3.3. Cubic root relative error (top), relative error constrained to ± 100% (middle), and absolute error (bottom) of calculated total H_2S concentrations from the OPUS sensor to control values, plotted over control concentrations. Measurements below OPUS and/or control LOD were removed.

The absolute error between raw sensor data and control in **Figure 3.3** showed that all methods had an increasing error over control concentration. This goes in line with the error over depth seen in **Figure 3.2** as total H_2S tend to increase with depth.

The uncertainty of the pH value could potentially influence the error to control – although it seem to have had a low effect around the chemocline (here found between 40-125 m), even though the ratio H_2S:HS^- could differ up to -12.90% when pH was positively adjusted, and 14.82% if pH was negatively adjusted (± SD of 0.06). The lower total H_2S concentration

at this depth (up to 28% of maximum concentration; max. 59 µM) meant a maximum concentration difference between 1.58-2.65 µM depending on method when a positive pH adjustment was applied, and between 1.81-3.04 µM when a negative pH adjustment was applied. In comparison, below 200 m the difference amounted to between 7.53-10.33 µM when positively adjusted, and 8.64-11.86 µM when negatively adjusted. ISD was in both scenarios least influenced out of all methods. The reason why the pH difference and thus the change in ratio may not have had a more dramatic influence on the total H_2S concentration may be due to the relatively low absorbance of the H_2S relative to the HS^- in the selected wavelength range. Nonetheless, there was a potential of the pH value to affect the relative error, although, since there is no simple way to determine which pH is closer to the truth (remember it was originally collected based on distance and density), no further investigation was made on this as false likelihoods could be introduced.

Despite having a large relative error below 10 µM control concentration, ISL had on average the lowest relative error at -1.7 % (**Table 3.2**). However, ISD had the lowest relative standard deviation at ± 41.5%, indicating this method as more stable. Excluding measurements below 10 µM control concentration gave ISD a relative SD at ± 12.3%, ISL at ± 14.0%, ISP at ± 15.1%, and ISQ at ± 18.5%. Despite the lower relative SD, ISD had the highest average relative error when excluding measurements below 10 µM at -20.4% while ISP had the lowest at -10.7%, closely followed by ISL at -10.9%. ISQ had 14.3% average relative error.

Table 3.2. Relative and absolute error between raw calculated total H_2S concentrations and control. Samples indicate the number of unique control measurements; however, since OPUS measurements below the cruise specific LOD were removed prior to calculations, the different methods have different number of samples.

Method	Relative error [%]		Absolute error [µM]		Samples
	Average	SD	Average	SD	[n]
ISD	-18.1	41.5	-10.45	9.59	113
ISL	-1.7	49.0	-5.98	8.43	115
ISP	-3.4	48.9	-5.65	8.23	115
ISQ	30.8	69.4	8.28	8.86	111

The Kruskal-Wallis rank sum test showed a difference in relative error to control between the four methods (chi-square = 193.38, p-value < 0.001, df = 3). The Dunn test with p-values adjusted after the Holm method confirmed a difference between all methods except between ISL and ISP (ISD vs. ISL: Z = -5.99; ISD vs. ISP: Z = -5.55; ISD vs. ISQ: Z = -13.81;

ISL vs. ISQ: Z = -7.90; p-value < 0.001 for all comparisons; ISL vs. ISP: Z = 0.44, p = 0.66). The similarities in SD of both relative and absolute error presented in **Table 3.2** makes it difficult to discern which method is closest to control, although a difference has been found statistically. Therefore, another visual representation will be used to discern the optimal method.

The Taylor diagram in **Figure 3.4** shows how each method relates to the control. The correlation to control was high for all methods, ranging between 0.987 to 0.989. The root mean square (RMS) error was nearly identical for ISD and ISL at 0.1373 and 0.1376 µM respectively, with ISP at 0.1452 µM, and ISQ slightly higher at 0.1644 µM. In terms of the normalized standard deviation, ISP had the closest resemblance to control at 0.92 µM, while ISD was slightly further away at 0.86 µM. Here, a normalized SD of 1 µM indicates that the method has the same variance as control.

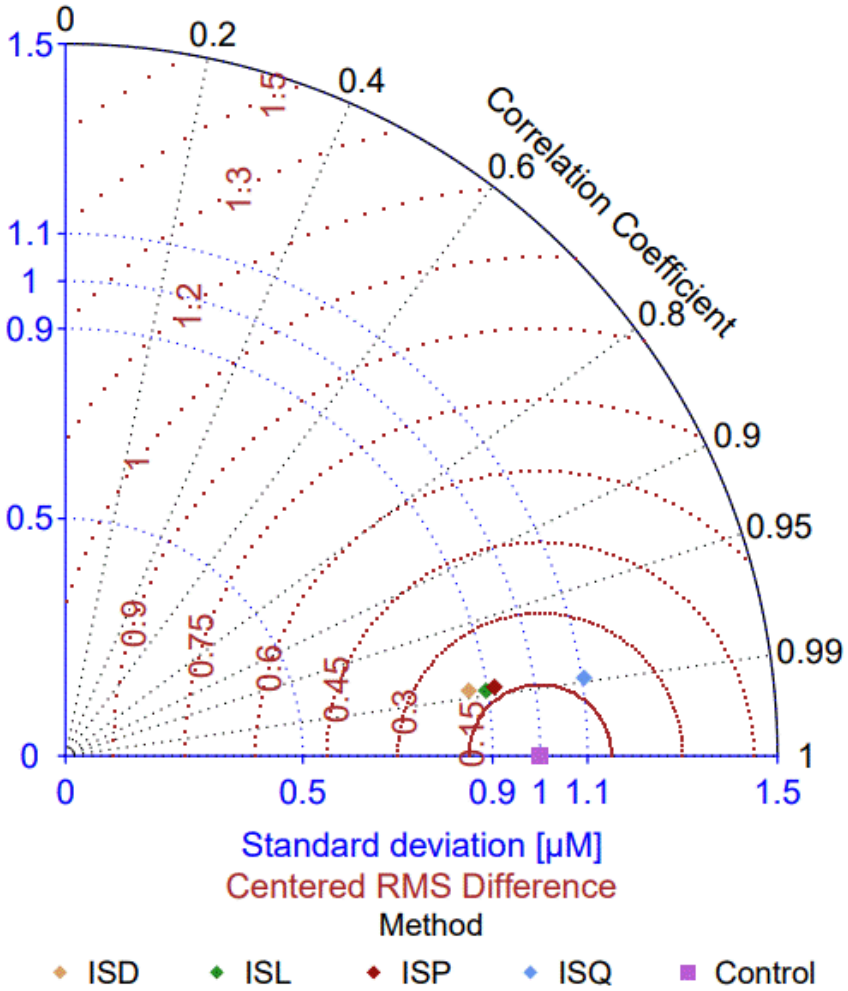

Figure 3.4. Taylor diagram of all methods using LOD adjusted raw data. The standard deviation is here normalized to the control SD.

To summarize, the hypothesis that all methods have equal error to control was rejected, however, the Taylor diagram could not clearly show which method had the closest outcome to

control. The ISD method had a lower RSM, relative error SD, as well as LOD over all cruises. No statistical difference could be found between ISL and ISP, and both methods had very similar relative error SD and LODs. ISQ on the other hand had a higher relative SD as well as LOD over all cruises, indicating that this method might not be as stable as the rest.

3.1.3 Correction when control values are present

In the previous section (**3.1.2**), results from equation **2.13** on calculated concentrations from OPUS measurements indicated that the outcome in most cases caught the pattern of the controls, but could have a relative error of -18.1 ± 41.5% for ISD, -1.7 ± 49% for ISL, -3.4 ± 48.9% for ISP, and 30.8 ± 69.4% for ISQ (excluding measurements below the LOD). Although the mean relative error for ISL and ISP was below or similar to reported values in literature (e.g. Meyer et al. (2018)), ISL, ISP, and ISQ had a larger variation than ISD. **Figure 3.2** and **Figure 3.3** show that the calculated concentrations and control are closely related, suggesting that an adjustment to the calculated concentrations may be useful. This section investigates the potential of a relative error correction on calculated concentrations from OPUS measurements. Another hypothesis testing was carried out to determine if a correction improved any of the methods, and if so, which method that would now be the better one. The two hypotheses are: 1) the relative error to control is the same for uncorrected and corrected values, and 2) all corrected methods have the same relative error to control.

As mentioned, all methods indicated a pattern to control over concentrations, with absolute error increasing over depth and control concentrations while relative error remained more or less stable. It was also found that the median of the "blank" measurements (non-Gaussian) were not 0 µM, thus all values were first adjusted on the median offset per cruise (equation **3.1**; **Table 3.3**). A correction factor (*Cf*) was calculated using the median adjusted OPUS concentrations directly against control (data pairs below $LOD_{control}$ were removed) in a linear regression going through origin, as shown in equation **3.1**. The factor was used to correct all median adjusted OPUS total sulfide concentrations. The correction factor was calculated per cruise as seasonal variations over the water column could affect the error.

$$[H_sS]_{t,control_i} = 0 + Cf \cdot \left(H_2S_{t,OPUS_i} - Mdn\left(H_2S_{t,OPUS_{blank}}\right)\right) \quad 3.1$$

where $\mathrm{Mdn}\left(\mathrm{H_2S_{t,OPUS_{blank}}}\right)$ is the median value of the OPUS measurements considered blanks.

Table 3.3. Median adjustment on total H_2S concentrations from the OPUS sensor measurements per cruse applied prior to calculation of correction factor. Numbers in brackets indicate the number of measurements used to derive the median.

Method	Median correction [µM]				
	EMB256	EMB261	EMB264	EMB271	EMB280
ISD	0.20 (13)	0.06 (77)	-0.53 (43)	-0.57 (9)	-0.20 (59)
ISL	2.00 (125)	0.48 (343)	3.70 (376)	3.25 (126)	1.38 (403)
ISP	1.13 (125)	-0.50 (343)	3.73 (376)	3.08 (126)	0.46 (403)
ISQ	-1.18 (125)	0.40 (343)	3.96 (376)	9.78 (126)	6.38 (403)

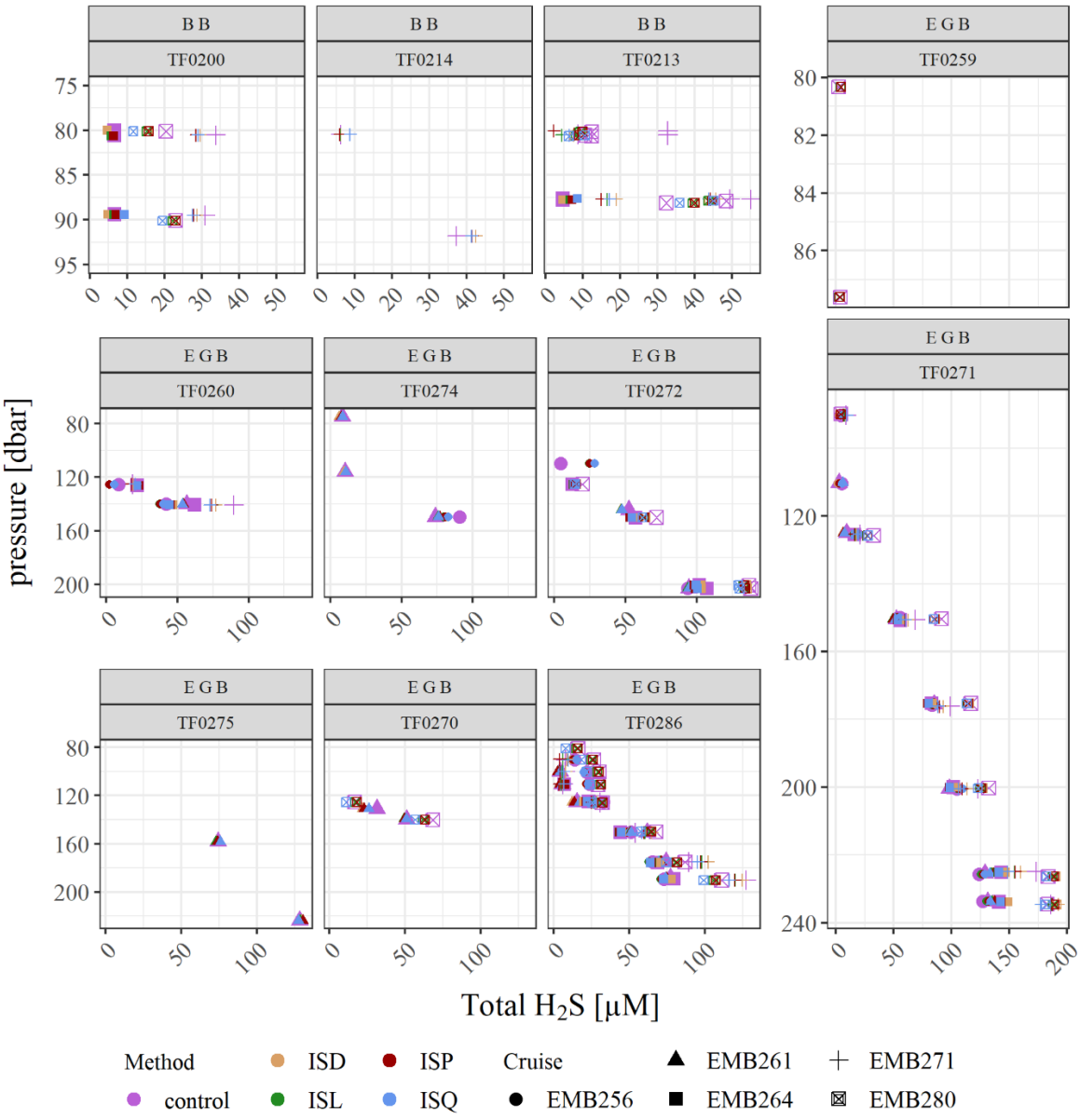

Figure 3.5. Profiles on corrected total H_2S concentrations for all four tested methods and control over pressure. Stations appear in the order as in the transect (see **Figure 2.8**), from the Bornholm Basin (BB) to Eastern Gotland Basin (EGB).

Since a correction was made based on all raw data, a new LOD was calculated on the adjusted data (**Table 3.4**). The difference to uncorrected data was mostly small, although combining all cruises showed that the LOD increased for ISD, while field SD increased for ISD, ISL, and ISP. Both the LOD and field SD decreased for ISQ. The new cruise specific LOD was applied before any further analysis.

Corrected profiles show little to no difference to control for all four methods in the Eastern Gotland Basin (EGB, **Figure 3.5**). The data of two stations positioned in the Bornholm Basin (BB), however, indicate a continuously higher deviation between all methods and control, especially effecting the July (EMB271) cruise.

Table 3.4. Summary of limit of blank (LOB), limit of detection (LOD), degrees of freedom (df), as well as blank and field standard deviations (SD) for corrected data. Outliers (defined as $\pm 1.5 \cdot \text{IQR}$ from the first and third quartile based on peak variation) were removed before calculating field SD. The LOD obtained for each cruise was applied on the data. Blank statistics presented for all cruises combined is meant for comparison only. Field SD for all cruises combined was calculated after the cruise specific LOD was applied and where more than one measurement was taken per control. The correction factors were obtained through equation **3.1** and values within brackets represent the number of measurements used**.** Control LOD = 2.36 µM, and control SD = 1.52 µM.

Cruise	Method	Correction	Blank				Field	
		factor	LOB [µM]	SD [µM]	df	LOD [µM]	SD [µM]	Samples
EMB256	ISD	1.14 (58)	0.36	0.35	12	0.96	0.78	32
	ISL	1.11 (58)	0.63	0.37	124	1.24	0.71	33
	ISP	1.10 (58)	0.42	0.37	124	1.03	0.72	33
	ISQ	0.92 (58)	2.05	0.99	124	3.68	0.87	33
EMB261	ISD	1.13 (66)	0.58	0.63	76	1.62	1.58	51
	ISL	1.11 (66)	0.76	0.55	342	1.66	1.40	53
	ISP	1.10 (66)	0.80	0.68	342	1.92	1.43	53
	ISQ	0.88 (66)	1.80	1.26	342	3.87	1.31	54
EMB264	ISD	1.14 (57)	2.13	1.32	42	4.31	0.71	38
	ISL	1.02 (57)	2.03	0.87	375	3.46	0.60	46
	ISP	1.00 (57)	1.95	0.88	375	3.40	0.59	46
	ISQ	0.83 (57)	4.02	2.38	375	7.94	0.82	35
EMB271	ISD	1.24 (93)	0.54	0.29	8	1.03	1.19	42
	ISL	1.13 (93)	1.34	0.58	125	2.29	1.06	42
	ISP	1.11 (93)	0.83	0.68	125	1.95	1.09	41
	ISQ	0.88 (93)	3.16	1.48	125	5.59	1.25	41
EMB280	ISD	1.24 (89)	1.12	0.59	58	2.09	0.85	79
	ISL	1.15 (89)	0.79	0.56	402	1.71	0.80	79
	ISP	1.14 (89)	1.16	0.63	402	2.20	0.80	79
	ISQ	0.92 (89)	2.19	1.65	402	4.91	0.91	71
All cruises combined	ISD	N/A	1.39	0.80	200	2.71	1.09	242
	ISL	N/A	1.05	0.64	1 372	2.11	0.96	253
	ISP	N/A	1.14	0.72	1 372	2.32	0.98	252
	ISQ	N/A	2.38	1.77	1 372	5.29	1.06	234

When comparing the corrected total H_2S to control for each profile, it became clearer which measurements deviated from the norm (**Figure 3.6**). Excluding station TF0286, which in general had a larger deviation throughout the whole water column, the measurements standing out came from the July (EMB271) cruise. In addition, at least two sets of measurements from the February (EMB256) cruise also deviated beyond 12.5 µM (at station TF0272 and TF0274).

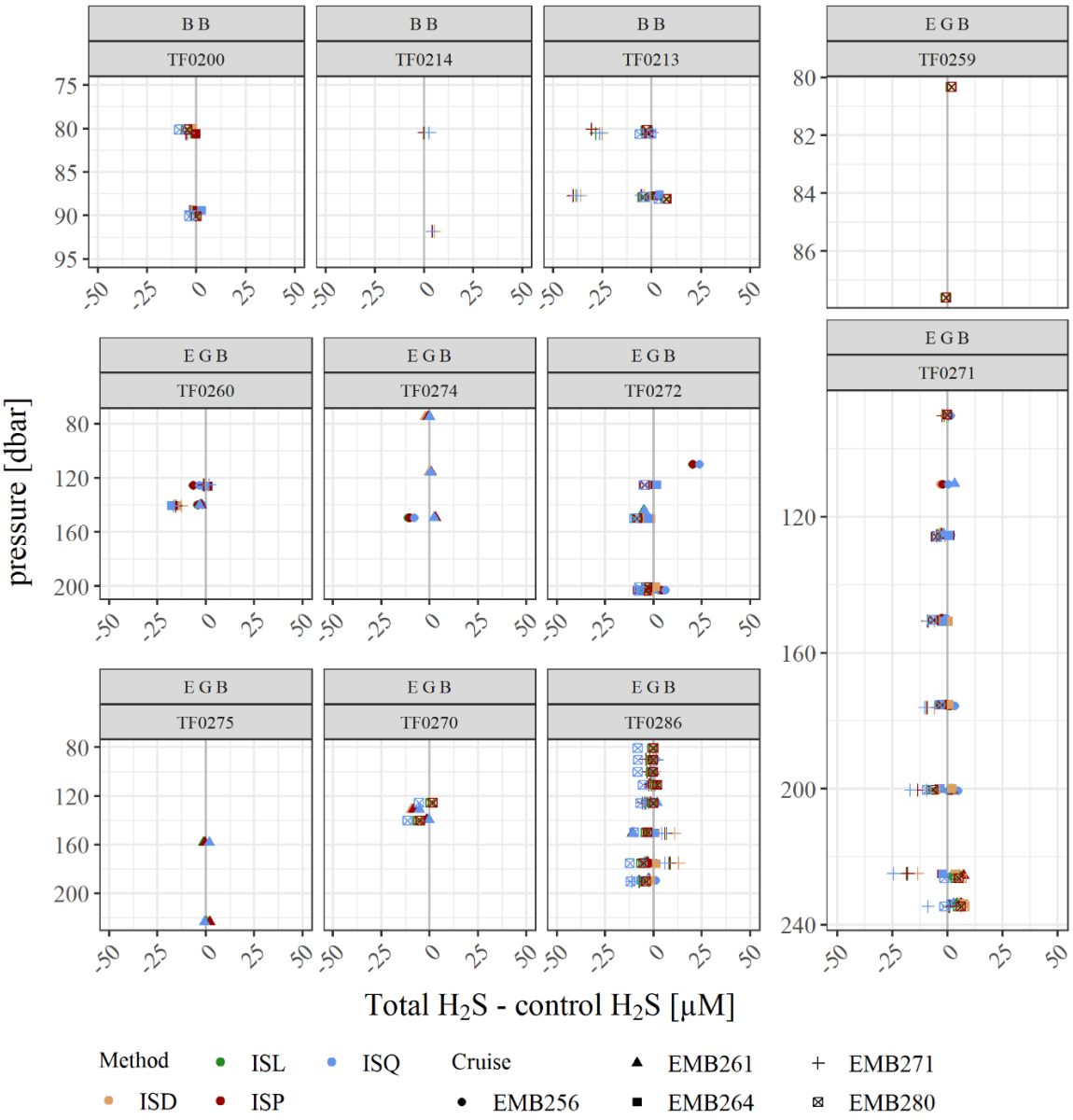

Figure 3.6. Difference between corrected OPUS concentrations and control for each profile, method, and cruise. Stations appear in the order as in the transect (see **Figure 2.8**), from the Bornholm Basin (BB) to Eastern Gotland Basin (EGB). Some variations can be observed; however, at least 97% of the data lies within ± 11.5 µM for all methods.

Figure 3.7 shows the absolute and relative error for all profiles combined. The relative error continued to show a large spread below 10 µM control concentrations for all methods

also after correction (**Figure 3.7**), however, the average relative error decreased for ISD (from -18.1 to -2.0%; **Table 3.2** and **Table 3.5**) and ISQ (from 30.8 to 0.9%), while ISL increased the average (from -1.7 to 3.8%). ISP remained rather unchanged going from -3.4 to -3.3%. ISQ was the only method that improved the relative SD when a correction was applied.

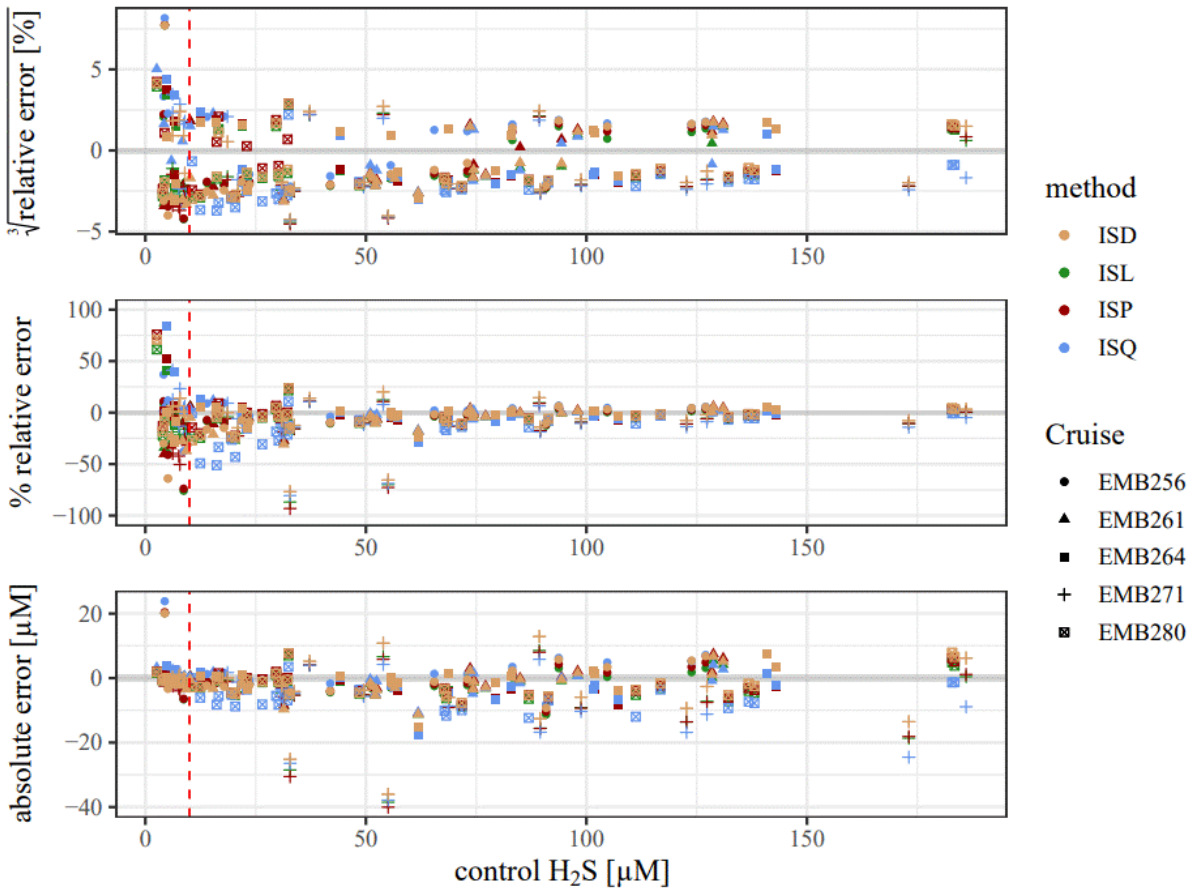

Figure 3.7. Difference between corrected total H_2S (OPUS) and control concentrations. OPUS values were corrected based on the slope (Cf) from the linear relationship to control values when going through origin (0,0).

Table 3.5. Relative and absolute error and SD of corrected data (total H_2S). The error indicates the mean difference to control, while the SD indicates the variance of the difference to control. Samples indicate the number of unique control samples at which multiple sensor measurements could have been taken.

Method	Relative error [%]		Absolute error [µM]		Samples
	Average	SD	Average	SD	[n]
ISD	-2.0	46.8	-1.55	6.35	113
ISL	-3.8	46.9	-2.85	6.41	115
ISP	-3.3	48.2	-2.50	6.70	115
ISQ	0.9	56.9	-3.13	7.23	111

Hypothesis 1 – equal error for corrected and uncorrected data:

The Kruskal-Wallis rank sum test indicated that ISD, ISP, and ISQ were different to their uncorrected counterpart (chi-square = 76.139, 6.103 and 75.056, respectively, with p-value < 0.001 for ISD and ISQ, and < 0.05 for ISP; ISL chi-squared = 2.2838 and p-value = 0.1307). A visual representation (**Figure 3.8**), using the Taylor diagram, showed that the corrected methods had, in general, a higher correlation and lower RMS to control than uncorrected methods. In addition, the normalized standard deviation indicated that all corrected methods had similar variance in the data as control. The first hypothesis, that corrected and uncorrected data have equal error, is therefore rejected for all methods except ISL. However, due to the improvements indicated in the Taylor diagram for ISL (triangle symbolizing corrected values is positioned behind ISP triangle; **Figure 3.8**), it is considered having undergone some improvements, although the statistical test does not show it.

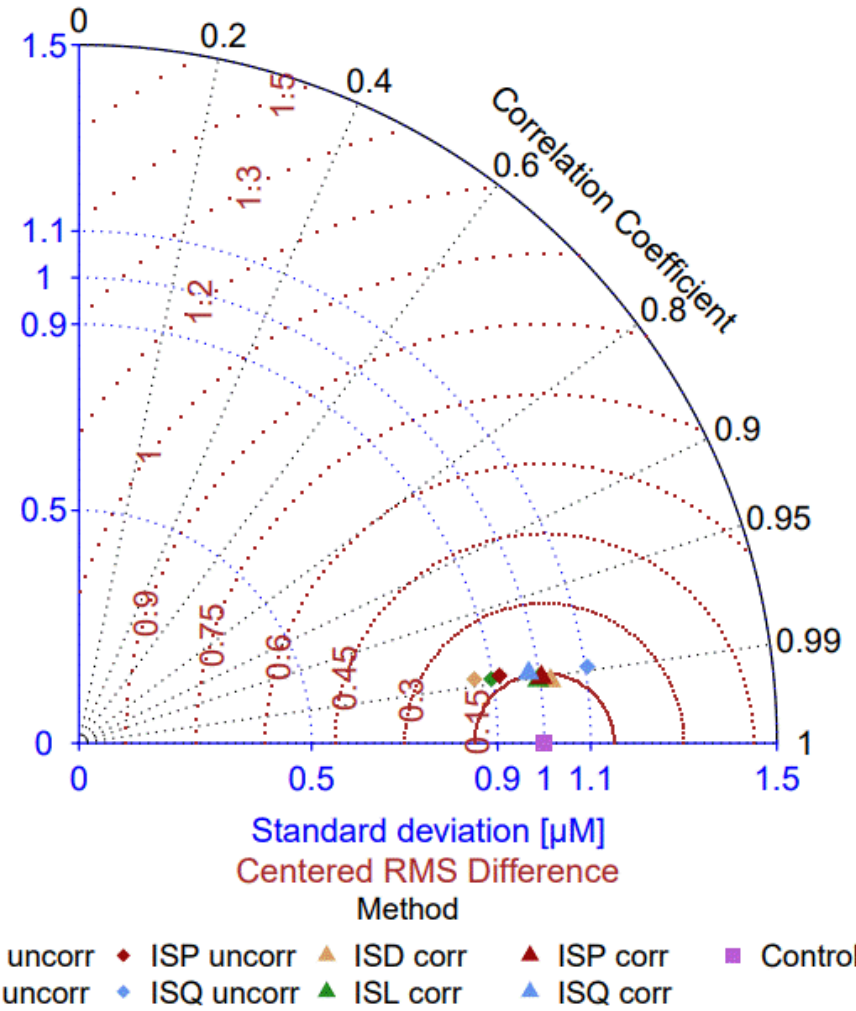

Figure 3.8. Taylor diagram of uncorrected (diamonds) and corrected (triangle) OPUS data against control (square).

Hypothesis 2 – all corrected methods have equal error:

From the previous hypothesis, it was concluded that a corrected and uncorrected method had different errors to control, and corrected data was in general closer to the control (**Figure 3.8**). This section aims to describe which of the four corrected methods give the best outcome overall.

The LOD of the corrected data was on average 2.71 µM for ISD, 2.11 µM for ISL, 2.32 µM for ISP, and 5.29 µM for ISQ, indicating a clear disadvantage for ISQ. In addition, the SD of the relative error to control varied up to 10.1% between the methods. The average relative error was lower for ISD compared to ISL and ISP (-2.0% vs. -3.8 and -3.3%, respectively), while ISQ had the lowest relative error at 0.9%. Nonetheless, all corrected methods were very similar in relation to the control (**Figure 3.8**). ISD had the highest correlation to control after correction at 0.9914, while ISL and ISP were close at 0.9908 and 0.9900, respectively. ISQ was further away at 0.9881.

Despite the arguably large SD of the relative error to control (all above 46%), all methods had similar variance in the data as control with a normalized SD to control at or around 1 µM (between 0.98 and 1.02 µM). The RMS error did, however, display some variation (ISD = 0.1340, ISL = 0.1350, ISP = 0.1417, and ISQ = 0.1502).

The Kruskal-Wallis rank sum test did not find any difference in relative error to control between the methods of corrected data (chi-squared = 3.5831, p-value = 0.3101, df = 3). Based on the data presented above, the second hypothesis, that all methods have equal relative error to control after correction cannot be rejected. Furthermore, although no significant difference could be found between the corrected methods it is recommended to use the ISD method if control measurements are taken and can be corrected for, as this method had the lowest relative error to control at -2.0 ± 46.8%, as well as the highest correlation to control. The average LOD of ISD corrected data is on par with control (ISD = 2.71 µM vs. control = 2.36 µM), and the field SD is generally better (ISD = 1.09 µM vs. control = 1.52 µM).

3.1.4 Evaluation of method

The aim of chapter **3.1** was to investigate which of the four methods ISD (derived background), ISL (linear background), ISP (poly-4 background), and ISQ (quadratic background), provide the most accurate estimation of *in-situ* total H_2S (free H_2S + HS^-) concentrations, and if a correction is needed post-regression.

From the concentration profiles in **Figure 3.1** and **Figure 3.2**, it became clear that all four methods tested, ISD, ISL, ISP, and ISQ, had a very good overlap between each other and

control, already in the unadjusted data. Because of these close relationships between the control and all methods, it is reasonable to conclude that the method with the least variation in the difference to control is the better method. A method with a low variance in the relative error to control is likely to be a more stable approach. A statistical difference was found between all unadjusted methods on their respective relative error to control (Kruskal-Wallis rank sum test), where ISD had a lower root-mean-square error (RMS), SD of relative error, as well as limit of detection (LOD) over all cruises. Adjusting the data on a regression line (equation **3.1**) affected the result for all methods except ISL. The biggest improvement on the average relative error to control was found for ISQ, which decreased the error by 97.08%, followed by ISD with 88.95%. In both scenarios, ISD was close to, or had the advantage over the other methods. This should not be surprising, since the background spectrum used here comes from a collection of "real world" samples, rather than an assumption of what it would look like, as is the case for ISL, ISP, and ISQ. In addition, variations in water properties occur on both spatial and temporal scales, and these variations will affect the calculations as the background spectrum can vary. Thus, the theory of an empirical background spectrum depends on the assumption that the background spectrum only changes in amplitude. Deriving a new background spectrum for each cruise, one can avoid this assumption since the natural variations will be taken into consideration. Although, the only way to ascertain the background spectrum with absolute certainty is to have control measurements off all known components for each sensor measurement. However, this approach is not feasible. Consequently, attempts must be made to apply or derive purely mathematical or empirical spectra.

Although a cruise specific background spectrum was used for ISD, no in depth analysis on the differences in the spectra has been added here. Nonetheless, it can be disclosed that minor variations were observed (**Figure 2.6**). Given the dynamics and ever-changing characteristics of the Baltic Sea, the use of a single spectrum for all seasons and years could be a far-fetched idea. This has also been discussed by Simis et al. (2017) who found that the spectral shape of CDOM may change from linear to exponential depending on the region within the Baltic Sea. With seasonal variations, the changing dynamics of the natural populations, and the unknown proportions of anthropogenic waste, it is plausible that the composition of the “background” of the Baltic Sea changes with both season and location. For the sake of argument, let us assume that such an idea is indeed feasible. If this is the case, the minor variations observed on the derived background spectra make sense. However, the rather small difference between all four methods (both unadjusted and adjusted) suggests that the assumption that a single empirical approach as a background spectrum is also applicable.

Field derived standard deviation of total H_2S concentration were lower for all methods compared to control (overall max. 1.20 µM for unadjusted ISQ vs. 1.52 µM for control). The normalized standard deviation for unadjusted data also indicated that the sensor data had similar internal variation as control for all methods. Thus, it can be concluded that the OPUS sensor is as precise as the long-used control method even when no adjustments are made, and regardless of which background method was used. Nonetheless, it should be noted that only ISD, with the *in-situ* derived background spectra, had an LOD below control for unadjusted data (on average 1.99 µM vs. control at 2.36 µM). The surprisingly high LOD for all other purely mathematical/empirical approaches may be due to a general offset (up to 9.78 µM for ISQ in July; EMB271), an adjustment that can be readily implemented.

Returning to the earlier point that a single background spectrum may be far-fetched. If the dynamics of the background spectrum of the Baltic Sea changes over seasons, there should be indications of some cruises being more accurate than others within the same empirical method (ISL, ISP, or ISQ; purely hypothetical mathematical functions). While the differences between the methods were small when all cruises were combined, examination of the LOD and median correction tables can provide insight into these discrepancies. Cruises EMB256, EMB261, and EMB280 (February, March, and November) tended to be more similar for unadjusted data, while EMB264 and EMB271 (May and July) showed differences. This could potentially advocate for a summer versus winter background spectrum. Nonetheless, the effects of *in-situ* variations of the unknown are probably not very strong since the overall profiles were in line with control for all cruises, and unless the interest is the chemocline it can be neglected since the difference to ISD was minimal.

Whether an adjustment is legitimate is a question that needs more attention. On the one hand, it has been demonstrated in this chapter that the four methods exhibit similarities already when unadjusted, and it is difficult to differentiate between them on the profiles presented here alone (**Figure 3.1**). The compelling overlap with control raises the question of whether the adjustment is truly justified. What if the application, or rather the preconception thereof, that an adjustment is "rather easy to apply" in fact impedes the development to understand the underlying reasons for the observed differences. Olson (2012) highlighted in his paper how the methylene blue method (here control) does not separate free and acid-labile H_2S, meaning the difference seen between the total H_2S derived from the OPUS sensor and the control may be due to the otherwise bound H_2S from free proteins and other substances. It should also be noted that the control samples were not filtered or otherwise modified prior to reagent addition. In comparison, the OPUS sensor can only measure the free total H_2S. The increased difference

between OPUS and control over depth could therefore be due to the bacterial assisted cell lysis coupled with the acidic solutions used in the control method that further degradation of bound H_2S (Olson, 2012), both of which would then increase the free total H_2S. On the other hand, the adjustments implemented here can be considered legitimate on the basis that it is impossible to achieve absolute perfection unless each element of the matrix being measured is fully understood. In addition, it is difficult to ascertain the extent to which bound total H_2S is released in the control samples. Consequently, adjustments then provide the optimal opportunity to account for the unknown and present data in the most accurate manner as long as the controls are considered accurate.

Although adjustments may serve a purpose in order to get values with the highest probability to be accurate, if the underlying data is too spread or samples non-homogenous, the correction may be faulty. For this reason, the number of measurements used to determine the correction is crucial. In this study, a minimum of 57 measurements were used to calculate the correction factor, giving a sturdy base. Only the February (EMB256) and July (EMB271) cruise had a lower number of measurements to calculate the median correction for ISD. However, the generally small correction that was applied (0.20 and -0.57 µM) should have an insignificant effect if slightly off the mark. The fact that both of these corrections were consistent with the other cruises strengthens their probable accuracy.

In the case where no controls can be taken, both ISL and ISP give similar results (unadjusted data). In addition, it would not be possible to make any corrections other than on the median offset, which again was similar between the two methods (less than 1 µM difference). However, since unadjusted ISL had a lower LOD (6.87 vs. ISP = 7.47 µM) as well as average relative error (-1.7 vs. ISP = -3.4%), it is suggested to use this method if no controls are collected. It should, however, be highlighted that both of these methods had a much higher LOD compared to control (2.36 µM), thus, it would seem that purely empirical methods are mainly applicable when total H_2S exceeds ca. 10 µM. In conclusion, if the aim is to measure sulfides below 10 µM, control measurements are needed, and if controls are collected, a derived background spectrum can account for unknown *in-situ* variations affecting the background spectrum.

3.2 Temporal and spatial variability of total H_2S in the Baltic Sea

3.2.1 Problem overview

Eutrophication and the expansion of anoxic zones (oxygen depletion) have been high on the agenda for countries surrounding the Baltic Sea in the past few years, and HELCOM (2013) has continuously monitored the status of this sea since 1979. Despite this increased interest, high resolution mapping of the spread of anoxic zones and the fluctuations therein is still poor. Mostly, data for such studies come from discrete measurements, from areas already known to be anoxic or suspected to be (e.g. routine monitoring cruises from IOW, Germany, and SMHI, Sweden). That makes these measurements highly susceptible to bias. Until now, there has not been a reliable *in-situ* measurement method to scrutinize a larger area and give a proper mapping of the anoxic zone. For the first time five transects of high-resolution *in-situ* total H_2S (H_2S_t; free H_2S + HS^-) have been compiled from different months in 2021. The objective of this chapter is twofold: firstly, to ascertain the distribution of anoxic water that has not yet been revealed; and secondly, to examine the potential of total H_2S observations within the sub-oxic zone.

3.2.2 Applied methodology

Building on the conclusions from chapter **3.1**, the ISD method was used to derive total H_2S from the OPUS data for the whole transect. The total H_2S (free H_2S + HS^-) concentrations obtained using the OPUS sensor were derived and corrected in the same manner as in chapter **3.1.3**, using equation **2.12** and **3.1**. All OPUS measurements were corrected using the median offset specific for each cruise (**Table 3.3**), as well as the correction factors from **Table 3.4** applied through equation **3.1**. The correction factors were obtained by using the slope between median corrected values and control concentrations (equation **3.1**; see section **3.1.3** for details). An example on the difference between corrected and uncorrected profiles can be seen in **Figure 3.9**.

OPUS standard deviation (SD) was on average 1.09 µM (field total H_2S), and the control SD was 1.52 µM (lab total H_2S). The theoretical limit of detection (LOD) of the oxygen sensor (SBE 43, Sea-Bird Scientific) was at 0.05 ml/l. Total H_2S is commonly presented as negative oxygen in ml/l as the required oxygen concentration needed to oxidize the sulfides (1 µM H_2S = -0.04478 ml/l O_2; Fonselius (1981)). To simplify the comparison to other literature the unit ml/l was used for oxygen concentrations (O_2 (µmol/l) = $44.6596 \cdot O_2(ml/l)$ at standard temperature and pressure; Bittig et al. (2018)).

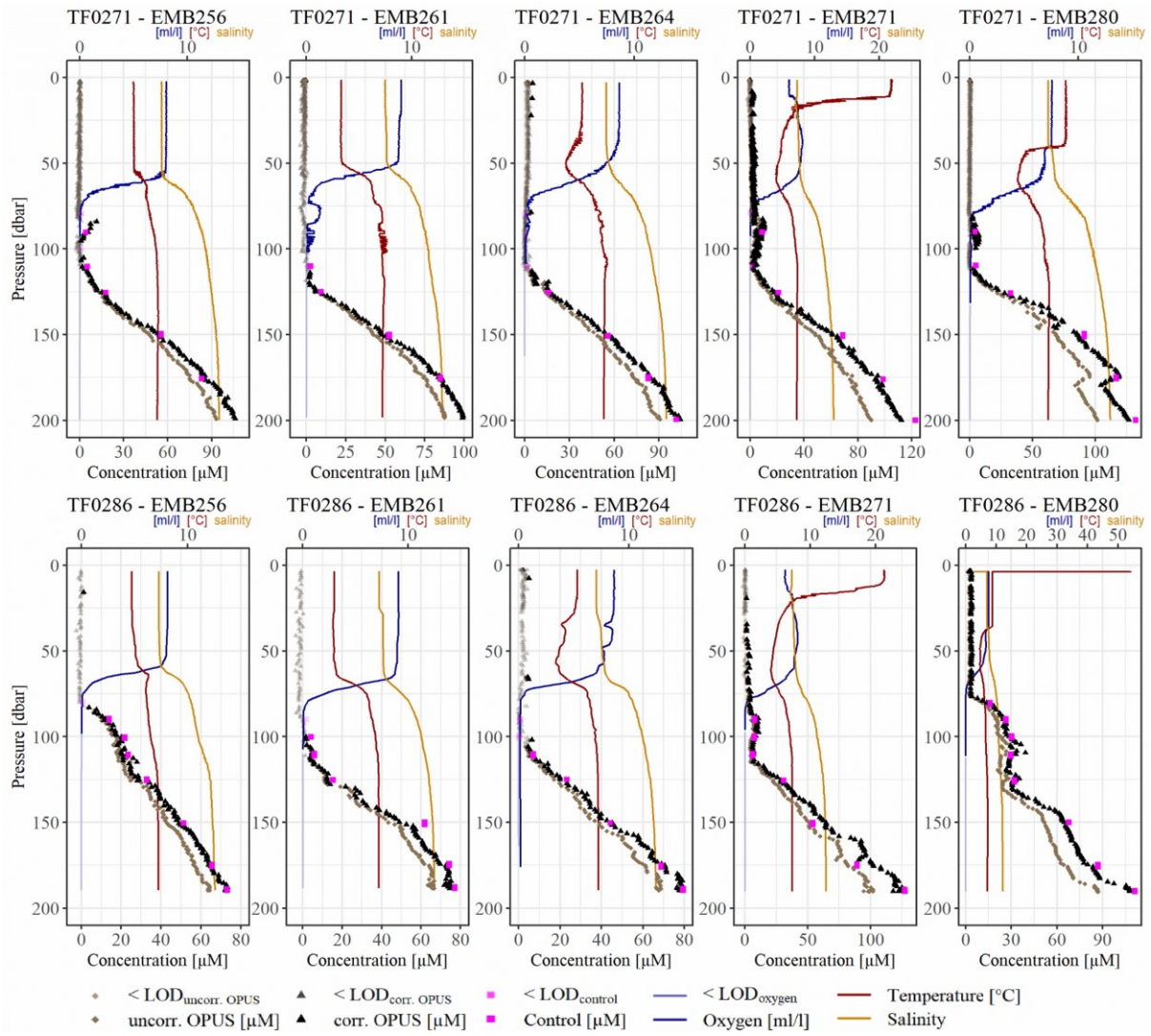

Figure 3.9. Corrected and uncorrected total H_2S profiles (OPUS sensor) from two stations in the Eastern Gotland Basin, measured during every cruise. Control values are from wet chemistry measurements.

The LODs for the OPUS sensor were already calculated in chapter **3.1.3**, and are presented in the figures here to highlight where total H_2S becomes detectable in each month. For some profiles, the limit of quantification (LOQ) is highlighted; however, this metric needs to be carefully applied. There is no general procedure to determine LOQ, as per definition, it will change depending on the question asked and the purpose of the evaluation. The LOQ is commonly calculated using the standard deviation (SD) of blank measurements multiplied with a suitable factor. Since an arbitrary depth range was used to estimate the blank values in chapter **3.1**, a smaller factor 5 has been used, to prevent overestimating the error. All limits for the OPUS sensor can be found in **Table 3.6**.

Table 3.6. Limit of detection (LOD), standard deviation (SD), and limit of quantification (LOQ) for the OPUS sensor (total H_2S) for each cruise.

Month	Cruise name	LOD [µM]	SD [µM]		LOQ [µM]
			blank	field	
February	EMB256	0.96	0.35	0.78	1.75
March	EMB261	1.62	0.63	1.58	3.15
May	EMB264	4.31	1.32	0.71	6.60
July	EMB271	1.03	0.29	1.19	1.45
November	EMB280	2.09	0.59	0.85	2.95

All calculations and profile plots were completed in RStudio, while plotting transects was done in Ocean Data View (ODV). Bathymetry data was collected from GEBCO. Transect figures were made by interpolating profile data over the whole transect using a DIVA software tool in ODV. The DIVA interpolation is done on a finite element grid, which considers boundaries (in this case the bathymetry). The gridding quality was set to 1.5, meaning that estimated values for the interpolation were not allowed to be further away from a real measurement than one length-scale (a distance measure used to allocate a quality value based on the distance between the estimate and the measurements used for the estimate). Interpolated values with a quality value above 1.5 were thus hidden. The estimated data misfit for the OPUS interpolations was in February $-6.62 \cdot 10^{-3}$ µM (mean) with a random mean square (rms) of 2.16 µM, mainly found in the deeper part of the Eastern Gotland Basin (below 75 m). These misfits in the interpolation between the data points can be disregarded, as the color scale does not show a resolution of this level. However, the estimated data misfit for control for the same transect was 0.86 µM (mean) with a rms of 10.56 µM. The higher rms value indicate that the border regions between the color levels may not be accurate, and one must be cautious when interpreting the total H_2S layers for control. The interpolation misfits remained small in the OPUS data in all other transects shown.

3.2.3 High resolution *in-situ* measurements vs. classical discrete monitoring data

The high resolution *in-situ* measurements (OPUS data) rendered a total number of 6293 measurements in February – of which 1643 measurements (26.1%) showed presence of sulfide above the LOD (0.96 µM) – compared to the classical monitoring data (control) using Niskin bottles which had a total of 23 measurements (20 > LOD, 2.36 µM; 87.0%). The number of total OPUS measurements dropped after the March cruise (EMB261), with November having

the least measurements as the weather conditions limited this cruise. However, both March and May indicated an overall lower number of measurements above LOD, 14.7% and 17.5% respectively, compared to July and November, which had 64.6% and 35.9%, respectively. The total number of OPUS measurements was 6333 in March (932 > LOD; 1.62 µM), 4048 in May (712 > LOD; 4.31 µM), 4007 in July (2589 > LOD; 1.03), and 3545 in November (1274 > LOD; 2.09 µM). For the same periods, the control data had a total number of 27, 29, 24, and 33 measurements (March, May, July, and November), amounting to 88.9%, 72.4%, 91.7%, and 90.9% above control LOD (**Table 3.7**).

Table 3.7. Summary of total H_2S data used in sections **3.2.3** and **3.2.4**. Control LOD was 2.36 µM. Cruise specific OPUS LOD was in order: 0.96, 1.62, 4.31, 1.03, and 2.09 µM, respectively.

Cruise	Control			OPUS		
	Total	> LOD	% > LOD	Total	> LOD	% > LOD
EMB256	23	20	87.0	6,293	1,643	26.1
EMB261	27	24	88.9	6333	932	14.7
EMB264	29	21	72.4	4048	712	17.6
EMB271	24	22	91.7	4007	2,589	64.6
EMB280	33	30	90.9	3545	1,274	35.9

Three main zones of total H_2S was found in the Eastern Gotland Basin from control measurements (**Figure 3.10**). The first zone of total H_2S around 0 µM stretched across the transect down to ca. 100 m, excluding the Arkona Basin and most of the Bornholm Basin as no interpolation could be made here. The second zone with total H_2S between 25-50 µM was spread within the Eastern Gotland basin around 100-150 m. The Gotland Deep contained the third zone of values exceeding 75 µM. Both the second and third zone followed the bathymetry well for the controls, and the third zone did not go on top the shelf in Eastern Gotland Basin nor over the sill separating the Gotland Deep from the northern part of the Eastern Gotland Basin. In comparison, the OPUS data not only showed that the third zone extended to outside the Gotland Deep, but also that the second zone was much thinner and more dynamic than seen from control data. Furthermore, the OPUS sensor measured concentrations up to 139.33 µM while the control only measured up to 127.03 µM.

The difference in vertical resolution and horizontal coverage between the control and OPUS data allowed the extent of the total H_2S to be determined with higher accuracy, as well as detection of previously unknown dynamics. In general, the OPUS measurements showed a

higher spatial variation compared to control (**Figure 3.10**; see also section **3.2.4**), with small areas of total H_2S around the oxic zone. The control LOD was computed as linear through the Eastern Gotland Basin, whereas the OPUS LOD showed intricate depth variations over the same distance. For both data sets, the onset of the LOD on the southern end of the Eastern Gotland Basin was situated in the same location. In addition, despite the high number of OPUS measurements in the Arkona and Bornholm Basins, no total H_2S was found here.

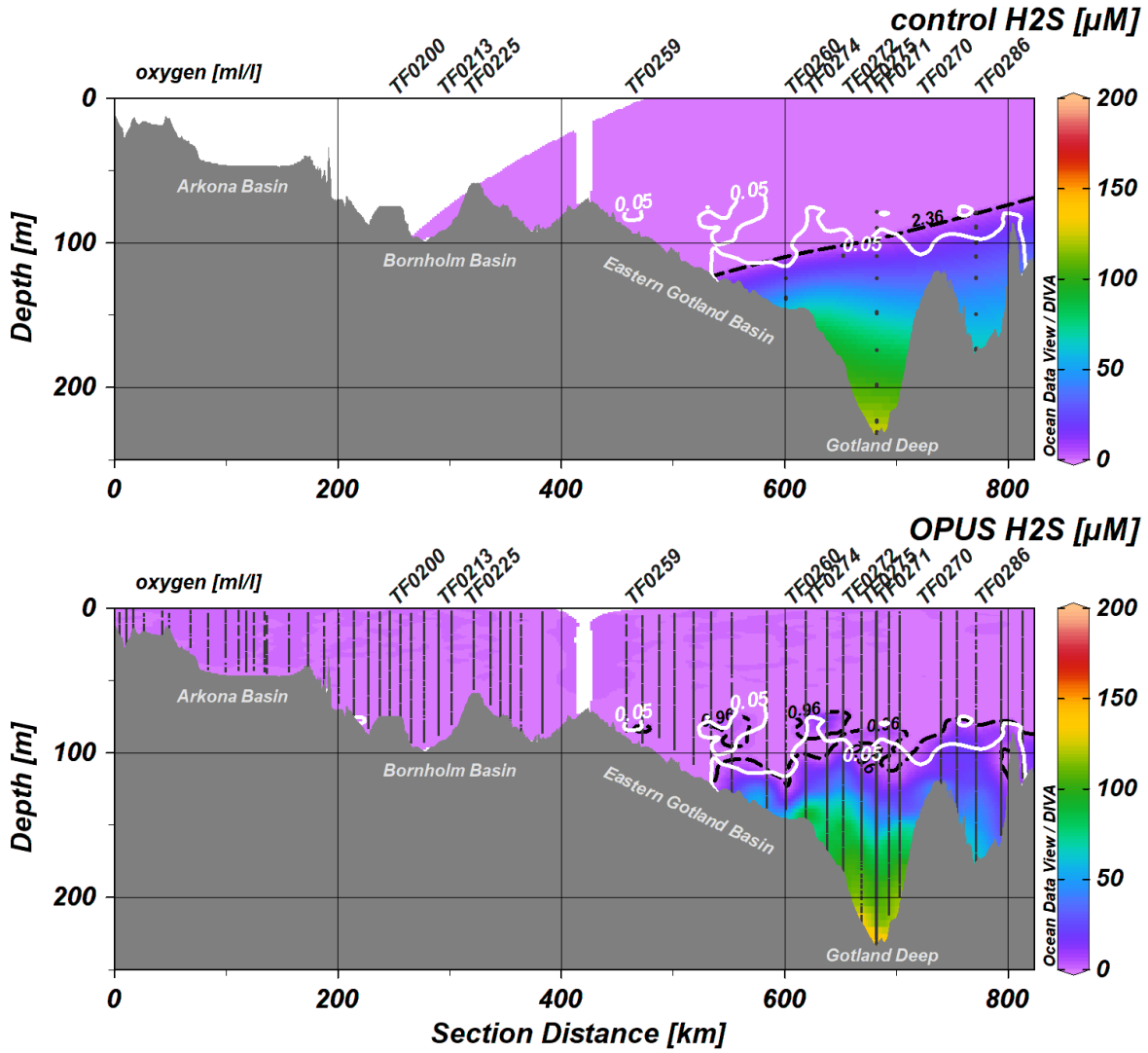

Figure 3.10. Transects of total H_2S concentrations (color) in February 2021 (EMB256). Top: control H_2S from Niskin bottle measurements. Black dots show the measurement locations. Bottom: corrected total H_2S from OPUS sensor measurements. Vertical black dots forming lines symbolizes where measurements were taken. Oxygen LOD (0.05 ml/l) are displayed in white solid lines, and total H_2S LOD (control = 2.36 µM and OPUS = 0.96 µM) in black dashed lines.

In contrast to the February data shown in **Figure 3.10**, the OPUS sensor detected total H_2S between the mainland Sweden and Bornholm in July (EMB271). Control measurements were only taken on the East-most station in **Figure 3.11**, here TF0200, and the shallowest measurement was taken where the increase of total H_2S reached its peak in the depths. The

control measurement cannot be used to estimate where the onset of total H_2S was, nor is it possible to determine how far the spread of total H_2S was in vertical and horizontal direction. The OPUS data, however, show similar increase in total H_2S around 75 m not only for TF0200 with the control measurements, but also for the two stations situated east of TF0200 and north-northeast of Bornholm Island. In addition, the OPUS data indicated that the increase in the bottom part of the profile might not be connected to sulfides measured higher up in the profile (TF0206 and TF0208 at ca. 65-75 m), meaning, there might be a vertical variation in total H_2S in this area. Such small-scale dynamics could not be seen in the control data.

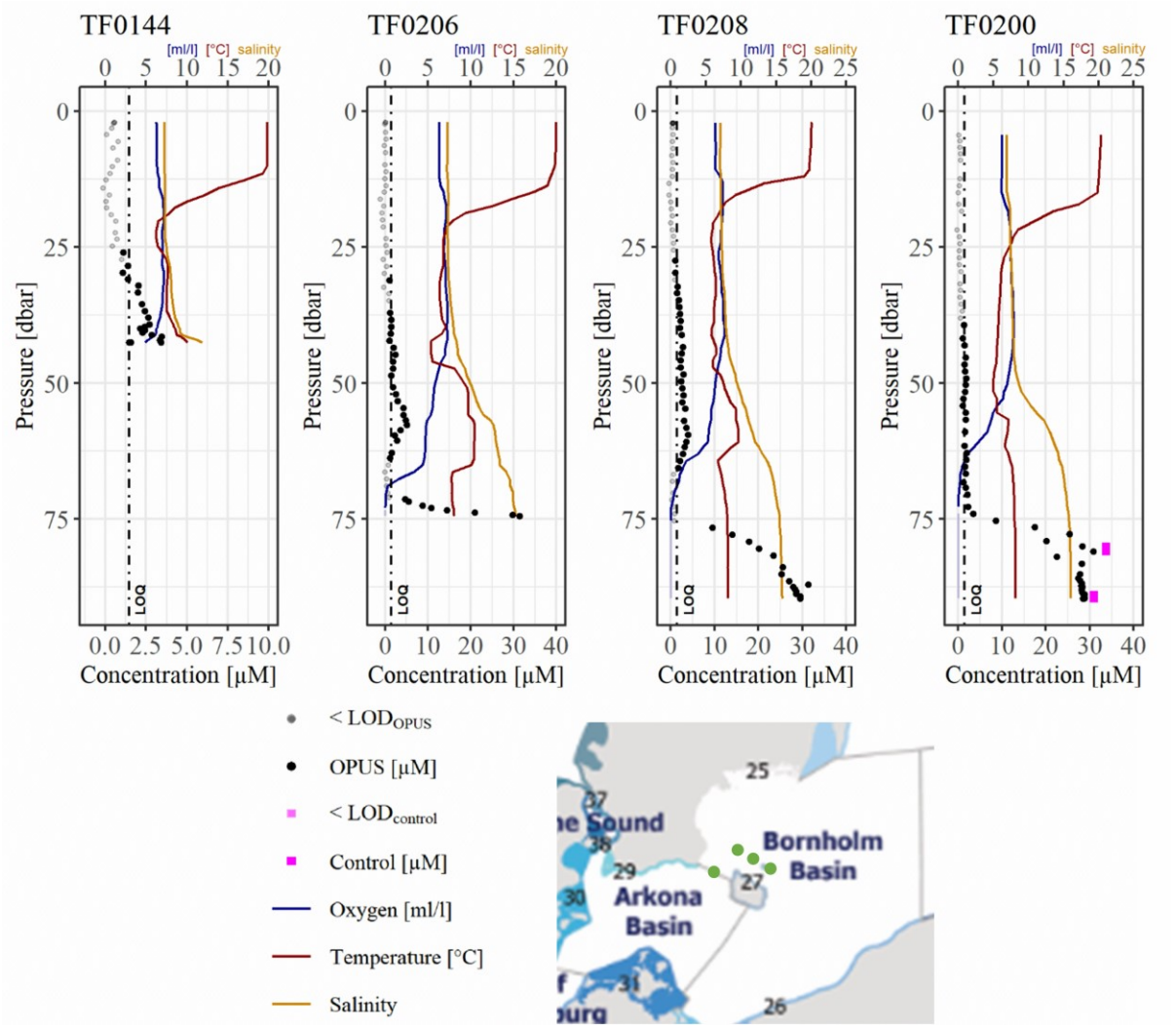

Figure 3.11. Profiles of total H_2S (OPUS [µM]) measured in July (EMB271) from west to north of Bornholm. Only station TF0200 had control measurements, although starting more than 40 m below the initial detection by the OPUS sensor, and almost 10 m below the initiation of the sharp total H_2S increase.

The Eastern Gotland Basin provided additional stations where a clear difference in vertical resolution between the control and OPUS data could be observed (**Figure 3.12**). At station TF0274 (on the edge of the southern continental slope before the Gotland Deep) in

March (EMB261) only three control measurements were taken. Similarly to what was observed at station TF0200 in July, the shallowest control point did not catch the onset of the increased sulfides. In addition, the OPUS data clearly showed that there was a local decrease in total H_2S between the 75 m (shallowest control point) and the approximately 120 m control point, which was not seen in the control data due to the lower resolution. This decrease stayed around the limit of quantification (LOQ), indicating a relatively strong connection between the peak formed between 75-100 m, and the continuous increase in the bottom waters (≥ 120 m).

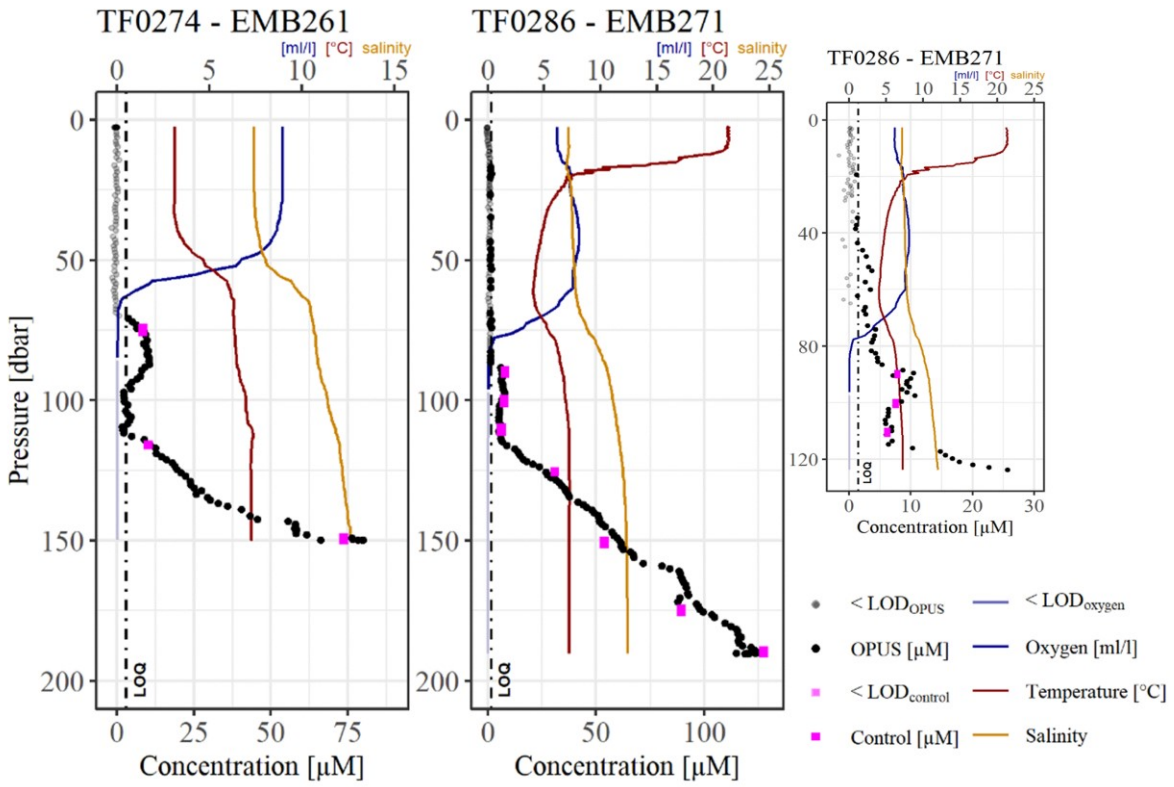

Figure 3.12. Two profiles in the Eastern Gotland Basin highlighting the difference in total H_2S between the control and OPUS data. The supporting oxygen, temperature, and salinity profiles are scaled to fit the plotting window, and should be read using the upper axis. Total H_2S is plotted on the lower x-axis.

On the other end of the Eastern Gotland Basin, at station TF0286 past the sill forming the northern boundary of the Gotland Deep, more control measurements were taken in July (EMB271). In contrast to the control measurements at station TF0274 in March (EMB261), controls at station TF0286 in July caught most of the extent of the local peak (**Figure 3.12**). The higher number of control measurements, and the lack of small-scale dynamics around 85-120 m gave similar outcome between the control and OPUS data. Nonetheless, looking closer at the shallower part of the profile as well as the deeper part (below 150 m), there are differences between the output from control patterns and OPUS data. In the shallower part of the profile, OPUS rendered concentrations above LOQ already around 40 m. In addition, the local total

H_2S peak at 90-100 m was a few µM higher for OPUS compared to control, which did not seem to have caught the absolute peak. In the lower part of the profile, OPUS measurements showed a dynamic pattern between the control measurements.

The difference in the spread of total H_2S between the OPUS and control method is also evident in **Figure 3.13**. The regions where total H_2S had been established by Feistel et al. (2016) in July 2021 were within the regions of the OPUS data. Noteworthy is that the OPUS data indicated a high total H_2S concentration between all three regions from the control data in the Eastern Gotland Basin (ca. 130 µM at station 272, and 55 µM at station 270), as well as a continuous total H_2S detection in the bottom waters all the way through to the southwestern Bornholm Basin. The OPUS measured concentrations between stations 224 and 253 in **Figure 3.13** (Bornholm Basin to southern Eastern Gotland Basin) are mainly low, although above the LOD at 1.03 µM. These values (except for two) are, however, below the control LOD at 2.36 µM.

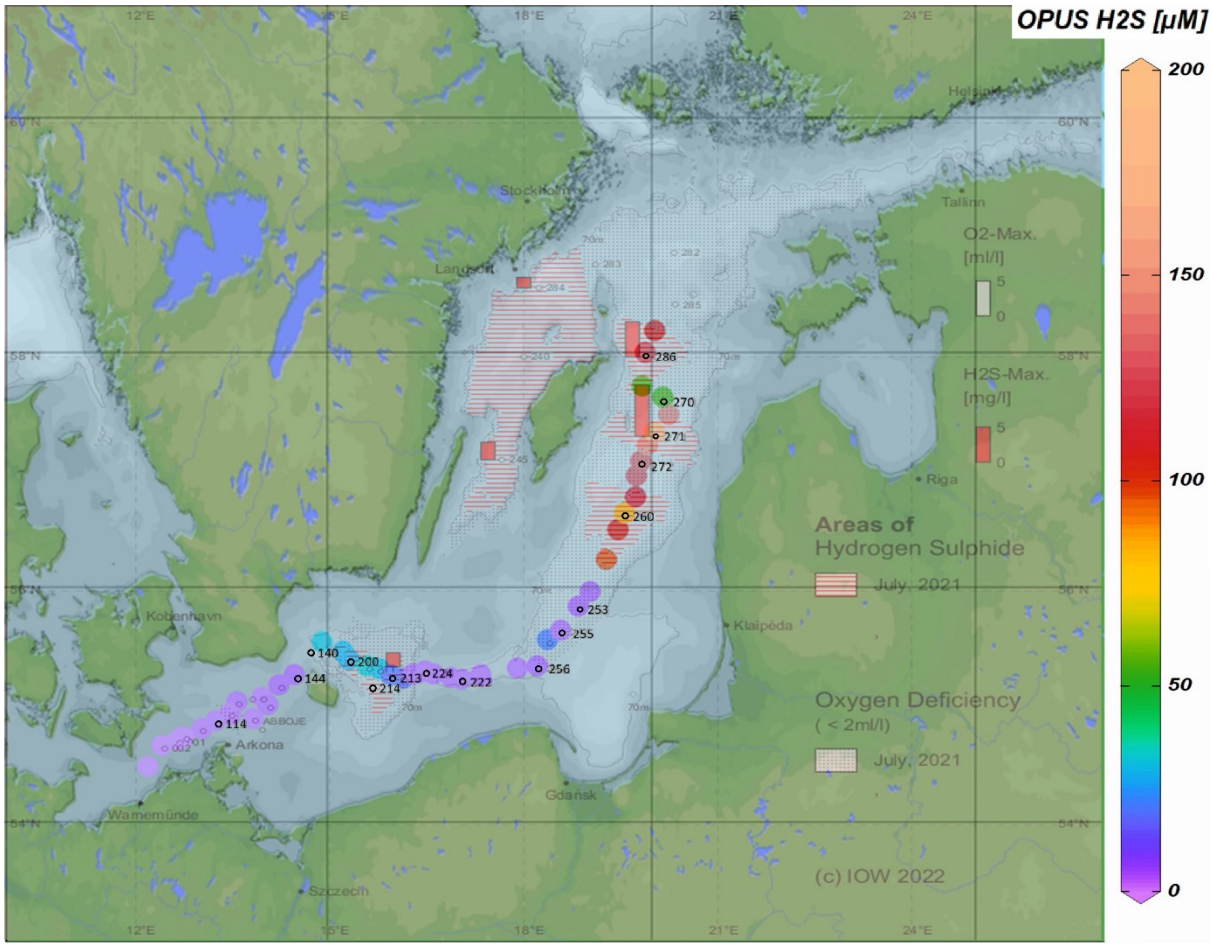

Figure 3.13. An overlay comparing the extent of total H_2S between OPUS (colored bar; µM) and control data (red staples and lined markings) in July 2021. The OPUS data are measurements from the deepest part of each cast and was put atop the map from Feistel et al. (2016), comprised of control measurements in "near bottom layer". The Western Gotland and the Northern Baltic Proper is not included. Purple 0-2.5 µM, dark blue 15-20 µM, light blue around 30 µM, green ca. 55 µM, yellow ca. 83 µM, and all varieties of red and beige above 95 µM. OPUS LOD was 4.31 µM.

3.2.4 High resolution (OPUS) total H_2S on spatial and temporal scales

The February (EMB256) and March (EMB261) data had low total H_2S concentrations in both Arkona and Bornholm Basin. Only 6 measurements were above total H_2S LOD in February (0.98-1.16 µM), and 3 in March (1.63-1.79 µM). However, none of these measurements was above total H_2S LOQ, as this limit was 1.75 µM and 3.15 µM, respectively. The first record of total H_2S above LOQ in either basins was therefore in May (EMB264), when the Bornholm Basin experienced concentrations up to 7.86 µM (LOQ = 6.60 µM). The bottom water of the Bornholm Basin was completely covered by sulfidic water in the July (EMB271) and November (EMB280) data (**Figure 3.14**), with station TF0213 measuring the highest concentration in both months (47.11 µM and 44.50 µM, respectively). In addition, traces of total H_2S were also measured at multiple stations in the Arkona Basin in July (up to 6.89 µM, LOQ = 1.45 µM**; Figure 3.14**). Only two such measurements were found above LOD in Arkona Basin in the November data (2.58 µM and 3.38 µM, LOQ = 2.95 µM).

Sulfidic water was present in a large portion of the Eastern Gotland Basin for all months investigated in 2021. Throughout the transect, sulfidic water was mainly found, but not limited to, below the oxygen limit (**Figure 3.15** and **Figure 3.17**). The spread of total H_2S from station TF0260, at the southern Gotland Deep trench, towards TF0259, at the beginning of the Eastern Gotland slope, had decreased from the February to March data. In addition, the valley seen at TF0260 in the February data was no longer seen in the March data. Rather, it would seem as the whole total H_2S profile had retracted toward the Gotland Deep, with the total H_2S valley, previously seen at station TF0260 in February, now being visible between stations TF0274 and TF0272 in March. The sulfidic bottom water emerged again towards the south in May, with station TF0262, situated between TF0259 and TF0260 at the southern edge of the sulfidic bottom water, having a strong gradient from OPUS LOD to 46.47 µM over the bottom 8 m of the water column. The same sharp increase could be observed in July. In summary, the sulfidic bottom water remained north of the 125 km mark for all cruises (**Figure 3.15**).

The overall highest concentration of total H_2S from the OPUS profiles was found in the bottom of the Gotland Deep for all months, with station TF0271 always giving the highest concentrations around 230-235 m. The February and March data had lower total H_2S concentrations in the Gotland Deep at 139 µM and 138 µM, respectively, compared to the other months. The increase of total H_2S in the Gotland Deep found in the May data (150 µM) had increased further in the July data (up to 193 µM). In the November data, total H_2S concentrations remained similar to the July data at 192 µM.

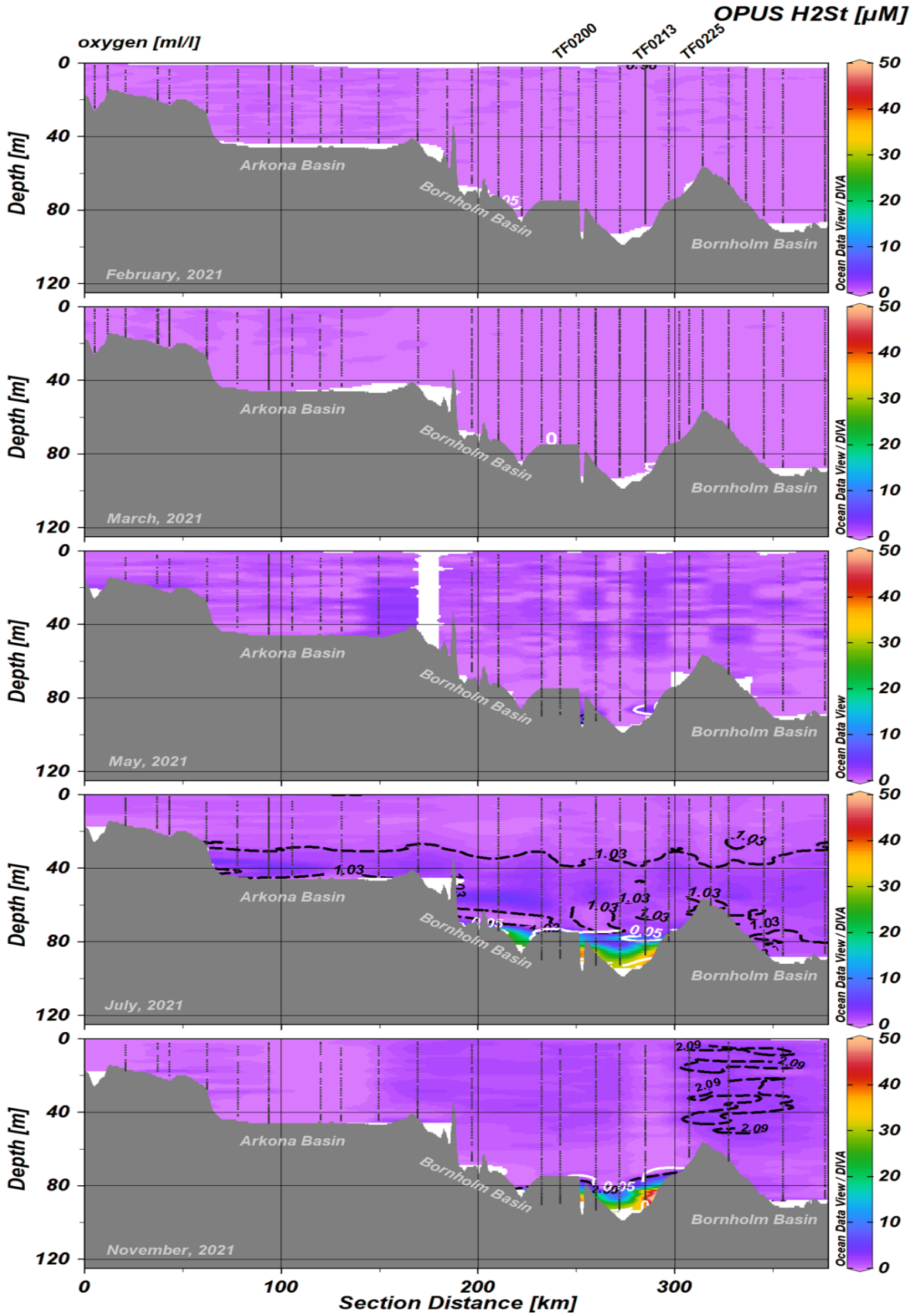

Figure 3.14. Transects from the five cruises showing the concentration of total H_2S from the OPUS sensor measurements (OPUS H_2St) from the Arkona and Bornholm Basin. White solid line indicates oxygen LOD. Black dashed lines indicate OPUS LOD along with the value for the respective months. If no black dashed lines are visible, there were no measurements above sensor LOD for that month.

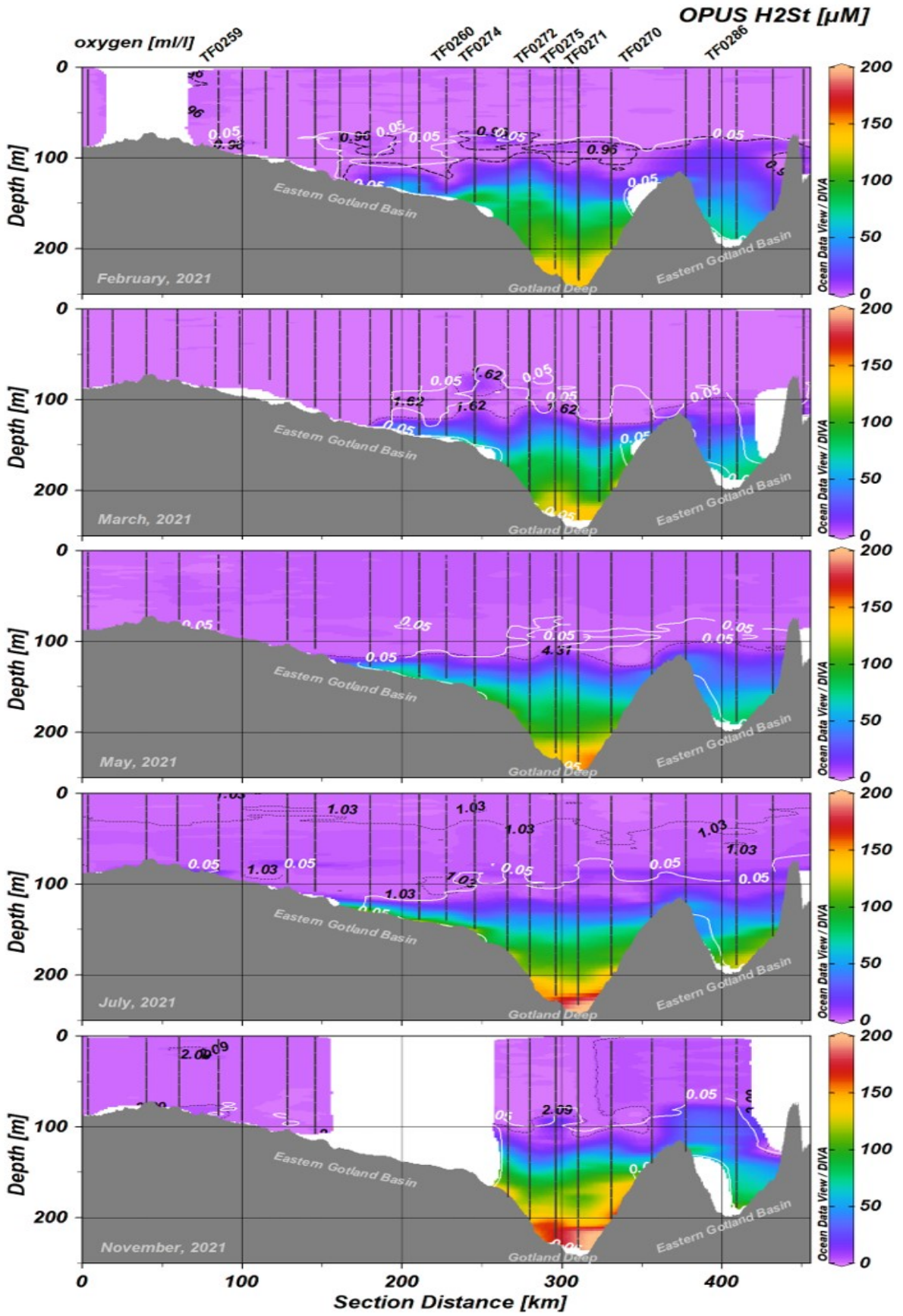

Figure 3.15. Transects from the five cruises showing the concentration of total H_2S from the OPUS sensor measurements (OPUS H_2St) in the Eastern Gotland Basin. White lines show oxygen sensor LOD, black dashed lines OPUS LOD for total H_2S.

Out of all five cruises, only the May data had an onset of total H_2S at approximately the same depth for all profiles in the Eastern Gotland Basin, around 120 m. All other cruises showed either plume structures (water masses with total H_2S separated from the sulfidic deep water) or breakoff phenomenon (areas with total H_2S that have a decrease in total H_2S, which connect to the sulfidic deep water) around the oxygen limit zone (oxygen LOD; **Figure 3.17**). Although the November cruise was highly affected by bad weather, rendering only 3545 measurements in total, the data not only caught a small plume around 450 km (onset of Eastern Gotland slope), but also indicated a second breakoff from the main sulfidic water around 675 km (above the Gotland Deep; **Figure 3.17**). The breakoff phenomenon was found in various areas in the February, March, and July data as well, mainly around 600 km (southern Gotland Deep trench) and 750 km (north of the Gotland Deep). The breakoffs were mainly between 75-100 meters, whereas any plumes could be found at even shallower depths (see section **3.2.5**).

The only occurrence of a total H_2S plume in either the Arkona or Bornholm Basin occurred in July (green areas in **Figure 3.16**). In fact, both basins experienced a plume, separated from one another and the sulfidic bottom water. The first plume began at the sill in southern Arkona Basin and stretched across approximately half of the main Arkona Basin. The plume started around 34 m depth and continued down to 45 m with a maximum total H_2S concentration of 6.89 µM. The second plume was found in the western part of the Bornholm Basin. The exact onset of the plume is difficult to determine due to the low number of profiles in the area, however, the available profiles indicate that the plume stretched between 51-63 m. Station TF0206 (Bornholm Basin) was situated in the main part of the second plume and total

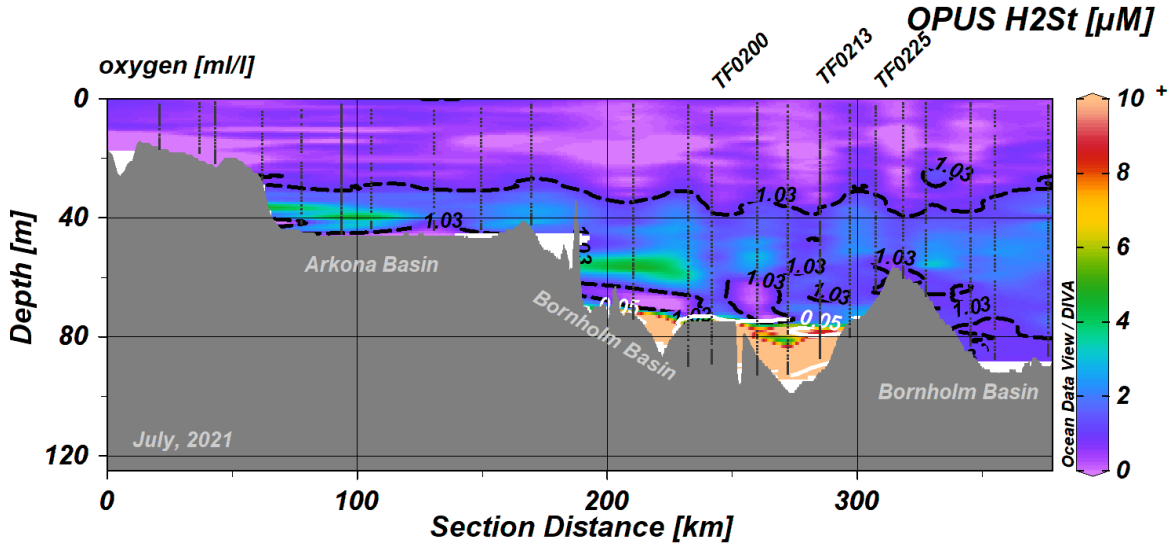

Figure 3.16. Highlight of plume structures (green) of total H_2S (OPUS H_2St) seen in the Arkona Basin and Bornholm Basin in July 2021 (EMB271). Black dashed lines show OPUS LOD for total H_2S and white solid lines oxygen LOD.

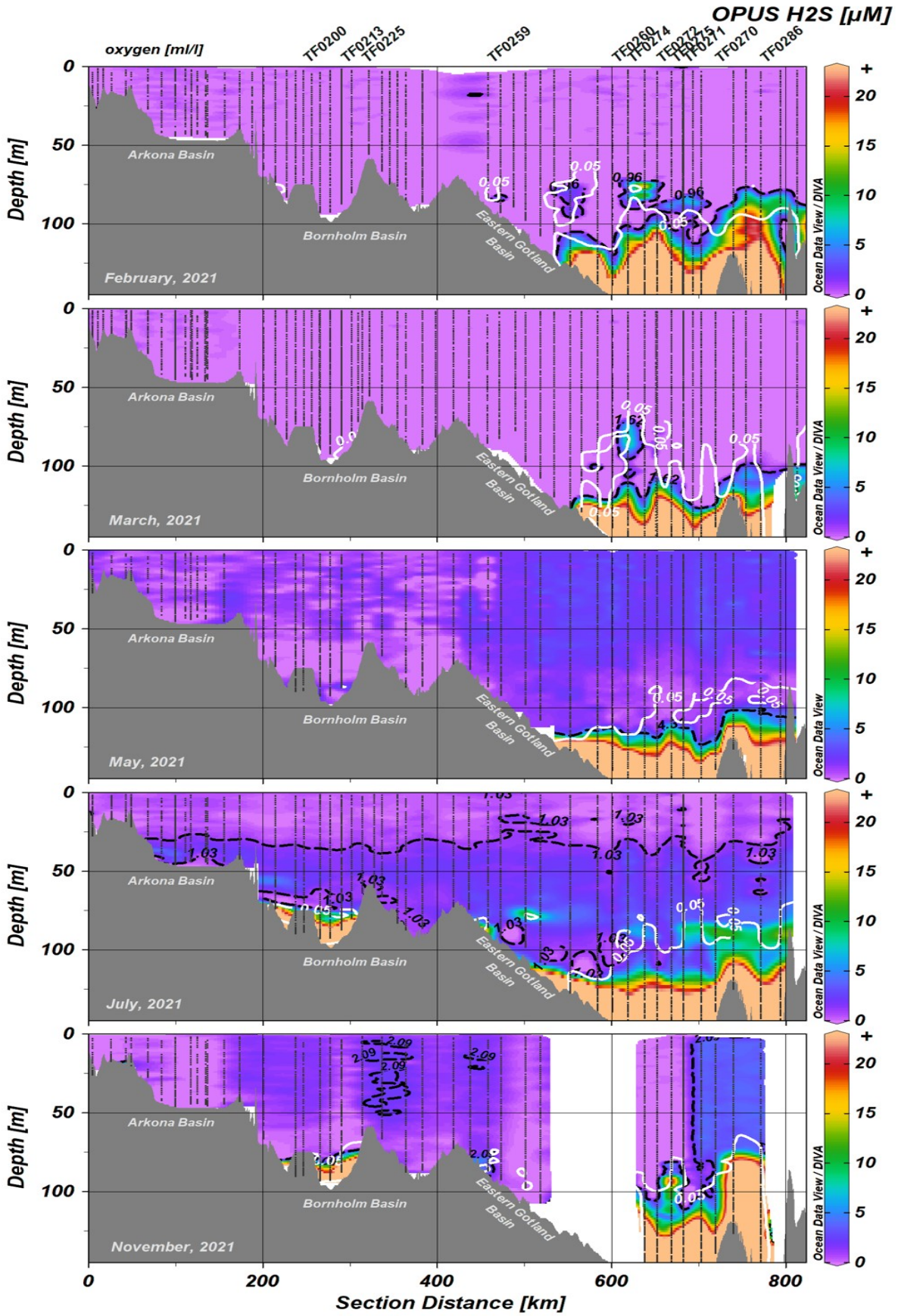

Figure 3.17. Transects from the five cruises highlighting the total H_2S concentrations from the OPUS sensor measurements (OPUS H_2St) around the chemocline. Black dashed lines indicate OPUS LOD for total H_2S, white solid lines oxygen sensor LOD.

H_2S concentrations were measured up to 5.12 µM. Since only two casts were taken – none of which were near the sill between the Arkona and Bornholm Basin – it could not be determined if this plume was a result from a natural release from e.g. sediments or originating elsewhere.

3.2.5 Co-occurrence of oxygen and total H_2S

This section investigates the natural occurrence of total H_2S, measured using the OPUS sensor, and oxygen, measured with an oxygen sensor on the CTD (see details in **3.2.2**). In most cases, the oxygen LOD was found at shallower depths than OPUS LOD for total H_2S (**Figure 3.15**), however, tendencies of overlap or a close relationship between the two LOD depths were also observed.

A first record of total H_2S within the sub-oxic zone in the Arkona and Bornholm Basins was recorded in February (**Table 3.8**). In total, six measurements were found above OPUS and oxygen LOD in February; however, none was above OPUS LOQ. The March and May data showed the same pattern. In March, three measurements were above OPUS and oxygen LOD, and in May, this number was four; again, none above OPUS LOQ (**Table 3.8**). It was not until July that more measurements were above OPUS and oxygen LOD in the Arkona and Bornholm Basins. In total, 492 measurements were above this limit, of which 310 measurements were also above OPUS LOQ (**Table 3.8**). The November data had again far less measurements above OPUS and oxygen LOD with 38 measurement, of which eight were above OPUS LOQ (**Table 3.8**).

Figure 3.18 shows five profiles from the Arkona and Bornholm Basins in July where total H_2S and oxygen was co-occurring. The stations were chosen to highlight the plume formations found in the Arkona and Bornholm Basins. Station TF0113 includes three casts from two different days.

Table 3.8. Number of OPUS measurements ($\mathbf{N_{total\ H_2S}}$) within the oxic/sub-oxic zone ($O_2 \geq 0.05$ ml/l) in the Arkona and Bornholm basin for each cruise.

Month	Cruise	Basin	$N_{total\ H_2S}$ in oxic/sub-oxic zone	
			Above total H_2S_{OPUS} and O_2 LOD	Above total H_2S_{OPUS} LOQ and O_2 LOD
February	EMB256	AB, BB	6	0
March	EMB261	AB, BB	3	0
May	EMB264	AB, BB	4	0
July	EMB271	AB, BB	492	310
November	EMB280	AB, BB	38	8

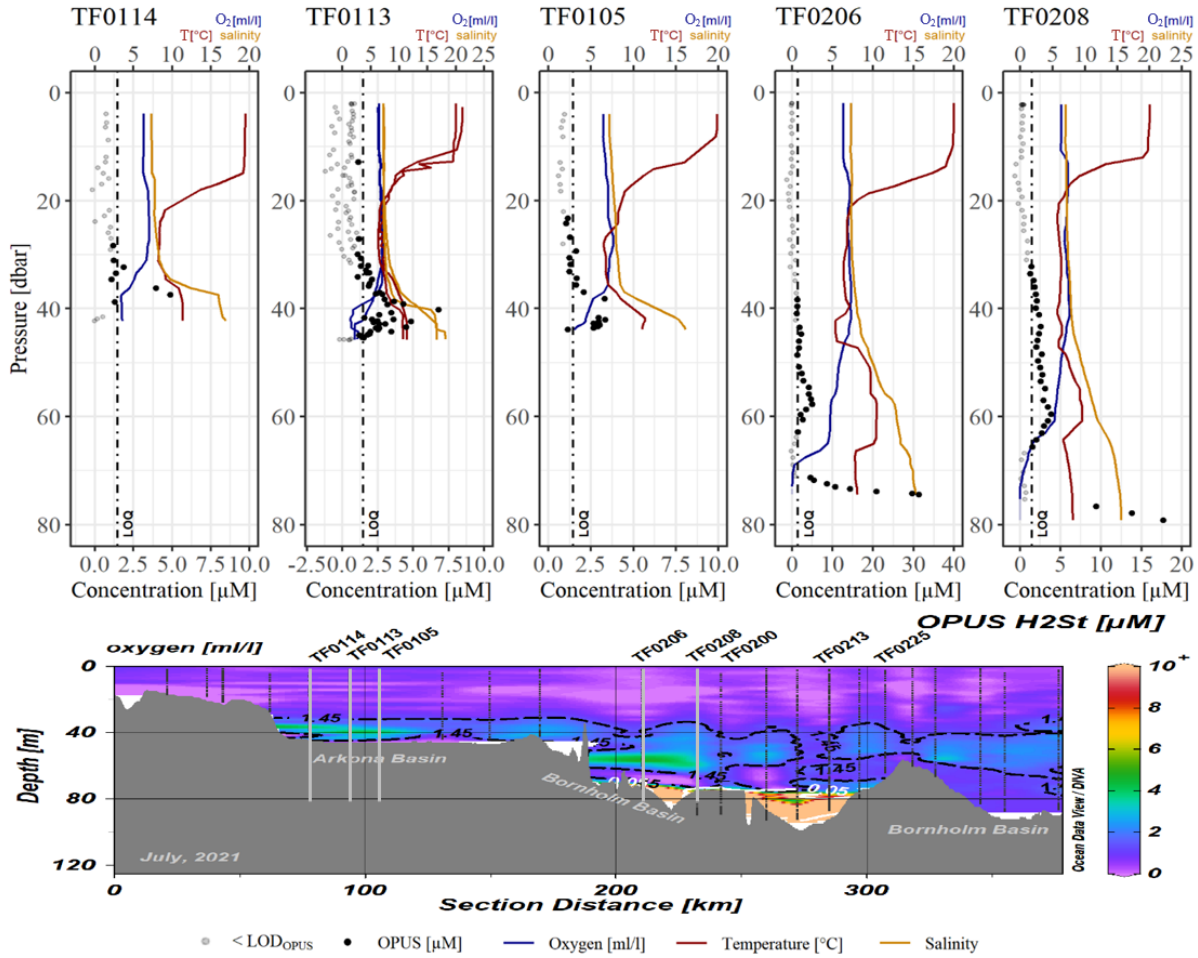

Figure 3.18. Profiles of total H_2S (OPUS [µM]) plumes in the Arkona Basin (first three) and the Bornholm Basin (TF0206 and TF0208) in July, 2021. The grey lines in the transect highlight the position of the profiles in order of appearance. Black dashed lines in the transect highlight OPUS LOD and the transect color shows the total H_2S concentration (OPUS H_2St).White solid line in the transect highlight oxygen LOD.

The large number of OPUS measurements above the LOD in the oxic/sub-oxic interface in the July data were spread relatively homogenous throughout the transect at 30-80 m depth (**Figure 3.16** and **Figure 3.18**). Two plume like structures, comprised of water masses with higher sulfidic concentrations than their surroundings, were also detected within this region. One of these plumes was found in the Arkona Basin, starting around 34 m depth and continuing down to 45 m with a maximum total H_2S concentration of 6.89 µM where oxygen was 1.92 ml/l (TF0113; **Figure 3.18**). It would require 0.31 ml/l oxygen to oxidize the amount of sulfides (going by the conversion from H_2S to negative oxygen by Fonselius (1981); 1 µM H_2S = -0.04478 ml/l O_2), and more than six times this amount was available, yet, total H_2S was measurable. Station TF0206 (Bornholm Basin) was situated in the main part of the second plume where up to 5.51 µM total H_2S was recorded at 72 m where oxygen was 0.07 ml/l (**Figure 3.18**). The level of oxygen available would not have been enough to oxidize the

sulfides, as 0.25 ml/l O_2 would be required. The local plume peaks found at stations TF0206 and TF0208 around 55-60 m were measured ca. 12-15 meters above the oxygen LOD. For the stations situated in the plume in the Arkona Basin, oxygen concentrations never went below LOD of 0.05 ml/l.

In contrast to the Arkona and Bornholm Basins, total H_2S was measured above the oxygen LOD for all months in the Eastern Gotland Basin; and exceeded total H_2S LOQ for all months except May (**Table 3.9)**. The number of measurements containing total H_2S within the oxic/sub-oxic zone ($O_2 \geq 0.05$ ml/l) far exceeded those in the Arkona and Bornholm basins. The July cruise had once again the highest number of total H_2S measurements within the oxic/sub-oxic zone, followed by the November cruise.

The Eastern Gotland Basin had multiple plumes around and above the oxygen LOD in the February data (**Figure 3.19**). One such plume of total H_2S was above the oxygen LOD at the southern Gotland Deep trench around station TF0274, with a large breakoff section of sulfidic water connected to the deep waters close by (stretching across the width of the Gotland Deep). In the plume between stations TF0274 and TF0272 at ca. 70-90 m depth, 3.37 µM total H_2S was measured (LOD = 0.96 µM, LOQ = 1.75 µM) when oxygen was 0.29 ml/l. To oxidize the total H_2S, a concentration of 0.15 ml/l O_2 would have been needed, less than what was available. In addition, for this particular plume, the maximum total H_2S concentration where oxygen was still detectable was 15.1 µM (O_2 = 0.06 ml/l). Here, not enough oxygen was available to oxidize all sulfides, as 0.68 ml/l O_2 would have been needed. The large section of sulfidic deep water in the northern part of the Eastern Gotland Basin had an onset when the oxygen sensor started to measure close to the LOD. However, it was not until ca. 25 m below this onset that the oxygen sensor continuously measured below LOD.

Table 3.9. Number of OPUS measurements ($\mathbf{N_{total\ H_2S}}$) within the oxic/sub-oxic zone ($O_2 \geq 0.05$ ml/l) in the Eastern Gotland basin for each cruise.

Month	Cruise	Basin	$N_{total\ H_2S}$ in oxic/sub-oxic zone	
			Above total H_2S_{OPUS} and O_2 LOD	Above total H_2S_{OPUS} LOQ and O_2 LOD
February	EMB256	EGB	32	15
March	EMB261	EGB	28	16
May	EMB264	EGB	12	0
July	EMB271	EGB	980	826
November	EMB280	EGB	311	249

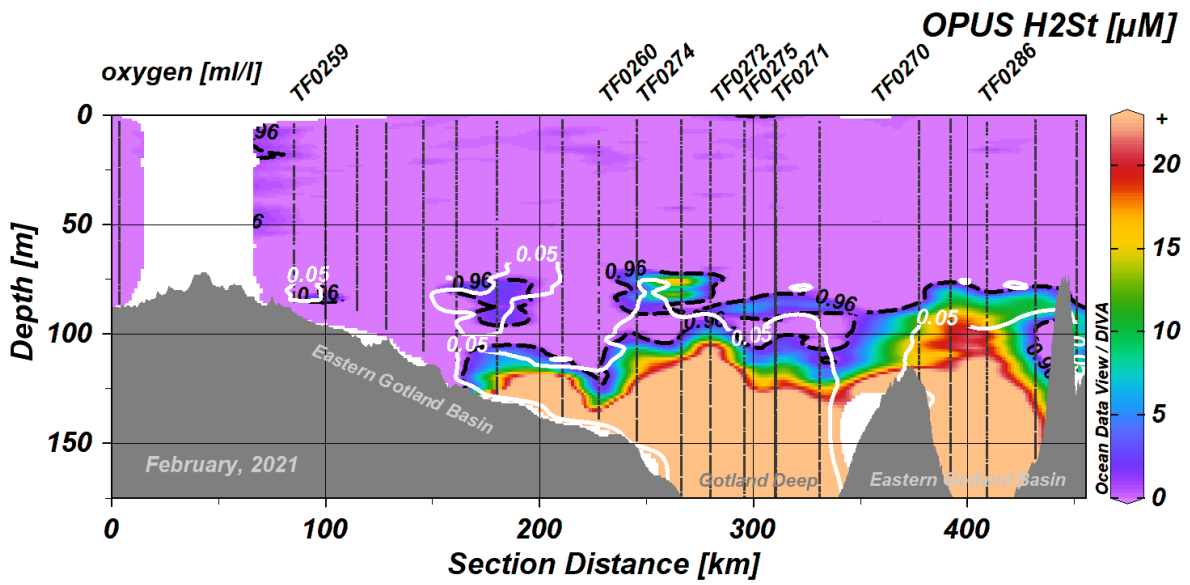

Figure 3.19. Total H_2S (OPUS H_2St) around the chemocline in February 2021, from OPUS measurements. Oxygen LOD displayed by solid white line and OPUS LOD for total H_2S by dashed black lines. For better visualization, total H_2S concentrations above 23 are all falling under the plus sign, colored light orange.

The March data had fewer plume structures compared to the February data (**Figure 3.20**), although, station TF0274 was still influenced by a plume. The onset of this plume was around 70 m depth, where oxygen was 0.07 ml/l, and extended for ca. 27 m. The oxygen sensor recorded values at or above LOD for the upper 20 m of this plume. The plume seemed to have two peaks of total H_2S. The first peak was found at 79 m where total H_2S was 8.39 µM and oxygen 0.06 ml/l. The second peak was found at 87 m where total H_2S was 9.27 µM and oxygen 0.05 ml/l. In both cases, the oxygen concentration was too low to oxidize the total H_2S as up to 0.38 ml/l and 0.42 ml/l O_2 would have been needed, respectively. Traces of total H_2S were also found at the oxygen LOD south of station TF0260 over the Eastern Gotland slope, where a larger plume area was visible in February. Here, only one total H_2S measurement was found above OPUS and oxygen LOD, measuring 4.44 µM total H_2S and 0.05 ml/l O_2. Up to 0.20 ml/l O_2 would have been needed to oxidize the sulfides. These traces were found ca. 4 m below the bottom part of the February plume, and ca. 22 m below the peak of the February plume (3.15 µM total H_2S at 78 m).

The July data, similar to the February and March data, showed plumes of total H_2S around or close to the oxygen LOD, as well as several hundred measurements of lower H_2S concentration in the oxic zone (**Figure 3.21**). The main sulfidic water mass (excluding the plumes) in the Eastern Gotland Basin, however, rarely extended above 100 m depth for any cruise.

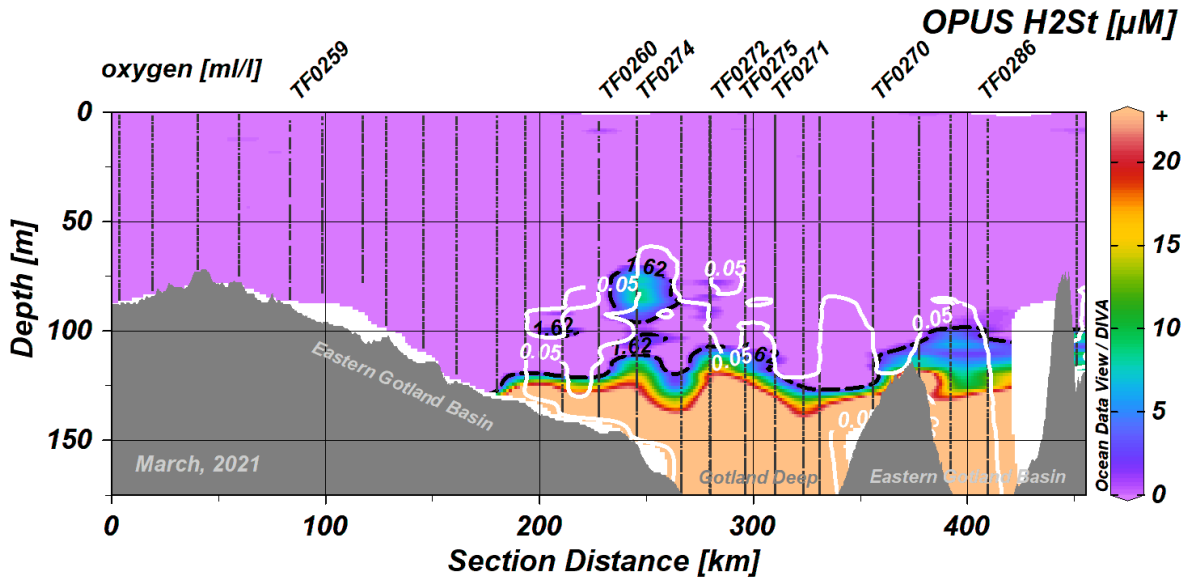

Figure 3.20. Plumes of total H_2S (OPUS H_2St) in the Eastern Gotland Basin in March, 2021. Oxygen LOD displayed by solid white line and OPUS LOD for total H_2S by dashed black lines.

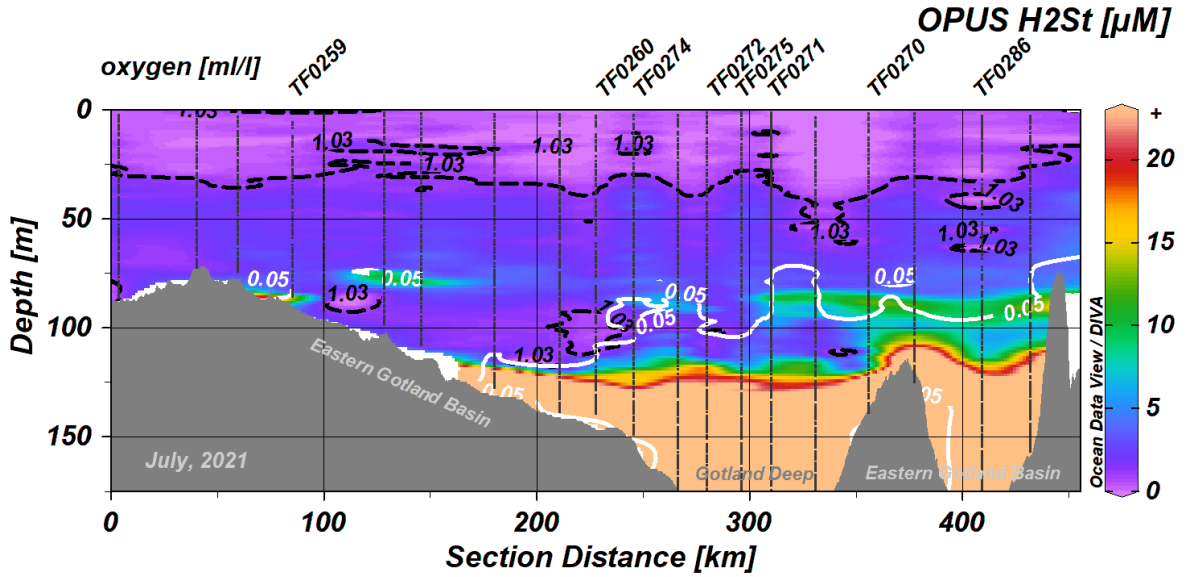

Figure 3.21. Highlight of total H_2S (OPUS H_2St) around the redox cline in July 2021, from OPUS measurements. Oxygen LOD displayed by solid white line and OPUS LOD for total H_2S by dashed black lines.

The widest plume for any of the months in the Eastern Gotland Basin was in July, around 80 m water depth, stretching from the Gotland Deep to the northern side of the Eastern Gotland Basin (**Figure 3.21**). Another total H_2S plume and elevated total H_2S concentrations were found at the same depth (80 m) over the Eastern Gotland slope and close to the sediments at the sill leading to the Bornholm Basin (at ca. 50 km in **Figure 3.21**).

Figure 3.22 shows five profiles within the plume structures in July. For all stations, a clear decrease in total H_2S could be observed below the first main increase around 80 m. Apart

from station TF0253, measurements never dropped below LOD, suggesting that the plume was never completely separated from the main sulfidic deep water mass. Between stations TF0270 and TF0277, a sharp gradient starting at about 80 m went from ca. 4 µM to 13 µM at 90 m. At the same depths, oxygen went from ca. 0.8 ml/l to 0.05 ml/l, with one measurement at the onset at station TF0286 of 0.13 ml/l. The generally low oxygen concentration at the onset of this large plume would not have been enough to oxidize the total H_2S. To oxidize 4 µM total H_2S, ca. 0.18 ml/l O_2 would be needed.

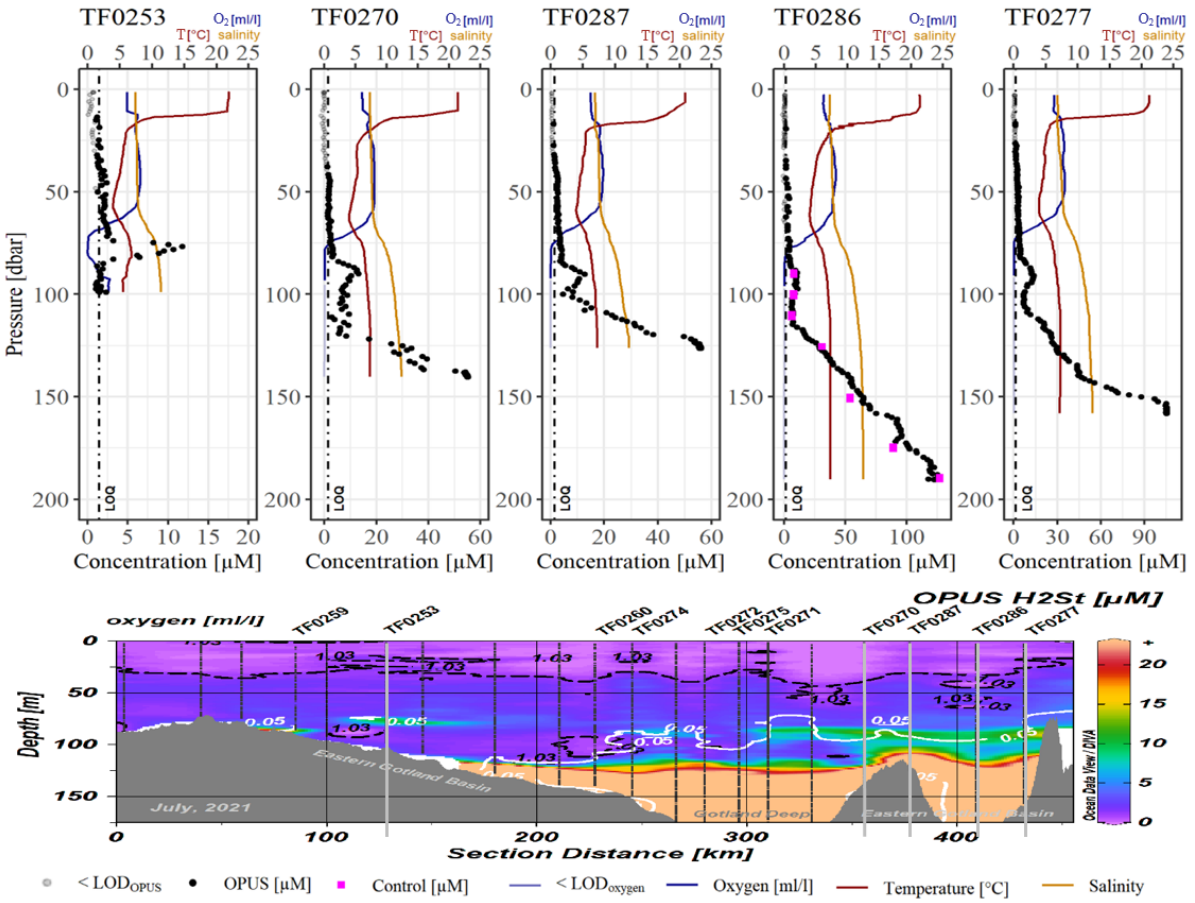

Figure 3.22. Profiles and transect of the chemocline in July 2021 showing plume structures above and around the oxygen LOD (white lines). Black dashed lines in the transect show OPUS LOD and color shows total H_2S concentrations from the OPUS data (OPUS H_2St). White solid line show oxygen LOD. Grey vertical lines in the transect show where the stations are positioned in order of the profiles.

The highest measured total H_2S concentration where oxygen was measurable in July was at 91.0 m on station TF0277, where total H_2S reached 13.6 µM and oxygen was found to be 0.05 ml/l (**Figure 3.22**). To oxidize this amount, 0.61 ml/l O_2 would be needed. In November, the same maximum was found at 97.3 m on station TF0271, where total H_2S was 5.12 µM and oxygen 0.06 ml/l. Here 0.23 ml/l O_2 would be needed. The maximum total H_2S concentration where oxygen was present was found at mid-depth also in the February and

March data, 76 m and 82 m, respectively. In February, 15.1 µM total H_2S was measured where oxygen was 0.06 ml/l, a total H_2S concentration which needs 0.68 ml/l O_2 to oxidize. In March, the concentration of total H_2S was lower, 9.05 µM, needing 0.41 ml/l O_2. However, only 0.05 ml/l O_2 was recorded. The May data had the shallowest depth where total H_2S and oxygen co-occurred at 3.5 m. Here 5.37 µM total H_2S was measured where oxygen recorded 8.87 ml/l. The 0.24 ml/l O_2 needed to oxidize the total H_2S is well within the limits of available oxygen, raising concerns for the accuracy of this measurement given the high LOD (4.31 µM). A closer look at the spectra recorded at the same depth showed that the aforementioned measurement diverted from the others (**Figure 3.23**). The reason for this discrepancy remains unclear; however, the observed change in spectral shape around 230 nm provided sufficient evidence to conclude that a higher total H2S concentration was present. Consequently, while the spectrum is distinct from the others in this location, the fitted concentration cannot be disregarded.

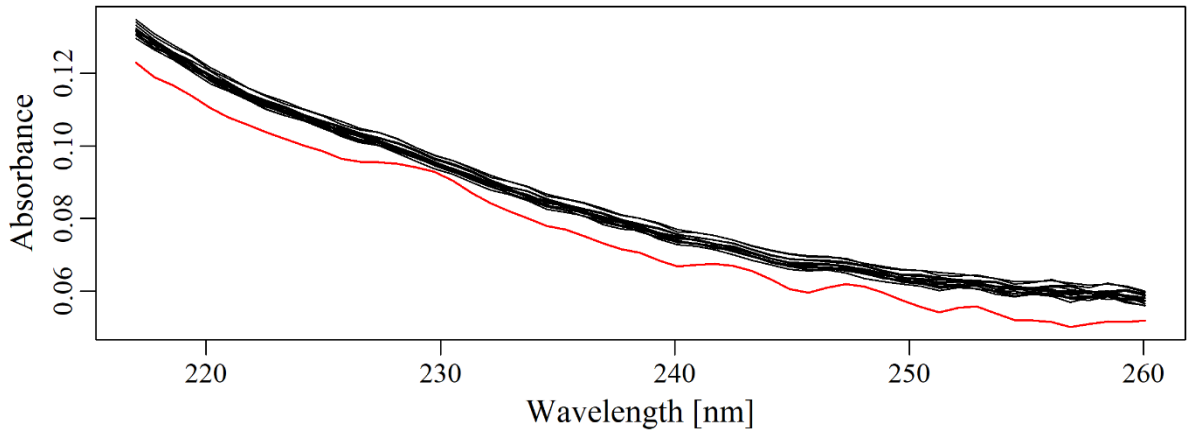

Figure 3.23. Absorbance spectra taken at 3.5 m where the shallowest total H_2S was found in May 2021. The red line is the spectrum that rendered 5.37 µM total H_2S. All black lines rendered total H_2S concentrations between 1.53 and 2.81 µM, all below cruise LOD (4.31 µM).

3.2.6 Relevance of total H_2S in the Baltic Sea

Up until now, the plausible spread of total H_2S has been estimated by looking at the spatially limited control data and linking them to sill locations, oxygen concentrations, and the smell of water samples. Feistel et al. (2016) raised the concern that historical data, which sometimes is of qualitative nature (e.g. presence of smells typical for H_2S), cannot be translated into quantitative measurements needed to fully understand the functioning of sulfidic systems, and where they occur. The limited number of measurements that is possible to make using the classical wet chemical approach also poses a significant risk at missing smaller patterns of total H_2S distribution. In addition, hydrogen sulfide concentrations are often presented as negative

oxygen or oxygen debt, and symbolize the amount of oxygen needed to oxidize the sulfide species before measureable oxygen can be acquired. This can lead to the interpretation that oxygen is unmeasurable where total H_2S is present. However, as pointed out by Avrahami and Golding (1968), hydrogen sulfide has a half-life of ca. 20 minutes when oxygen concentrations are as high as 3.8 ml/l, which would be above the sub-oxic zone. Here, the total H_2S was purposefully not reported as negative oxygen, as the intention was to investigate if both compounds could be detected simultaneously. The high-resolution OPUS data presented in this chapter has given a unique insight into the distribution of total H_2S, and proven the existence of total H_2S plumes within the low oxygen zone (LOZ); a phenomenon especially observable in the Eastern Gotland Basin.

The difference in resolution between the OPUS sensor and the discrete measurements for controls did not only shed light on the dynamic upper layer of total H_2S in relation to oxygen, but also showed how the internal structures of total H_2S changed over depth for each month studied. Potential oxygen intrusions below 100 m, an area signified as the stratification zone, have been discussed in literature (e.g. Hietanen et al., 2012; Kamyshny et al., 2013; Holtermann et al., 2020), and evidence of the same phenomenon has been uncovered here. Going back to **Figure 3.10** and **Figure 3.17** and comparing the oxygen LOD to the total H_2S LOD, an intrusion of oxygen into the sulfidic zone below 100 m (close to station TF0260) was seen from the OPUS data in February, but not from the control data. In addition, the OPUS data, compared to the control data, showed multiple plumes of total H_2S around and above the oxygen LOD. The figures also show that intrusions of oxygen found in single profiles might just be a characteristic in that particular area, and separation could be found close by. In addition, this demonstrates that limited oxygen and total H_2S co-existence does occur in the Baltic Sea, and is not restricted to the open ocean or the Black Sea (e.g. Sorokin, 1972; Luther & Tsamakis, 1989).

As pointed out by Kelley et al. (2016), species of fish had different gene expressions depending on the concentrations of sulfides in their environment. The species studied there, however, all lived in environments that were classified as either sulfidic or non-sulfidic areas, meaning the species were under similar stress at all times. However, here the high-resolution OPUS H_2S data showed that the extent and concentration of total H_2S in the Baltic Sea changed over various time scales; not only over months with the five cruises, but also between days or even hours on the same station. This level of diurnal variance requires the organisms to have a rapid response system, similar to the one reported in the soil amoeba by Lloyd (2006), where a rapid increase in H_2S caused some of the electron pathways to be shut down, while others

remained open, or the alternative oxidase (AOX) pathway reported in a lugworm (Tobler et al., 2016), which can maintain its activity also under the influence of H_2S (see also **Table 3.10**). A response system or ability to change gene expression could be a solution for organisms that are under either periodic sulfidic influence or mobile enough to seek out areas with less sulfides.

Anoxic marine zones, areas signified by oxygen concentration in the nM region and below, have been found to be inhabited by anammox bacteria, while regions with higher oxygen levels in the vicinity were dominated by bacteria that aerobically oxidize ammonium to nitrate (Ulloa et al., 2012). The nitrification and de-nitrification processes are tightly coupled to the oxygen levels, but not much is known about the influence of sulfides when oxygen is present. Berg et al. (2015) conducted an experiment on a branch of the ammonia-oxidizing archaea found in the Baltic Sea, phylum *Thaumarchaeota*, where samples collected from the Gotland Deep area were spiked with sulfides. The results showed that the nitrification process was significantly reduced after adding 4.1 µM of H_2S, and in most samples halted after adding 8.3 µM of H_2S. In February 2021, the first cruise for this thesis and the cruise with the highest total H_2S concentration within the sub-oxic zone, total H_2S reached a maximum of 15.1 µM. This concentration would be enough to stop any nitrification process by the ammonia-oxidizing archaea. Nonetheless, the majority of the measurements containing total H_2S within the sub-oxic zone in February (85%) was at or below 4.1 µM; at which concentration the nitrification process was only reduced (Berg et al., 2015). The only exception regarding the 4.1 µM threshold was in May where all measurements above total H_2S LOD in the oxic/sub-oxic zone were between 4.1 and 8.3 µM total H_2S; at which concentration the nitrification process had stopped in most, but not all samples (Berg et al., 2015). As plume structures changed over time, free-floating microorganisms may have maintained nutrient cycling despite the periodic increase in sulfides. Furthermore, the SQR pathway in mammalian colonocytes can efficiently detoxify up to 10 µM H_2S (Tobler et al., 2016), providing temporary protection from sporadic plume structures. Nonetheless, as summarized by Carstensen and Conley (2019), persistent hypoxia (< 2 ml/l O_2), which is coupled to the concentration of total H_2S, leads to a decline in the macrofauna diversity, and may not be able to recover unless aided by undisturbed communities in the vicinity. The macrofauna diversity is one of the corner stones for a sustainable environment, and a loss in biodiversity could affect other trophic levels in the system, as degradation and burial of nutrients may be reduced.

Increasing hydrogen sulfide concentrations have been reported for the Baltic Sea over the last century (Fonselius & Valderrama, 2003; Feistel et al., 2016), and the ecosystem effects of sulfidic waters are an important issue for HELCOM (in the context of oxygen debt;

HELCOM (2023)). Throughout the year presented in this chapter, total H_2S increased. The difference in total H_2S concentrations between the March/May and July/November data aligns with previous findings in the Baltic Sea (Perner et al., 2022). However, this increase cannot be linked to sensor drift as the data was corrected on control values. Further research is needed to know if the increase is due to inter-annual variability, or if it is following the trend shown by e.g. Fonselius and Valderrama (2003).

Table 3.10. Summary of literature on effects and use of the sulfur cycle and its components.

Keyword	Effects	Area studied	Reference
Sulfur cycle	Sulfate assimilation is vastly done by phototrophic organisms; Sulfate reducing bacteria; diurnal H2S release;		Hansen et al. (1978); Sievert et al. (2007); Kamyshny et al. (2013); Deng et al. (2018); Hu et al. (2018); Dahl (2020)
	Upwelling and plume formations in OMZ supports chemolitoautotrophs	Peru	Schunck et al. (2013)
	Sources and sinks	Remote oceanic atmosphere and open ocean	Shooter (1999)
	Higher anaerobic and aerobic sulfide oxidation rates than abiotic rates	photo- and chemolitotrophs	Sorokin (1972); Luther et al. (2011)
	magnetotactic bacteria as sulfide shuttle	Lake Yuqiao	Li et al. (2020)
H_2S	Toxicity: Spread, metabolism		Evans (1967); Beauchamp et al. (1984); Guidotti (1996); Kabil and Banerjee (2010)
	Protection against toxicity	Soil amoeba	Lloyd et al. (1981)
	Electron donor; signaling molecule	chemo-/photolitotrophic bacteria, yeast, higher organisms, humans	Lloyd (2006); Olson and Straub (2016); Giuffrè and Vicente (2018); Dahl (2020)
	Pathways for production and catabolism	Metazoans and higher organisms	Olson and Straub (2016); Tobler et al. (2016)
	Temporal variability	Gulf of Finland	Kankaanpää and Virtasalo (2017)
Sulfides	Adaptation; evolution	Crustacea, Ostracoda; fish, fungi	Jahn et al. (1996); Martin et al. (2003); Kelley et al. (2016)
	History		Szabo (2018)
Hypoxia	Release of N and P; Biomass loss	Baltic Sea	Diaz and Rosenberg (2008); Conley et al. (2009); Carstensen and Conley (2019)

CHAPTER 4. CONCLUSIONS

This thesis has investigated 1) which regression method would be most suitable to use for detecting total H_2S using the OPUS UV sensor in the Baltic Sea, and 2) the spatial and temporal distribution of total H_2S along a transect going from the Arkona Basin to the Eastern Gotland Basin.

The initial results showed that the accuracy of the OPUS sensor in relation to wet chemistry control data was relatively good when measuring total H_2S (free H_2S + HS^-) using a derived background spectrum (ISD) from field samples of known total H_2S and NO_3 concentrations. In fact, the limit of detection for total H_2S was lower for this method compared to the wet chemistry control method (on average 1.99 µM ± 0.93 µM vs. 2.36 ± 1.52 µM). Although the limit of detection was higher for the other three methods (between 6.87 µM and 16.45 µM; SD between 0.87 µM and 1.20 µM), the average relative error to control was smaller for the linear (ISL) and poly-4 (ISP) methods (-1.7% and -3.4%, respectively) compared to the derived method (-18.1%). The quadratic method (ISQ) had the highest average relative error to control at 30.8%.

Improvements were made to the accuracy of the OPUS data when correcting the processed total H_2S on a median offset, as well as on the slope between these corrected values and the controls. The Kruskal-Wallis rank sum test showed that the results from the ISD, ISP, and ISQ methods were different to their uncorrected counterpart, and further investigation showed that the outcomes had improved. When applied, the greatest improvement in the relative error to control was found for the ISQ method, which decreased the error by 97.08% from its original value (to 0.9%). The ISD method also displayed a large decrease of 88.95% from its original value (to -2.0%). Despite the improvements observed for the ISQ method, the SD remained large compared to the other methods (56.9% or 7.23 µM compared to the best method ISD at 46.8% or 6.35 µM). Nevertheless, the Kruskal-Wallis rank sum test could not find any difference between the corrected data and control for any of the methods. The overall improved result of the ISD method, as well as the fact that the derived background spectrum can account for seasonally variable unknown components in the water column, was the reason for selecting this method for the second part of this thesis.

The spatial and temporal investigation of total H_2S from the high-resolution OPUS data revealed several plumes of total H_2S within or close to the oxic/sub-oxic zone. In addition, the main sulfidic deep waters had a much more dynamic upper layer than previously seen from the control data. When comparing the distribution of sulfidic bottom water from the control data

(maps generated by “near bottom” control samples) to the OPUS measured profile data, it became evident that the extent of sulfidic bottom water differed. Most of the Eastern Gotland Basin was covered in sulfidic water according to the OPUS data, whereas the computed maps from the control data indicated that there were three areas with total H_2S, separated from one another.

The higher resolution in the OPUS data has not only allowed for a better understanding of the spatial distribution of sulfidic deep wasters, but also shown co-occurrence of total H_2S and oxygen. The July cruise was especially affected in all three basins, whereas the February, March, May, and November cruises mainly displayed such characteristics in the Eastern Gotland Basin. Only scattered measurements of total H_2S and oxygen co-occurrence was found for these latter months in the Arkona and Bornholm Basins.

The plumes found in the Eastern Gotland Basin tended to be around the same spot for the different cruises. One plume was often encountered over the Eastern Gotland slope, one over the southern Gotland Deep trench, and a third plume or breakoff from the sulfidic deep waters at the northern Gotland Deep trench stretching northward. Given that none of these plumes or breakoffs were found during the May cruise, they are most likely not permanent. Since a large portion of these plumes also have lower total H_2S concentration, it is likely that any samples previously taken through Niskin bottles around these areas have missed the center of the plumes and oxidized enough to be below the limit of detection.

Determining where sulfidic water is present, and at which concentration, is crucial for understanding the complex sulfur cycle. While it is acknowledged that photo- and chemolitotrophs, in addition to higher organisms, are capable of utilizing diverse forms of sulfur ions for cellular functionality and signaling (see e.g. **Table 3.10**), the distribution patterns of these ions in the Baltic Sea are not yet fully understood. The data presented here showed that plumes of total H_2S were periodically found around the OMZ, but the concentrations found within these plumes were within the limits for maintaining detoxification and nitrification processes. However, it is important to monitor not only the occurrence of plume structures but also the concentrations as well. With increasing total H_2S concentrations, the chemocline may move towards the sea surface (Kump et al., 2005), allowing more sulfidic bottom water to expand upwards, which may result in plume structures with concentrations high enough to affect the detoxification pathways of various organisms.

REFERENCES

Addison, C., Gamlen, G., & Thompson, R. (1952). 70. The ultra-violet absorption spectra of sodium hyponitrite and sodium α-oxyhyponitrite: the analysis of mixtures with sodium nitrite and nitrate. *Journal of the Chemical Society (Resumed)*, 338-345. https://doi.org/10.1039/JR9520000338

Armstrong, F. A. J., & Boalch, G. T. (1961). Ultra-violet Absorption of Sea Water. *192*(4805), 858-859. https://doi.org/10.1038/192858b0

Avrahami, M., & Golding, R. M. (1968). The oxidation of the sulphide ion at very low concentrations in aqueous solutions. *Journal of the Chemical Society A: Inorganic, Physical, Theoretical*, 647. https://doi.org/10.1039/j19680000647

Beauchamp, R. O., Jr., Bus, J. S., Popp, J. A., Boreiko, C. J., & Andjelkovich, D. A. (1984). A critical review of the literature on hydrogen sulfide toxicity. *Crit Rev Toxicol*, *13*(1), 25-97. https://doi.org/10.3109/10408448409029321

Berg, C., Vandieken, V., Thamdrup, B., & Jürgens, K. (2015). Significance of archaeal nitrification in hypoxic waters of the Baltic Sea. *The ISME Journal*, *9*(6), 1319-1332. https://doi.org/10.1038/ismej.2014.218

Bhuiyan, M. M. U., Rahman, M., Naher, S., Shahed, Z. H., Ali, M. M., & Islam, A. R. M. T. (2024). Oxygen declination in the coastal ocean over the twenty-first century: Driving forces, trends, and impacts. *Case Studies in Chemical and Environmental Engineering*, *9*, 100621. https://doi.org/10.1016/j.cscee.2024.100621

Bittig, H., Körtzinger, A., Johnson, K., Claustre, H., Emerson, S., Fennel, K., Garcia, H., Gilbert, D., Gruber, N., Kang, D.-J., Naqvi, W., Prakash, S., Riser, S., Thierry, V., Tilbrook, B., Uchida, H., Ulloa, O., & Xing, X. (2018). *SCOR WG 142: Quality Control Procedures for Oxygen and Other Biogeochemical Sensors on Floats and Gliders. Recommendations on the conversion between oxygen quantities for Bio-Argo floats and other autonomous sensor platforms*. https://doi.org/10.13155/45915

Björck, S. (1995). A review of the history of the Baltic Sea, 13.0-8.0 ka BP. *Quaternary International*, *27*, 19-40. https://doi.org/10.1016/1040-6182(94)00057-c

Blackford, J., Bull, J. M., Cevatoglu, M., Connelly, D., Hauton, C., James, R. H., Lichtschlag, A., Stahl, H., Widdicombe, S., & Wright, I. C. (2015). Marine baseline and monitoring strategies for carbon dioxide capture and storage (CCS). *International Journal of Greenhouse Gas Control*, *38*, 221-229. https://doi.org/10.1016/j.ijggc.2014.10.004

Burbery, L., Abraham, P., Wood, D., & De Lima, S. (2021). Applications of a UV optical nitrate sensor in a surface water/groundwater quality field study. *Environmental Monitoring and Assessment*, *193*(5). https://doi.org/10.1007/s10661-021-09084-0

Callbeck, C. M., Canfield, D. E., Kuypers, M. M. M., Yilmaz, P., Lavik, G., Thamdrup, B., Schubert, C. J., & Bristow, L. A. (2021). Sulfur cycling in oceanic oxygen minimum zones. *Limnology and Oceanography*, *66*(6), 2360-2392. https://doi.org/10.1002/lno.11759

Canfield, D. E. (2004). The evolution of the Earth surface sulfur reservoir. *American Journal of Science*, *304*(10), 839-861.

Carstensen, J., & Conley, D. J. (2019). Baltic Sea Hypoxia Takes Many Shapes and Sizes. *Limnology and Oceanography Bulletin*, *28*(4), 125-129. https://doi.org/10.1002/lob.10350

Charlson, R. J., Anderson, T. L., & McDuff, R. E. (1992). 13 The Sulfur Cycle. In S. S. Butcher, R. J. Charlson, G. H. Orians, & G. V. Wolfe (Eds.), *International Geophysics* (Vol. 50, pp. 285-300). Academic Press. https://doi.org/10.1016/S0074-6142(08)62696-0

Cline, J. D., & Richards, F. A. (1969). Oxygenation of hydrogen sulfide in seawater at constant salinity, temperature and pH. *Environmental Science & Technology*, *3*(9), 838-843. https://doi.org/10.1021/es60032a004

Commission, E. (2020). *REPORT FROM THE COMMISSION TO THE EUROPEAN PARLIAMENT AND THE COUNCIL on the implementation of the Marine Strategy Framework Directive (Directive 2008/56/EC)*. Brussels: COM(2020) 259 final

Conley, D. J., Björck, S., Bonsdorff, E., Carstensen, J., Destouni, G., Gustafsson, B. G., Hietanen, S., Kortekaas, M., Kuosa, H., Markus Meier, H. E., Müller-Karulis, B., Nordberg, K., Norkko, A., Nürnberg, G., Pitkänen, H., Rabalais, N. N., Rosenberg, R., Savchuk, O. P., Slomp, C. P., . . . Zillén, L. (2009). Hypoxia-Related Processes in the Baltic Sea. *Environmental Science & Technology*, *43*(10), 3412-3420. https://doi.org/10.1021/es802762a

Dahl, C. (2020). A biochemical view on the biological sulfur cycle. *Environmental technologies to treat sulfur pollution: principles and engineering*, *2*, 55-96. https://doi.org/10.2166/9781789060966_0055

de Fommervault, O. P., D'Ortenzio, F., Mangin, A., Serra, R., Migon, C., Claustre, H., Lavigne, H., d'Alcala, M. R., Prieur, L., Taillandier, V., Schmechtig, C., Poteau, A., Leymarie, E., Dufour, A., Besson, F., & Obolensky, G. (2015). Seasonal variability of nutrient concentrations in the Mediterranean Sea: Contribution of Bio-Argo floats. *Journal of Geophysical Research-Oceans*, *120*(12), 8528-8550. https://doi.org/10.1002/2015jc011103

de Jonge, V. N., Elliott, M., & Brauer, V. S. (2006). Marine monitoring: Its shortcomings and mismatch with the EU Water Framework Directive's objectives. *Marine Pollution Bulletin*, *53*(1), 5-19. https://doi.org/10.1016/j.marpolbul.2005.11.026

Deng, Q., Wu, X., Wang, Y., & Liu, M. (2018). Activity Characteristics of Sulfate Reducing Bacteria and Formation Mechanism of Hydrogen Sulfide. *Applied Ecology and Environmental Research*, *16*(5), 6369-6383. https://doi.org/10.15666/aeer/1605_63696383

Diaz, R., & Rosenberg, R. (2008). Spreading Dead Zones and Consequences for Marine Ecosystems. *Science (New York, N.Y.)*, *321*, 926-929. https://doi.org/10.1126/science.1156401

Dunn, O. J. (1964). Multiple Comparisons Using Rank Sums. *Technometrics*, *6*(3), 241-252. https://doi.org/10.2307/1266041

EEA. (2023). How climate change impacts marine life. (22/2023). Retrieved 04.12.2024, from https://www.eea.europa.eu/publications/how-climate-change-impacts (12.11.2024)

Evans, C. L. (1967). THE TOXICITY OF HYDROGEN SULPHIDE AND OTHER SULPHIDES. *Quarterly Journal of Experimental Physiology and Cognate Medical Sciences*, *52*(3), 231-248. https://doi.org/10.1113/expphysiol.1967.sp001909

Feistel, S., Feistel, R., Nehring, D., Matthäus, W., Nausch, G., & Naumann, M. (2016). *Hypoxic and anoxic regions in the baltic Sea, 1969 - 2015* (Meereswiss. Ber., Issue.

Finch, M. S., Hydes, D. J., Clayson, C. H., Weigl, B., Dakin, J., & Gwilliam, P. (1998). A low power ultra violet spectrophotometer for measurement of nitrate in seawater: introduction, calibration and initial sea trials. *377*(2-3), 167-177. https://doi.org/10.1016/s0003-2670(98)00616-3

Fonselius, S. (1981). Oxygen and hydrogen sulphide conditions in the Baltic Sea. *Marine Pollution Bulletin*, *12*(6), 187-194. https://doi.org/10.1016/0025-326X(81)90169-7

Fonselius, S., & Valderrama, J. (2003). One hundred years of hydrographic measurements in the Baltic Sea. *Journal of Sea Research*, *49*(4), 229-241. https://doi.org/10.1016/s1385-1101(03)00035-2

Foster, P., & Morris, A. W. (1971). The use of ultra-violet absorption measurements for the estimation of organic pollution in inshore sea waters. *5*(1), 19-27. https://doi.org/10.1016/0043-1354(71)90059-5

Frank, C., Meier, D., Voß, D., & Zielinski, O. (2014). Computation of nitrate concentrations in coastal waters using an in situ ultraviolet spectrophotometer: Behavior of different computation methods in a case study a steep salinity gradient in the southern North Sea. *Methods in Oceanography*, *9*, 34-43. https://doi.org/10.1016/j.mio.2014.09.002

Giuffrè, A., & Vicente, J. B. (2018). Hydrogen Sulfide Biochemistry and Interplay with Other Gaseous Mediators in Mammalian Physiology. *Oxidative Medicine and Cellular Longevity*, *2018*, 6290931. https://doi.org/10.1155/2018/6290931

Grashoff, K., Ehrhardt, M., & Kremling, K. (1983). Methods of seawater analysis, 2nd edn. Verlag Chemie. In: Weinheim.

Guenther, E. A., Johnson, K. S., & Coale, K. H. (2001). Direct Ultraviolet Spectrophotometric Determination of Total Sulfide and Iodide in Natural Waters. *Analytical Chemistry*, *73*(14), 3481-3487. https://doi.org/10.1021/ac0013812

Guidotti, T. L. (1996). Hydrogen Sulphide. *Occupational Medicine*, *46*(5), 367-371. https://doi.org/10.1093/occmed/46.5.367

Gustafsson, B. G. (2000). Time-Dependent Modeling of the Baltic Entrance Area. 1. Quantification of Circulation and Residence Times in the Kattegat and the Straits of the Baltic Sill. *Estuaries*, *23*(2), 231. https://doi.org/10.2307/1352830

Hansen, M. H., Ingvorsen, K., & Jøgensen, B. B. (1978). Mechanisms of hydrogen sulfide release from coastal marine sediments to the atmosphere. *Limnology and Oceanography*, *23*(1), 68-76. https://doi.org/10.4319/lo.1978.23.1.0068

HELCOM. (2013). *HELCOM Monitoring and Assessment Strategy*. Copenhagen

HELCOM. (2023). State of the Baltic Sea. Third HELCOM holistic assessment 2016-2021. Baltic Sea Environmental Proceedings n°194.

Hietanen, S., Jäntti, H., Buizert, C., Jürgens, K., Labrenz, M., Voss, M., & Kuparinen, J. (2012). Hypoxia and nitrogen processing in the Baltic Sea water column. *Limnology and Oceanography*, *57*(1), 325-337. https://doi.org/10.4319/lo.2012.57.1.0325

Holtermann, P., Prien, R., Naumann, M., & Umlauf, L. (2020). Interleaving of oxygenized intrusions into the Baltic Sea redoxcline. *Limnology and Oceanography*, *65*(3), 482-503. https://doi.org/10.1002/lno.11317

Hopkins, C. (2000). Overview of monitoring in the Baltic Sea. *Report to the Global Environment Facility/Baltic Sea Regional Project. AquaMarine Advisers*.

Hu, X., Liu, J., Liu, H., Zhuang, G., & Xun, L. (2018). Sulfur metabolism by marine heterotrophic bacteria involved in sulfur cycling in the ocean. *Science China Earth Sciences*, *61*(10), 1369-1378. https://doi.org/10.1007/s11430-017-9234-x

Jahn, A., Gamenick, I., & Theede, H. (1996). Physiological adaptations of Cyprideis torosa (Crustacea, Ostracoda) to hydrogen sulphide. *Marine Ecology Progress Series*, *142*, 215-223. https://doi.org/10.3354/meps142215

Jenkyns, H. C. (2010). Geochemistry of oceanic anoxic events. *Geochemistry, Geophysics, Geosystems*, *11*(3), n/a-n/a. https://doi.org/10.1029/2009gc002788

Johnson, K. S., & Coletti, L. J. (2002). In situ ultraviolet spectrophotometry for high resolution and long-term monitoring of nitrate, bromide and bisulfide in the ocean. *Deep-Sea Research Part I-Oceanographic Research Papers*, *49*(7), 1291-1305. https://doi.org/10.1016/S0967-0637(02)00020-1

Johnson, K. S., Coletti, L. J., & Chavez, F. P. (2006). Diel nitrate cycles observed with in situ sensors predict monthly and annual new production. *Deep Sea Research Part I: Oceanographic Research Papers*, *53*(3), 561-573. https://doi.org/10.1016/j.dsr.2005.12.004

Johnson, K. S., Plant, J. N., Coletti, L. J., Jannasch, H. W., Sakamoto, C. M., Riser, S. C., Swift, D. D., Williams, N. L., Boss, E., Haëntjens, N., Talley, L. D., & Sarmiento, J. L. (2017). Biogeochemical sensor performance in the SOCCOM profiling float array. *Journal of Geophysical Research: Oceans*, *122*(8), 6416-6436. https://doi.org/10.1002/2017jc012838

Kabil, O., & Banerjee, R. (2010). Redox Biochemistry of Hydrogen Sulfide. *Journal of Biological Chemistry*, *285*(29), 21903-21907. https://doi.org/10.1074/jbc.r110.128363

Kamyshny, A., Yakushev, E. V., Jost, G., & Podymov, O. I. (2013). Role of Sulfide Oxidation Intermediates in the Redox Balance of the Oxic–Anoxic Interface of the Gotland Deep, Baltic Sea. In E. V. Yakushev (Ed.), *Chemical Structure of Pelagic Redox Interfaces: Observation and Modeling* (pp. 95-119). Springer Berlin Heidelberg. https://doi.org/10.1007/698_2010_83

Kankaanpää, H. T., & Virtasalo, J. J. (2017). Rapid fluctuations in the northern Baltic Sea H2S layer. *Journal of Marine Systems*, *176*, 24-37. https://doi.org/10.1016/j.jmarsys.2017.07.001

Kelley, J. L., Arias-Rodriguez, L., Patacsil Martin, D., Yee, M.-C., Bustamante, C. D., & Tobler, M. (2016). Mechanisms Underlying Adaptation to Life in Hydrogen Sulfide–Rich Environments. *Molecular Biology and Evolution*, *33*(6), 1419-1434. https://doi.org/10.1093/molbev/msw020

Kõuts, M., Maljutenko, I., Elken, J., Liu, Y., Hansson, M., Viktorsson, L., & Raudsepp, U. (2021). Recent regime of persistent hypoxia in the Baltic Sea. *Environmental Research Communications*, *3*(7), 075004. https://doi.org/10.1088/2515-7620/ac0cc4

Krauss, W., & Brügge, B. (1991). Wind-Produced Water Exchange between the Deep Basins of the Baltic Sea. *Journal of Physical Oceanography*, *21*(3), 373-384. https://doi.org/https://doi.org/10.1175/1520-0485(1991)021<0373:WPWEBT>2.0.CO;2

Kruskal, W. H., & Wallis, W. A. (1952). Use of Ranks in One-Criterion Variance Analysis. *Journal of the American Statistical Association*, *47*(260), 583-621. https://doi.org/10.2307/2280779

Kuijpers, A., Kunzendorf, H., Rasmussen, P., Sicre, M.-A., Ezat, U., Fernane, A., & Weckström, K. (2012). The Baltic Sea inflow regime at the termination of the Medieval Climate Anomaly linked to North Atlantic circulation. *Baltica*, *25*(1), 57-64. https://doi.org/10.5200/baltica.2012.25.05

Kump, L. R., Pavlov, A., & Arthur, M. A. (2005). Massive release of hydrogen sulfide to the surface ocean and atmosphere during intervals of oceanic anoxia. *Geology*, *33*(5), 397-400. https://doi.org/10.1130/g21295.1

Langergraber, G., Fleischmann, N., & Hofstädter, F. (2003). A multivariate calibration procedure for UV/VIS spectrometric quantification of organic matter and nitrate in wastewater. *Water Science and Technology*, *47*(2), 63-71. https://doi.org/10.2166/wst.2003.0086

Lass, H. U., & Mohrholz, V. (2003). On dynamics and mixing of inflowing saltwater in the Arkona Sea. *Journal of Geophysical Research: Oceans*, *108*(C2). https://doi.org/https://doi.org/10.1029/2002JC001465

Lass, H. U., Mohrholz, V., & Seifert, T. (2005). On pathways and residence time of saltwater plumes in the Arkona Sea. *Journal of Geophysical Research: Oceans*, *110*(C11). https://doi.org/10.1029/2004jc002848

Lehmann, A., & Hinrichsen, H.-H. (2003). Water, heat and salt exchange between the deep basins of the Baltic Sea. *Boreal Environment Research*, *7*, 405-415.

Lehmann, A., Myrberg, K., Post, P., Chubarenko, I., Dailidiene, I., Hinrichsen, H.-H., Hüssy, K., Liblik, T., Meier, H. E. M., Lips, U., & Bukanova, T. (2022). Salinity dynamics of

the Baltic Sea. *Earth System Dynamics*, *13*(1), 373-392. https://doi.org/10.5194/esd-13-373-2022

Li, J., Liu, P., Wang, J., Roberts, A. P., & Pan, Y. (2020). Magnetotaxis as an Adaptation to Enable Bacterial Shuttling of Microbial Sulfur and Sulfur Cycling Across Aquatic Oxic-Anoxic Interfaces. *Journal of Geophysical Research: Biogeosciences*, *125*(12). https://doi.org/10.1029/2020jg006012

Linnet, K., & Kondratovich, M. (2004). Partly Nonparametric Approach for Determining the Limit of Detection. *Clinical Chemistry*, *50*(4), 732-740. https://doi.org/10.1373/clinchem.2003.029983

Liu, Z., Deng, Z., Davis, S. J., & Ciais, P. (2024). Global carbon emissions in 2023. *Nature Reviews Earth & Environment*, *5*(4), 253-254. https://doi.org/10.1038/s43017-024-00532-2

Lloyd, D. (2006). Hydrogen sulfide: clandestine microbial messenger? *Trends in Microbiology*, *14*(10), 456-462. https://doi.org/10.1016/j.tim.2006.08.003

Lloyd, D., Kristensen, B., & Degn, H. (1981). Oxidative Detoxification of Hydrogen Sulphide Detected by Mass Spectrometry in the Soil Amoeba Acanthamoeba castellanii. *Microbiology*, *126*(1), 167-170. https://doi.org/10.1099/00221287-126-1-167

Luther, G. W., Findlay, A. J., Macdonald, D. J., Owings, S. M., Hanson, T. E., Beinart, R. A., & Girguis, P. R. (2011). Thermodynamics and Kinetics of Sulfide Oxidation by Oxygen: A Look at Inorganically Controlled Reactions and Biologically Mediated Processes in the Environment. *Frontiers in Microbiology*, *2*. https://doi.org/10.3389/fmicb.2011.00062

Luther, G. W., & Tsamakis, E. (1989). Concentration and form of dissolved sulfide in the oxic water column of the ocean. *Marine Chemistry*, *27*(3), 165-177. https://doi.org/10.1016/0304-4203(89)90046-7

Malone, T. C., & Newton, A. (2020). The Globalization of Cultural Eutrophication in the Coastal Ocean: Causes and Consequences [Review]. *Frontiers in Marine Science*, *7*. https://doi.org/10.3389/fmars.2020.00670

Martin, W., Rotte, C., Hoffmeister, M., Theissen, U., Gelius-Dietrich, G., Ahr, S., & Henze, K. (2003). Early Cell Evolution, Eukaryotes, Anoxia, Sulfide, Oxygen, Fungi First (?), and a Tree of Genomes Revisited. *IUBMB Life*, *55*(4-5), 193-204. https://doi.org/10.1080/1521654031000141231

Matsushita, B., Yang, W., Chang, P., Yang, F., & Fukushima, T. (2012). A simple method for distinguishing global Case-1 and Case-2 waters using SeaWiFS measurements. *ISPRS Journal of Photogrammetry and Remote Sensing*, *69*, 74-87. https://doi.org/10.1016/j.isprsjprs.2012.02.008

Meier, H. E. M. (2005). Modeling the age of Baltic Seawater masses: Quantification and steady state sensitivity experiments. *Journal of Geophysical Research: Oceans*, *110*(C2). https://doi.org/10.1029/2004jc002607

Meyer, D., Prien, R. D., Rautmann, L., Pallentin, M., Waniek, J. J., & Schulz-Bull, D. E. (2018). In situ Determination of Nitrate and Hydrogen Sulfide in the Baltic Sea Using an Ultraviolet Spectrophotometer. *Frontiers in Marine Science*, *5*. https://doi.org/10.3389/fmars.2018.00431

Millero, F. J. (1986). The thermodynamics and kinetics of the hydrogen sulfide system in natural waters. *Marine Chemistry*, *18*(2), 121-147. https://doi.org/10.1016/0304-4203(86)90003-4

Millero, F. J., Hubinger, S., Fernandez, M., & Garnett, S. (1987). Oxidation of H2S in seawater as a function of temperature, pH, and ionic strength. *Environmental Science & Technology*, *21*(5), 439-443. https://doi.org/10.1021/es00159a003

Millero, F. J., Plese, T., & Fernandez, M. (1988). The dissociation of hydrogen sulfide in seawater1. *Limnology and Oceanography*, *33*(2), 269-274. https://doi.org/10.4319/lo.1988.33.2.0269

Nehir, M., Esposito, M., Begler, C., Franke, C., Zielinski, O., & Achterberg, E. P. (2021). Improved Calibration and Data Processing Procedures of OPUS Optical Sensor for High-Resolution in situ Monitoring of Nitrate in Seawater [Original Research]. *Frontiers in Marine Science*, *8*(805). https://doi.org/10.3389/fmars.2021.663800

Noto, V. D., & Mecozzi, M. (1997). Determination of Seawater Salinity by Ultraviolet Spectroscopic Measurements. *Applied Spectroscopy*, *51*(9), 1294-1302. http://as.osa.org/abstract.cfm?URI=as-51-9-1294

Nygård, H., Lindegarth, M., Darr, A., Dinesen, G. E., Eigaard, O. R., & Lips, I. (2020). Developing benthic monitoring programmes to support precise and representative status assessments: a case study from the Baltic Sea. *Environmental Monitoring and Assessment*, *192*(12). https://doi.org/10.1007/s10661-020-08764-7

Olson, K. R. (2012). A Practical Look at the Chemistry and Biology of Hydrogen Sulfide. *Antioxidants & Redox Signaling*, *17*(1), 32-44. https://doi.org/10.1089/ars.2011.4401

Olson, K. R., & Straub, K. D. (2016). The Role of Hydrogen Sulfide in Evolution and the Evolution of Hydrogen Sulfide in Metabolism and Signaling. *Physiology*, *31*(1), 60-72. https://doi.org/10.1152/physiol.00024.2015

Perner, M., Wallmann, K., Adam-Beyer, N., Hepach, H., Laufer-Meiser, K., Böhnke, S., Diercks, I., Bange, H. W., Indenbirken, D., Nikeleit, V., Bryce, C., Kappler, A., Engel, A., & Scholz, F. (2022). Environmental changes affect the microbial release of hydrogen sulfide and methane from sediments at Boknis Eck (SW Baltic Sea). *Frontiers in Microbiology*, *13*. https://doi.org/10.3389/fmicb.2022.1096062

Plant, J. N., Sakamoto, C. M., Johnson, K. S., Maurer, T. L., & Bif, M. B. (2023). Updated temperature correction for computing seawater nitrate with in situ ultraviolet spectrophotometer and submersible ultraviolet nitrate analyzer nitrate sensors. *Limnology and Oceanography: Methods*. https://doi.org/10.1002/lom3.10566

Poornima, D., Shanthi, R., Ranith, R., Senthilnathan, L., Sarangi, R. K., Thangaradjou, T., & Chauhan, P. (2016). Application of in-situ sensors (SUNA and thermal logger) in fine tuning the nitrate model of the Bay of Bengal. *4*, 9-17. https://doi.org/10.1016/j.rsase.2016.04.002

Rabalais, N. N. (2019). Ocean deoxygenation from eutrophication (human nutrient inputs). In *Ocean deoxygenation: Everyone's problem - Causes, impacts, consequences and solutions.* (pp. 117-135). IUCN. https://doi.org/10.2305/IUCN.CH.2019.13.en

Reverberi, A. P., Klemeš, J. J., Varbanov, P. S., & Fabiano, B. (2016). A review on hydrogen production from hydrogen sulphide by chemical and photochemical methods. *Journal of Cleaner Production*, *136*, 72-80. https://doi.org/10.1016/j.jclepro.2016.04.139

Sakamoto, C. M., Johnson, K. S., & Coletti, L. J. (2009). Improved algorithm for the computation of nitrate concentrations in seawater using an in situ ultraviolet spectrophotometer. *Limnology and Oceanography: Methods*, *7*(1), 132-143. https://doi.org/10.4319/lom.2009.7.132

Sakamoto, C. M., Johnson, K. S., Coletti, L. J., & Jannasch, H. W. (2017). Pressure correction for the computation of nitrate concentrations in seawater using an in situ ultraviolet spectrophotometer. *Limnology and Oceanography: Methods*, *15*(10), 897-902. https://doi.org/10.1002/lom3.10209

Samset, B. H., Lund, M. T., Fuglestvedt, J. S., & Wilcox, L. J. (2024). 2023 temperatures reflect steady global warming and internal sea surface temperature variability. *Communications Earth & Environment*, *5*(1). https://doi.org/10.1038/s43247-024-01637-8

Schneider, B., Dellwig, O., Kuliński, K., Omstedt, A., Pollehne, F., Rehder, G., & Savchuk, O. (2017). Biogeochemical cycles. In *Biological oceanography of the Baltic Sea* (pp. 87-122). Springer. https://doi.org/10.1007/978-94-007-0668-2_3

Schunck, H., Lavik, G., Desai, D. K., Großkopf, T., Kalvelage, T., Löscher, C. R., Paulmier, A., Contreras, S., Siegel, H., Holtappels, M., Rosenstiel, P., Schilhabel, M. B., Graco, M., Schmitz, R. A., Kuypers, M. M. M., & Laroche, J. (2013). Giant Hydrogen Sulfide Plume in the Oxygen Minimum Zone off Peru Supports Chemolithoautotrophy. *Plos One*, *8*(8), e68661. https://doi.org/10.1371/journal.pone.0068661

Shooter, D. (1999). Sources and sinks of oceanic hydrogen sulfide – an overview. *Atmospheric Environment*, *33*(21), 3467-3472. https://doi.org/10.1016/S1352-2310(98)00364-1

Siang, H. Y., Tahir, N. M., Malek, A., & Isa, M. A. M. (2017). Breakdown of hydrogen sulfide in seawater under different ratio of dissolved oxygen/hydrogen sulfide. *Malaysian Journal of Analytical Sciences*, *21*, 1016-1027. https://doi.org/10.17576/mjas-2017-2105-03

Sievert, S. M., Kiene, R. P., & Schulz-Vogt, H. N. (2007). The Sulfur Cycle. *Oceanography*, *20*(2), 117-123. https://doi.org/10.5670/oceanog.2007.55

Simis, S. G. H., Ylöstalo, P., Kallio, K. Y., Spilling, K., & Kutser, T. (2017). Contrasting seasonality in optical-biogeochemical properties of the Baltic Sea. *Plos One*, *12*(4), e0173357. https://doi.org/10.1371/journal.pone.0173357

Snoeijs-Leijonmalm, P., & Andrén, E. (2017). Why is the Baltic Sea so special to live in? In *Biological oceanography of the Baltic Sea* (pp. 23-84). Springer. https://doi.org/10.1007/978-94-007-0668-2_2

Sorokin, Y. I. (1972). The Bacterial Population and the Processes of Hydrogen Sulphide Oxidation in the Black Sea. *ICES Journal of Marine Science*, *34*(3), 423-454. https://doi.org/10.1093/icesjms/34.3.423

Stramma, L., & Schmidtko, S. (2019). Global evidence of ocean deoxygenation. In *Ocean deoxygenation: Everyone's problem - Causes, impacts, consequences and solutions.* (pp. 25-36). IUNC. https://doi.org/10.2305/IUCN.CH.2019.13.en

Szabo, C. (2018). A timeline of hydrogen sulfide (H2S) research: From environmental toxin to biological mediator. *Biochemical Pharmacology*, *149*, 5-19. https://doi.org/10.1016/j.bcp.2017.09.010

Tabibzadeh, S. (2016). Nature creates, adapts, protects and sustains life using hydrogen sulfide. *Front. Biosci*, *21*(3), 528-560. https://doi.org/10.2741/4407

Takeda, K., & Fujiwara, K. (1993). Determination of nitrate in natural waters with the photo-induced conversion of nitrate to nitrite. *Analytica Chimica Acta*, *276*(1), 25-32. https://doi.org/10.1016/0003-2670(93)85035-i

Taylor, K. E. (2001). Summarizing multiple aspects of model performance in a single diagram. *Journal of Geophysical Research: Atmospheres*, *106*(D7), 7183-7192. https://doi.org/10.1029/2000jd900719

Tobler, M., Passow, C. N., Greenway, R., Kelley, J. L., & Shaw, J. H. (2016). The Evolutionary Ecology of Animals Inhabiting Hydrogen Sulfide–Rich Environments. *Annual Review of Ecology, Evolution, and Systematics*, *47*(1), 239-262. https://doi.org/10.1146/annurev-ecolsys-121415-032418

Tuttle, J. H., & Jannasch, H. W. (1977). Thiosulfate stimulation of microbial dark assimilation of carbon dioxide in shallow marine waters. *Microbial Ecology*, *4*(1), 9-25. https://doi.org/10.1007/bf02010426

Ulloa, O., Canfield, D. E., Delong, E. F., Letelier, R. M., & Stewart, F. J. (2012). Microbial oceanography of anoxic oxygen minimum zones. *Proceedings of the National Academy of Sciences*, *109*(40), 15996-16003. https://doi.org/10.1073/pnas.1205009109

Wenzel, T. (2024). *Molecular and Atomic Spectroscopy*. LibreTexts. https://chem.libretexts.org/@go/page/182364

Zielinski, O., Voß, D., Saworski, B., Fiedler, B., & Körtzinger, A. (2011). Computation of nitrate concentrations in turbid coastal waters using an in situ ultraviolet spectrophotometer. *Journal of Sea Research*, *65*(4), 456-460. https://doi.org/10.1016/j.seares.2011.04.002

DOCTORAL COMMITTEE

1st Referee

Prof. Dr. rer. nat. Joanna Waniek

Leibniz Institute for Baltic Sea Research – Warnemünde

Department: Marine Chemistry

2nd Referee

Prof. Dr. rer. nat. Arne Körtzinger

GEOMAR Helmholtz-Zentrum für Ozeanforschung Kiel

Department: Marine Biogeochemistry

Day of submission: 13.02.2025

Day of defense: 03.06.2025

CURRICULUM VITAE

CONTACT INFORMATION:	Malin M. Waern Leibniz Institute for Baltic Sea Research – Warnemünde Department: Marine Chemistry malin.waern@uni-rostock.de
EDUCATION:	University of Rostock / IOW *PhD student, Germany | 2020 – 2025* University of Gothenburg *Master's degree in Marine Science, Sweden | 2018 – 2020* University of Southampton *Erasmus+, Southampton, England | 2017 – 2018* University of Gothenburg *Bachelor's degree in Marine Science, Sweden | 2015 – 2018*
CERTIFICATES:	IOW statistics workshop *Series organized by IOW's PhD network, Germany | 2023* KFT Scientific Diver Nitrox *Dive certificate for Scientific Diver with mixed gases, Germany | 2022* DGUV Scientific Diver *Dive certificate for European Scientific Diver, Germany | 2021* SSI Enriched Air Nitrox *Dive certificate Nitrox up to EAN40, Sweden | 2018* PADI Advanced open water diver *Dive certificate 30 m, Sweden | 2015* PADI Open water *Dive certificate 15 m, Sweden | 2015*
PUBLICATIONS AND PRESENTATIONS:	Gustafsson, M., Strand, Å., Laugen, A.T., Albretsen, J., André, C., Broström, G., Jorde, P. E., Knutsen, H., Ortega-Martinez, O., Sodeland, M., **Waern, M.**, Wrange, A.-L., & De Wit, P. (2024). Unlocking the secret life of blue mussels: Exploring connectivity in the Skagerrak through biophysical modeling and population genomics. *Evolutionary Applications*, 17, e13704. https://doi.org/10.1111/eva.13704 **Waern M.**, Floth-Peterson M., Prien R., Bittig H. Nutrient monitoring via UV spectroscopy – A way to improve our understanding of ecosystems in the Baltic Sea? modified version, Poster ICYMARE – International Conference for Young Marine Researchers, 15-16.09.2022, Bremerhaven, Germany **Waern M.**, Floth-Peterson M., Prien R., Bittig H. Nutrient monitoring via UV spectroscopy – A way to improve our

understanding of ecosystems in the Baltic Sea? Poster Advisory Board IOW, 29.06.2022, Warnemünde, Germany

Waern M., Strand Å., Effects of Pacific oysters on the blue mussel population in Sweden – implications for restoration. Poster ASSG – Association of Scottish Shellfish Growers conference, 30.10.2019, Oban, Scotland